DOE/BC/14934-8
(OSTI ID: 5126)

INCREASING WATERFLOOD RESERVES IN THE WILMINGTON OIL FIELD THROUGH IMPROVED RESERVOIR CHARACTERIZATION AND RESEROIR MANAGEMENT

Annual Report
March 20, 1996 – March 21, 1997

By
Roger Koerner, City of Long Beach
Don Clarke, City of Long Beach
Scott Walker, Tidelands Oil Production Co.
Chris Phillips, Tidelands Oil Production Co.
John Nguyen, Tidelands Oil Production Co.
Dan Moos, Stanford University
Kwasi Tagbor, MPI

April 1999

Work Performed Under Contract No. DE-FC22-95BC14934

City of Long Beach
Long Beach, California

National Petroleum Technology Office
U. S. DEPARTMENT OF ENERGY
Tulsa, Oklahoma

DOE/BC/14934-8
Distribution Category UC-122

Increasing Waterflood Reserves in the Wilmington Oil Field through Improved Reservoir Characterization and Reservoir Management

By
Roger Koerner, City of Long Beach
Don Clarke, City of Long Beach
Scott Walker, Tidelands Oil Production Co.
Chris Phillips, Tidelands Oil Production Co.
John Nguyen, Tidelands Oil Production Co.
Dan Moos, Stanford University
Kwasi Tagbor, MPI

April 1999

Work Performed Under Contract DE-FC22-95BC14934

Prepared for
U.S. Department of Energy
Assistant Secretary for Fossil Energy

Gary Walker, Project Manager
National Petroleum Technology Office
P.O. Box 3628
Tulsa, OK 74101

Prepared by
City of Long Beach
Dept.of Oil Properties
211 E. Ocean Blvd – Suite 500
Long Beach, CA 90802

TABLE OF CONTENTS

APPENDICES and FIGURES

Foreword

This project is intended to increase recoverable waterflood reserves in slope and basin reservoirs through improved reservoir characterization and reservoir management. The particular application of this project is in portions of Fault Blocks IV and V of the Wilmington Oil Field, in Long Beach, California, but the approach is widely applicable in slope and basin reservoirs. Transferring technology so that it can be applied in other sections of the Wilmington Field and by operators in other slope and basin reservoirs is a primary component of the project.

Abstract

This project used advanced reservoir characterization tools, including the pulsed acoustic cased-hole logging tool, geologic three-dimensional (3-D) modeling software, and commercially available reservoir management software to identify sands with remaining high oil saturation following waterflood. Production from the identified high oil saturated sands was stimulated by recompleting existing production and injection wells in these sands using conventional means as well as a short radius redrill candidate.

Although these reservoirs have been waterflooded over 40 years, researchers have found areas of remaining oil saturation. Areas such as the top sand in the Upper Terminal Zone Fault Block V, the western fault slivers of Upper Terminal Zone Fault Block V, the bottom sands of the Tar Zone Fault Block V, and the eastern edge of Fault Block IV in both the Upper Terminal and Lower Terminal Zones all show significant remaining oil saturation. Each area of interest was uncovered emphasizing a different type of reservoir characterization technique or practice. This was not the original strategy but was necessitated by the different levels of progress in each of the project activities.

Executive Summary

Waterflood oil recovery in the Wilmington Field has historically been inefficient due to a variety of factors, including reservoir heterogeneity, poor sweep efficiency, high water cut, and poor injection profiles. Sands with high remaining oil saturation are still present despite extensive waterflooding, but locating these sands has been difficult.

Reservoir management software has identified areas of potentially high remaining oil saturation in both the Upper Terminal Zone and the Lower Terminal Zone of Fault Block IV. A pulsed acoustic cased-hole logging tool was run in potential recompletion

candidates and recovered compressional wave data from which porosities were calculated. Unfortunately, shear wave data were not recovered therefore acoustically derived saturations cannot be predicted for the Fault Block IV wells. An optimized remedial recompletion was completed on well Y-63 in the Upper Terminal Zone of Fault Block IV, and well Z-223 of Upper Terminal Zone Fault Block V. These wells are doing better than offset production wells.

Examination of recent electric logs (E-logs) revealed sands with remaining high oil saturation in the Tar Zone and Upper Terminal Zone of Fault Block V. A deterministic 3-D model was built around the Upper Terminal Zone recompletion candidate Well J-120. Well J-120 was recompleted and returned to production. Production results greatly exceeded expectation. A deterministic 3-D model was also built around the Tar Zone recompletion candidate Well J-15. Well J-15 was also recompleted and returned to production. Production results were also greater than anticipated.

Introduction

This project uses advanced reservoir characterization tools, including the pulsed acoustic cased-hole logging tool, geologic (3-D) modeling software, and commercially available reservoir management software to identify sands with remaining high oil saturation following waterflood. Production from the identified high oil saturation sands will be exploited by recompleting existing idle production and injection wells in these sands using conventional means as well as a short radius redrill candidate.

Discussion

● Reservoir Characterization

Theoretical relationships, confirmed by laboratory and field data, suggest that hydrocarbon-bearing rocks in situ can be differentiated from rocks containing brines using sonic velocity measurements. Rock-log and fluid-log models are needed to calibrate, interpret, and understand the acoustic log data[1].

Because hydrocarbons in situ generally have much lower bulk moduli and densities than brines, replacing water with hydrocarbons lowers the compressional velocity and increases slightly the shear wave velocity. Williams[2] presented convincing evidence that hydrocarbons could be detected from the difference between measured Vp/Vs and that

predicted for a water saturated rock from shear wave velocity as shown in Figure 1 comparing wells M-499 and 167-W[3]. Because the water delineation line is similar for clean and clay-bearing sands, virtually the same relationship can be used to detect hydrocarbons in both, eliminating the need for an independent lithology indicator. However, because of the lack of quantitative physical models to predict the effect, this technique has been applied with caution and a limited degree of success.

Researchers have developed a rock model which relates frame moduli to porosity in unconsolidated sands found in the Wilmington Field and other slope and basin reservoirs.

The reservoir characterization portion of the DOE project incorporated the refinement and application of rock-log models for relationships between elastic-wave velocities measured using the dipole logging tool, and the oil saturation and porosity within the reservoir. Existing theoretical models were evaluated for application to the Wilmington Field. Several of these models were applied to predict the magnitude of the effect of saturation on velocities. Laboratory data were collected in actual samples of reservoir rock and in sand-clay mixtures, to better define the relationships between elastic moduli and reservoir properties. The most appropriate model was then applied to predict porosity and constrain saturation using the existing log data.
An investigation of uncertainty in predictions revealed that while primary-wave (P-wave) data alone could be used in ideal circumstances to predict saturation, secondary-wave (S-wave) velocities are required to refine the results and improve confidence. The results indicated that monopole and dipole logs can be used to predict porosity and to differentiate between potentially productive and non-productive sands in the Wilmington field.

The theoretical rock physics part of the DOE project has two main thrusts: (a) first-principle-based models for relating the elasticity of the high-porosity sediment frame to porosity and mineralogy; and (b) models for relating sonic P- and S-wave velocities to the properties of the pore fluid. The latter models are intended to be used in the inversion mode i.e., for inferring pore fluid type (hydrocarbons versus brine) from sonic. An important by-product of this modeling is a theory for estimating permeability from porosity and velocity.

Elasticity of High-porosity Sediments

By analyzing several data sets for sandstones of up to 40% porosity, we concluded that there are two end-member velocity-porosity trends. One is for rocks where the diagenetic cement fills the grain contacts thus reinforcing the sediment's frame (e.g., quartz rims growing on sand grains), and the other is for rocks where the cement is

deposited away from the grain contacts (e.g., mica and clay in the pore space). In the first case, both P- and S-wave velocities are high even in a high-porosity sandstone. In the second case, at the same high porosity, the velocities are low. In reality, many rocks fall between these two end members: often both contact and non-contact cement are present. However, it appears that the Wilmington oil-bearing rocks can be accurately described by the low-velocity end member. We have successfully used this theory to infer porosity from behind-casing dipole data.

Saturation and Velocity

A standard way of relating the properties of the pore fluid (compressibility and density) to sonic velocity is by using Gassmann's equation. The assumption behind this approach is that the phases of the pore fluid (e.g., oil and brine) are homogeneously mixed at the pore scale, which allows for calculating the compressibility of the "effective" pore fluid. A different situation is where the two (or more) phases of the pore fluid are situated in patches and do not co-exist in every pore. Of course, these two situation have to be treated as the end members of the general case where both patchy and homogeneous situations are present. We provide a theory for calculating the effective elastic properties of rock with patchy saturation. By using a field example, we show that such a situation can indeed exist in situ. In practice, quantitative saturation values cannot be obtained even if the fluid distribution is known, without knowing the compliances of the fluid endmembers.

Permeability

Similar to the elasticity of rock, its permeability depends not only on porosity, but also on the position of the pore-filling cement. At the same porosity, it is larger for the contact-cement case than for the other end member--the non-contact-cement case. By using a field example, we show that by relating permeability to the amount of the non-contact cement, we achieve a much more accurate trend that by relating it to porosity. This new parameter, the volumetric fraction of the non-contact cement in the rock, can be found from porosity and velocity.

Uncertainty

In earlier work it was demonstrated that porosity and fluid saturation could be inferred from acoustic P-wave data even in the absence of S-wave data. However, interpretation of seismic velocities in terms of fluid saturations are not unique. Velocities are affected not only by the pore fluids we wish to detect, but also by variations in porosity, clay content, pressure, and temperature. Statistical analytical methods to investigate uncertainties in these predictions were applied to a synthetic example conditioned on laboratory data, and to a real well log example in a shaly sand reservoir from the Gulf of Mexico. The results showed that while in some cases shear wave data may not help to reduce the uncertainty,

in other situations, noisy S-wave data along with noisy P-wave data can convey more information than perfect P-wave data alone. By implication, knowledge of lithology in addition to P- and S-wave velocity it should be possible to refine the interpretations further. Such information may be available for application to cased holes using gamma-ray logs or older open-hole logs.

Laboratory Results

More than thirty laboratory tests of unconsolidated samples were acquired during the course of this project. Measurements of bulk and shear modulus and ultrasonic P- and S-wave velocities were carried out in the majority of these experiments while varying confining pressure from zero to 30 Mpa, corresponding to a depth of burial of more than 1524m (5000'). Initial tests were completed on archived cores with residual fluids intact, and on archived cores after cleaning to remove tars. Tests on cores recovered during the project and stored under refrigeration were carried out in a similar fashion. Synthetic samples of Ottawa sand mixed with wetted clays were tested to investigate the importance to this project of frequency dependence of the measured moduli.

The results revealed that one, porosities could be predicted using the Hashin-Shtrikman Lower Bound (HSLB) model for unconsolidated materials. However, the results need to be corrected slightly (approximately 3 to 5 porosity units up or down) for the effects of varying confining or pore fluid pressures. Two, saturation with fluids caused changes in properties consistent with the Gassmann relations used to model the field data. Three, significant irreversible compaction occurs on loading, preventing the use of a single sample to study the effects of fluid replacement. This required more measurements than originally expected to fully describe the properties of these materials in the presence of different types of pore fluids. Four, the dry frame moduli were frequency dependent due to the presence of clays and mica. This frequency dependence was in addition to an expected dispersion associated with pore fluids.

The laboratory data were sufficient to demonstrate that the theoretical rock-log models were accurate and general enough to allow application to fields such as Wilmington. Furthermore, they allowed us to "calibrate" the models against theoretical predictions from contact theory. They revealed that care must be taken when applying laboratory data to the field to incorporate both frame and fluid related dispersion.

Field Application

Porosity

Porosity estimation techniques based on the theoretical model appropriate for the Wilmington Field were applied to shear-wave data from two wells, for comparison to alternative porosity estimation techniques. In the cased well porosities predicted acoustically were in excellent agreement with density-derived porosities in sands, and were lower in shales, and thus were more likely to be measures of the effective porosity. Importantly, the sonic porosity was more reliable in bad hole sections due to its insensitivity to variations in hole size. In a second well, sonic porosities obtained in the open hole were smaller than neutron porosities and slightly larger than density porosities.

Saturation

Acoustic data from two wells was used to evaluate the ability to predict saturation. In one well for which open-hole estimates from Archie's Law were used to select perforation intervals, the acoustic prediction was in qualitative agreement with Archie's Law estimates of saturation. By selecting those zones, it was demonstrated that the sonic data in Wilmington were consistent with ALHI empirical predictions, in that high oil saturation zones lay below the ALHI "water line". Data from an injector, in which intervals subject to injection could be isolated from those which were not subject to injection using a gamma-ray log, revealed that the data lay above the water line, consistent with being fully watered-out. These two empirical tests revealed both that the acoustic technique could be used to predict the presence of hydrocarbons, and that it could also be used to identify fully watered-out zones.

Lithology Effects

The field data revealed the presence of lithology effects not predicted by the original Williams ALHI paper. These included scatter in the water-saturated data above the ALHI "water line". They are not likely to be important in qualitative applications of acoustic saturation prediction. Theoretical modeling revealed that these effects are due to the presence of feldspars and other grains in addition to quartz, and can to first order be accounted for using a gamma-ray log to determine the relative volume of quartz in relation to other minerals in the rock matrix. Further work would be necessary to quantify the effect.

Monopole and dipole shear sonic logs can provide accurate compressional and shear wave velocities in cased holes, even in shallow, unconsolidated sands such as in the Wilmington Field. Porosity can be determined from shear wave velocity, provided an appropriate transform is used. Qualitatively, acoustic logs can be used to locate bypassed oil.

● Reservoir Engineering

Oil field reservoir and production engineering analysis for the Wilmington Field first required locating, inputting, quality controlling, storing, and manipulating enormous amounts of data. This was a monumental task that we originally underestimated. Production data from the early life of the field was missing or only available on hard copy. The missing data was located at government agencies such as the City of Long Beach's Department of Oil Properties (DOP) and the California Department of Oil and Gas and Geothermal Resources (CDOGGR). Zones of interest were prioritized for engineering studies. Waiting for all zones to be input and quality controlled before starting our studies would have reduced the time allocated for analysis.

The first zone of interest completed was the Upper Terminal Zone of Fault Block IV. Researchers generated numerous cumulative production bubble maps, cumulative injection bubble maps, daily production maps, and isocut maps. These maps revealed an area on the east side of the fault block against the Harbor Entrance Fault that appeared to have low cumulative oil recovery. Idle well Y-63, originally scheduled for abandonment, was recompleted in the Upper Terminal Zone across the "Hx", "J", "Y", and "K" sands. It currently produces 121.4 m^3/d (763 b/d) gross, 3.8 m^3/d (24 b/d) net, for a 96.7% water cut with 15.2 m (50') of fluid over the pump.

Remaining zones are under study and will eventually generate recompletion candidates similar to well Y-63. These candidates will be recompleted during the second budget period.

In zones where data input and manipulation were not completed, researchers scanned the log files for newer electric logs which would indicate bypassed oil. Another technique for finding bypassed oil was to identify anomalous production well characteristics such as lower than average water cuts, high oil production rates, and high water production rates. These practices generated recompletion candidates Y-30, J-15, and J-120.

Idle well Y-30 penetrates the Lower Terminal Zone of Fault Block IV and is set to be recompleted in the "AB", "AC", and "AD" sands. Studies showed that surrounding Lower Terminal Zone production wells produce with higher than field average oil cuts and with excellent productivity. Also, Y-30 penetrates the zone close to the Harbor Entrance Fault and could produce oil that might be banked under and against the fault. This fault structure is under further analysis with the 3-D geologic modeling software. Production

data for well Y-30 is not available since the well has not been recompleted.

Fault Block V recompletion candidate J-15 was generated from recent electric logs that passed through the Tar Zone and anomalous neighboring Tar Zone production wells. Penetrating logs over a 30-year period showed little change in the resistivities of the "F_1" and "F_o" sands of the Tar Zone despite heavy waterflooding. This well was recompleted with a novel steam consolidation technique discussed in the recompletion activity. It currently produces 87.8 m^3/d (552 b/d) gross, 7.3 m^3/d (46 b/d) net, for a 91.7% water cut with 455 m (1494') of fluid over the pump.

Fault Block V recompletion candidate J-120 was also generated from recent electric logs that passed through the Upper Terminal Zone. They showed the "Hxo" sand in this area of the Upper Terminal Zone has not been adequately drained. As little activity has taken place in this sand for the last 30 years it is likely to have bypassed oil. A review of all producers and injectors open to the "Hxo" sand revealed no injection and only a few old wells capable of producing from this sand. Further development of the bypassed reservoir was ideally suited for our geologic 3-D modeling. This prospective reservoir was not just a bypassed area in a known sand but a bypassed sand in a known reservoir.

● Deterministic 3-D Geologic Modeling

The majority of 3-D modeling took place on the "Hxo" sand of the Upper Terminal Zone in Fault Block V. A working deterministic 3-D geologic model was developed and scattered data for the "Hx_1", "Hxo", "Hx_2", and "Hx" sands were used to define model layers (Appendix 1). The model uncovered a flawed interpretation to the west of the Daisy Avenue Fault which defines the boundary between fault blocks V and VI. The 3-D geologic model pointed to a fault splay as a preferable interpretation supported by the distribution of scattered data from the four modeled layers. The fault splay interpretation is structurally consistent with other parts of the Wilmington Field.

Once the deterministic 3-D model was created, the next step was to model parameters within the layers. Oil saturation was modeled (Fig. 2) with initial oil saturation and current oil saturation maps created. Also, sand percentage and oil volumes were modeled and mapped. The oil volume mapping of the "Hxo" sand estimated original oil in place at 540,844 m^3 (3.4 million stock tank barrels) of which 445,401 m^3 (2.8 million stock tank barrels) is bypassed oil. Idle well J-120 was selected for recompletion in the "Hxo" sand based upon our geologic model and reservoir engineering work discussed earlier. The

well was producing 56.0 m^3/d (352 b/d) gross, 16.9 m^3/d (106 b/d) net, for a 69.9% water cut with 668 m (2190') of fluid over pump before sanding up. Well J-120 is scheduled for our novel steam consolidation process.

The geologic model was also used to develop our short-radius horizontal recompletion candidate. To plan a horizontal well properly, strict geologic control is required to keep the well in the target sand. The "Hxo" sand is only 4.6-6.1m (15'-20') in thickness so our margins of safety were quite small. Tidelands Oil has recent experience drilling horizontal wells and found that a 5-foot target window was attainable.

By investigating to the west of the original project area, we were able to determine that there is a stratigraphic change that is controlling the oil saturation. It was noticed early in the project life that the original oil saturation is lower to the west.

Logs from wells penetrating the area as far as 305m (1000') to the west were correlated and the model was expanded. It was found the targeted zone has decreased oil saturation, becomes thinner and shalier to the west. A facies boundary was drawn to make it clear the planned well course should not be drilled too far west. The Hxo layer was subdivided based on the bottom of the oil sand and the top of the highest resistivity streak seen in the logs. These horizons were included in the model as the HxoB (bottom of sand) and HxoJ layers. Cross sections and maps were created so the horizontal well could be planned.

Researchers were successful using the 3-D model for geosteering. The cross sections and maps were highly accurate providing for a successful project. We managed to split the distance the horizontal lateral was contained in the HxoJ and the sand lobe above. It should be noted that the HxoB and HxoJ layers were defined for this project only and do not reside in the permanent data base. The markers were identified on the electric logs and placed in the modeling software data base and then exported so they could be used to create the 3-D model.

The model was good for organizing so we could pinpoint problems that occurred at the rig site. One such problem was found when it was noticed that the Measurement While Drilling (MWD) values the directional engineer was plotting on his maps showed the well to be on course in the section view and was clearly low with respect to the well plan from our cross section. It turned out the directional vendor was not using the correct magnetic declination and they were using an inappropriate vertical section plane. They could not

correct the maps in time and we had to geosteer and control the directional entirely from our cross sections.

● Pulsed Acoustic Logging

Log data from recompletion candidates Z-223 and Z-27 were analyzed for useable acoustic data. Only a few short intervals were found to be useful. Researchers logged both wells with a nuclear device for comparative purposes and found reasonable agreement between acoustically derived results and nuclear derived results.

The ability to detect the formation shear wave has been greatly hampered by the strong presence of Stonely (tube) waves arriving simultaneously with formation signals. In modeling wave propagation in cased holes research suggested that good cement/casing bond can actually *degrade* low frequency waveforms in certain situations. Trapped energy is propagated more efficiently when cement/casing thickness is large and the formation is soft. This effect was realized in Wilmington Field logging runs where the initial acoustic tool design yielded better results due to its lack of energy output below 1 kHz. Neither standard casing bond logs nor specialty logs that measure the azimuthal variation of bond using acoustic techniques provided clear predictions of the quality of the multi-pole acoustic logs.

Cased hole shear wave logging in slope and basin clastic reservoirs like Wilmington is extremely difficult due to both wellbore conditions and the similarity of the dipole mode moveout and that of the Stonely (tube) wave. When a shear wave is recorded it is possible to discriminate between watered out and potentially productive zones.

● Recompletions

Conventional recompletions in the Wilmington Field have been done by perforating and gravel packing a slotted liner across the perforated interval for sand control. In some cases, recompletions using inner liners have exhibited unusually high initial decline rates. To offset this situation an optimized recompletion technique was developed. Two wells were recompleted with the optimized technique, wells Z-223 and Y-63.

Well Z-223 is a Fault Block V Upper Terminal Zone recompletion candidate that we

conventionally perforated across the "Hx", "J", "Z", and "W" sands with tubing conveyed guns. Perforations were 1.27 cm (0.5") in size, four holes per foot. A wire wrapped screen with 0.025 cm (0.010") mesh slots was gravel packed across the perforated interval with 30-40 gravel for sand control. The well was placed on production in December 1996 (Fig. 3) but appeared to be damaged despite our "optimized" recompletion. Well Z-223 was acid stimulated and returned to production. Production currently stands at 158.1 m^3/d (994 b/d) gross, 3.8 m^3/d (24 b/d) net, for a 97.6% water cut with 4.9 m (16') of fluid over the pump.

Although Z-223 is performing slightly better than the average Upper Terminal Zone well, production results thus far are disappointing.

Well Y-63 is a Fault Block IV Upper Terminal Zone recompletion candidate that we conventionally perforated across the "Hx", "J", "Y", and "K" sands with wireline conveyed guns. Perforations were 1.22 cm (0.48") in size, six holes per foot. A wire wrapped screen with 0.025 cm (0.010") mesh slots was gravel packed across the perforated interval with 30-40 gravel for sand control. The well was placed on production in December 1996 (Fig. 4). Production currently stands at 121.4 m^3/d (763 b/d) gross, 3.8 m^3 (124 b/d) net, for a 96.9% water cut with 15.2 m (50') of fluid over the pump. Production results are lower than estimated but the well may be cleaning up. Y-63 is performing better than offset wells in an area of the reservoir considered wet.

Two wells, J-120 and J-15, were recompleted with extreme overbalanced perforating, sand consolidated with one cycle of steam injection, and placed on production. The novel steam consolidation technique involves selectively perforating the target sands with one to four 0.635 cm (0.25") perforations per foot, placing the interval on steam injection until the total injected volume reaches 119.3 m^3 (750 bcwe) steam per perforation, and placing the well on production. This technique has been empirically developed. Lab studies are under way to replicate and comprehend the mechanisms involved.

Well J-120 is a Fault Block V Upper Terminal Zone recompletion candidate that we perforated across the "Hxo" sand with tubing conveyed guns and extreme overbalanced. Perforations were 1.22 cm (0.48") in size, 1.25 holes per foot. This well took 2,991 m^3 (18,800 barrels) of cold water equivalent steam injection for sand consolidation. J-120 was shut in for soaking in late August 1996 and placed on production in October 1996. Oil production peaked at 37.7 m^3/d (237 b/d) net with only a 32.3% water cut in early December 1996 (Fig. 5). Unfortunately, during an attempt to increase production, J-120 was brought on production at twice the planned gross production rate and sanded up

immediately. A review of the consolidation operation showed we did not reach the empirically derived steam volume of 119.3 m^3 (750 barrels) per perforation needed for full sand consolidation. Well J-120 is scheduled for a reconsolidation application with steam. Before sanding up in late January 1997, J-120 was producing 56.0 m^3/d (352 b/d) gross, 16.9 m^3 (106 b/d) net, for a 69.9% water cut with 668 m (2190') of fluid over the pump.

The average producer in the Upper Terminal Zone Fault Block V reservoir produces only 4.0 m^3/d (25 b/d) net with a 97.4% water cut. An encouraging sign is the production temperature of J-120 was almost back to a pre-steam temperature suggesting thermal benefits were neglible at the time of failure. We anticipated that when the well cooled off after producing back the injected heat the oil production might fall off quickly. This was not the case. Gross and net productivities were much higher with the steam recompletion technique compared with the "optimized" waterflood recompletion. With the 3-D geologic model as a tool, we are recompleting other candidate wells and further developing the "Hxo" reservoir.

Well J-15 is a Fault Block V Tar Zone recompletion candidate that we perforated across the "F_1" and "F_o" sands with tubing conveyed guns and extreme overbalanced. Perforations were 1.22 cm (0.48") in size, 1.25 holes per foot. This well took 14,762 m^3 (92,800 bcwe) steam for sand consolidation. J-15 was shut in for soaking in late August 1996 and placed on production in late October 1996. J-15 currently produces 87.8 m^3/d (552 b/d) gross, 7.3 m^3/d (46 b/d) net, for a 91.7% water cut with 455 m (1494') of fluid over the pump (Fig. 6). This production is much higher than the production from well A-173 which was recompleted using an "optimized" recompletion. Well A-173 is completed in the same sands as J-15 and currently produces 21.3 m^3/d (134 b/d) gross, 2.1 m^3/d (13 b/d) net, for a 90.3% water cut with 2.7 m (9') of fluid over the pump Figure 7. Production well Z1-7 was also completed in the same sands as wells J-15 and A-173, but with the older recompletion techniques. Well Z1-7 produces 11.8 m^3/d (74 b/d) gross, 1.4 m^3/d (9 b/d) net, for an 87.8% water cut with 0 m (0') of fluid over the pump, much lower than well J-15 and slightly lower than well A-173.

Due to the extremely successful production results from wells J-120 and J-15, Tidelands Oil is completing all future wells in a similar manner whenever possible. Recompletion candidate well Z-61 is a Tar Zone well similar to J-15. Both wells were recompleted in the "F_1" and "F_o" sands. Researchers tried to make the Z-61 recompletion more cost effective by wireline perforating instead of tubing conveyed perforating. The number of perforations per foot were also reduced as it seems productivity is not a problem with the steam consolidation technique. Z-61 will be under going steam consolidation with a portable steam generator. Permits have been applied for and the well is ready to take

steam.

The short radius horizontal redrill is another technique to recover bypassed oil and avoid the substantial production decline experienced in conventional Wilmington recompletions. This technique is very expensive compared to the optimized or steam consolidation recompletion and requires a thorough cost/benefit analysis. Well J-17 is a short radius horizontal well redrilled in the "Hxo" sand (Fig. 8) but not completed as of this report date. Production results should be available at future industry meetings and in our final DOE technical report.

Well J-17 was horizontally redrilled to the relatively thin (4.6m) "Hxo" sand using intermediate radius directional tools from a point approximately 61 vertical meters (200 vertical ft) above the target zone. The directional plan included building to 90 inclination and then turning the well 103 to the left while maintaining 90 of angle. This was accomplished using Logging While Drilling / Measurement While Drilling (LWD/MWD) tools and a production hoist with rental hydraulic sub-base, mud pump and mud pit.

We were able to use a different type of LWD and evaluate the advantages and disadvantages. The vendor we used utilized 'pulse' technology instead of a 'carrier wave' to transmit the LWD and MWD signals. We also elected to use a battery power source instead of the power turbine as we had used in the past.

The advantage of the battery power source was it provided continuous power to the telemetry system so the signals could be reliably transmitted to the surface. When used in the past, the turbine would not generate enough power when the bit drilled shale and the mud thickened causing a decrease in the RPM.

The downhole LWD recording device contained multiple resistivity equivalent curves. There were amplitude curves and phase curves at two different frequencies. Although for this project, the deep tools were not useful as the sands are thin and the deep reading measurements averaged the low resistivity shales. The disadvantages are two-fold. There was a 61 m/hr (200 ft/hr) limit on the drilling for both LWD and for down hole recording. We could have easily exceeded that and reached 183 m/hr (600 ft/hr) and successfully recorded data at the surface and down hole for previous projects. The second issue involved the resistivity curves displayed at the surface. The plan was to monitor the induction curve separation to place the well near the top of the sand. The 'pulse' technology only allows two curves of information when in rotating mode and not in the

correctional or 'sliding' mode. When sliding the limited information carried on the pulse is prioritized so the tool face is continuously output sacrificing one of the LWD resistivity curves. The higher technology of the carrier wave is the preferred method if resistivity curve separation is being used for geosteering. If the 'pulse' technology is used more emphasis needs to be placed on the geological modeling for geosteering.

Also, the directional proposal was too severe to be consistently and efficiently executed as planned on the first attempt. The 244m (800') of drilling only in the oriented mode at high dogleg rates required numerous conditioning runs using a bullnose hole-opener and three point reamer plus mud lubricants to allow the tools to slide. An attempt to run a smaller dogleg directional assembly without a conditioning run resulted in unintentionally sidetracking the hole while spudding and reaming to bottom.

A performance based contract for the directional services is needed to insure that the directional contractor is fully focused on the project. The directional and logging while drilling services are by far the most expensive aspect of drilling such a well. Errors or omissions by the directional contractor that prolong the job should not be rewarded.

A production hoist has sufficient pulling capacity to redrill most wells in the Wilmington Field. In conjunction with a rental hydraulically powered sub-base, it was possible to perform the necessary drilling and tool handling functions. However, make-up and break-out of HWDP, drill collars and directional tools were slow and time consuming. Due to the small amount of drop available from the pitcher nipple to the shale shaker, a larger than normal pitcher and flowline are required to avoid flow over the top of the pitcher nipple.

Correct cement volumes and displacements are required for a good primary cement job on the liner. A slight amount of washout results in a significant percentage of excess cement required to fully cement the liner. There is no caliper log with the LWD tools as is normally used to determine the correct cement volume. Pumping a tracer or dyed fluid while on bottom prior to pulling out to run the liner could be used to determine the total hole volume, from which the liner annulus volume could be calculated.

As of March 1997, researchers have recompleted five (5) wells which have produced a total of 4,776 m^3 (30,024 bbls) of stock tank oil. Individual cumulative oil production is as follows:

J-7	3,361	bbls
J-15	7,277	bbls
J-120	14,995	bbls
Y-63	2,118	bbls
Z-223	2,283	bbls
Total:	30,024	bbls

● Technology Transfer

Tech transfer has taken place throughout the course of the project. Technical papers and presentation have been given at local, regional, and national meetings of professional societies such as the Society of Petroleum Engineers (SPE), American Association of Petroleum Geologists (AAPG), Society of Professional Well Log Analysts (SPWLA), Society of Exploration Geophysics (SEG), American Geophysical Union (AGU), and Petroleum Technology Transfer Council (PTTC).

Activities during the project year include the following:

Researchers made a presentation on the acoustic tool performance in both cased hole and open hole at the "Dipole Sonic Symposium" organized by the Society of Exploration Geophysicists in Tulsa, OK, in April, 1996.

A field trip to the Wilmington Field for the American Association of Petroleum Geologists (AAPG) in association with the 1996 national meeting in San Diego, May 18, 1996.

An article was also be placed in the AAPG guidebook for the national meeting from Moos, Walker, Clarke: "Sonic Logging to Detect Bypassed Hydrocarbons in the Wilmington Field, CA." May 18, 1996. (Appendix 2)

Researchers presented a paper at the AAPG national meeting in San Diego: Moos, Hooks, Walker: "Acoustic Logging Through Casing to Detect Hydrocarbons and Determine Porosity in the Wilmington Field, CA" May 21, 1996.

Researchers planned the Stanford Rock and Borehole Geophysics Project Annual Meeting June 19-21, 1996. Papers written and presented included:

Chang, Zoback, Moos: "Viscoelasticity and Dispersion in Unconsolidated Reservoir Rocks from the Wilmington Field, California". (Appendix 3)

Chang, Zoback, Moos: "A Comparison of Dynamic and Static Moduli in Unconsolidated Reservoir Rocks from the Wilmington Field, California". (Appendix 4)

Moos, Hooks, Walker: "Hydrocarbon Saturation Determination from Sonic Log Data". (Appendix 5)

Dvorkin et al: "Identifying Patchy Saturation from Well Logs". (Appendix 6)

Researchers presented a paper to the Geophysical Research Letters titled: "Application of theoretically derived rock physic relationships for clastic rocks to log data from the Wilmington Field, CA". (Appendix 7)

Researchers participated in the Ocean Drilling Program Downhole Measurements Panel Meeting in Salt Lake City, Utah. DOE results were disseminated to other attendees.

Researchers made a presentation in September, 1996 on the Waterflood Project status to the Department of Energy (DOE), California Department of Oil and Gas (CDOG), California State Lands Commission, along with representatives from state and federal government in Long Beach, CA.

Researchers attended the Society of Professional Well Log Analysts (SPWLA) Symposium on "Petrophysics in 3-D" in Taos, New Mexico in October, 1996.

Amoco visited Stanford University and discussed a collaborative effort on analyzing dipole data.

Researchers presented papers at the November, 1996 Society of Exploration Geophysics (SEG) Annual Meeting in Denver, CO. Also at the meeting, researchers held a workshop on problems associated with data acquisition of dipole and monopole data at Wilmington in conjunction with the Shear-Wave Special Interest Group of the Log

Characterization Consortium.

Researchers made three presentations in November, 1996 on the Waterflood Project status to the Petroleum Technology Transfer Council (PTTC) meetings held in Bakersfield, Ventura, and Long Beach, CA. Researchers also hosted a "point-counterpoint" discussion on oil detection behind pipe.

Clarke, D., City of Long Beach: Oral presentation on "New Ways To Do Geology", PTTC Workshop on California Geology With and Without Computer Graphics, USC campus, Los Angeles, CA, 15 Jan 1997.

Phillips, C.,Tidelands Oil Production Company, Clarke, D., City of Long Beach, An, L., University of Southern California: Oral presentation on "Case Histories - DOE Supported Projects, Thermal Flood, Tar Zone, Wilmington Oil Field", PTTC Workshop on California Geology With and Without Computer Graphics, USC campus, Los Angeles, CA, 15 Jan 1997

Tidelands Oil Production Company: Discussed novel sand consolidation well completion technique developed through DOE project with John Horstkoetter, Mark Vandergon, and William Grames of BP Exploration (Alaska) Inc., Jim Spearman of BJ Services Company, and Dave Dillon of Centrilift Pumps, Inc., meeting in Long Beach, CA, 13 February 1997.

Researchers submitted a paper to the June, 1997 International Rock Mechanics Meeting titled: "Anelasticity and Dispersion in Dry Unconsolidated Sands", Chang, Moos and Zoback. (Appendix 8)

Researchers submitted a paper to the June, 1997 SPE Western Regional Meeting titled: "Locating and Producing Bypassed Oil: A D.O.E. Project Update. (Appendix 9)

Researchers submitted a paper to the 1997 American Association of Petroleum Geologists Meeting titled: "Fluid Detection and Porosity Determination using Acoustic Logs in the Wilmington Field, CA".

Researchers updated the project's World Wide Web homepage at http://pangea.stanford.edu/~moos/DOE_home.html (Appendix 10)

Tidelands Oil and USC have developed a CD-ROM multimedia presentation on the history of this project and our mid-term project. This historical record will be updated periodically and available to other operators and the public in general. Periodically, CD's would be produced and distributed to other organizations as part of our continued technical transfer commitment. (Appendix 11 CD-ROM included)

References

1. D. Moos, J. Dvorkin, A. Hooks, *Application of Theoretically Derived Rock Physics Relationships for Clastic Rocks to Log Data - Example from the Wilmington Field, CA*, paper prepared for special issue of Geophysical Research Letters on Core/Log/Seismic Integration, January 1996.

2. D. Williams, *The Acoustic Log Hydrocarbon Indicator,* paper W for Society of Professional Well Log Analysts 31st Annual Logging Symposium, June 1990.

3. D. Moos, S. Hara, C. Phillips, A. Hooks, K. Tagbor, *Field Test of Acoustic Logs for Measuring Porosity and Oil Saturation in a Mature Waterflood in the Wilmington Field, CA*, paper SPE 29655 presented at the Society of Petroleum Engineers Western Regional Meeting, Bakersfield, CA, March 1995.

Results - ALHI at Wilmington

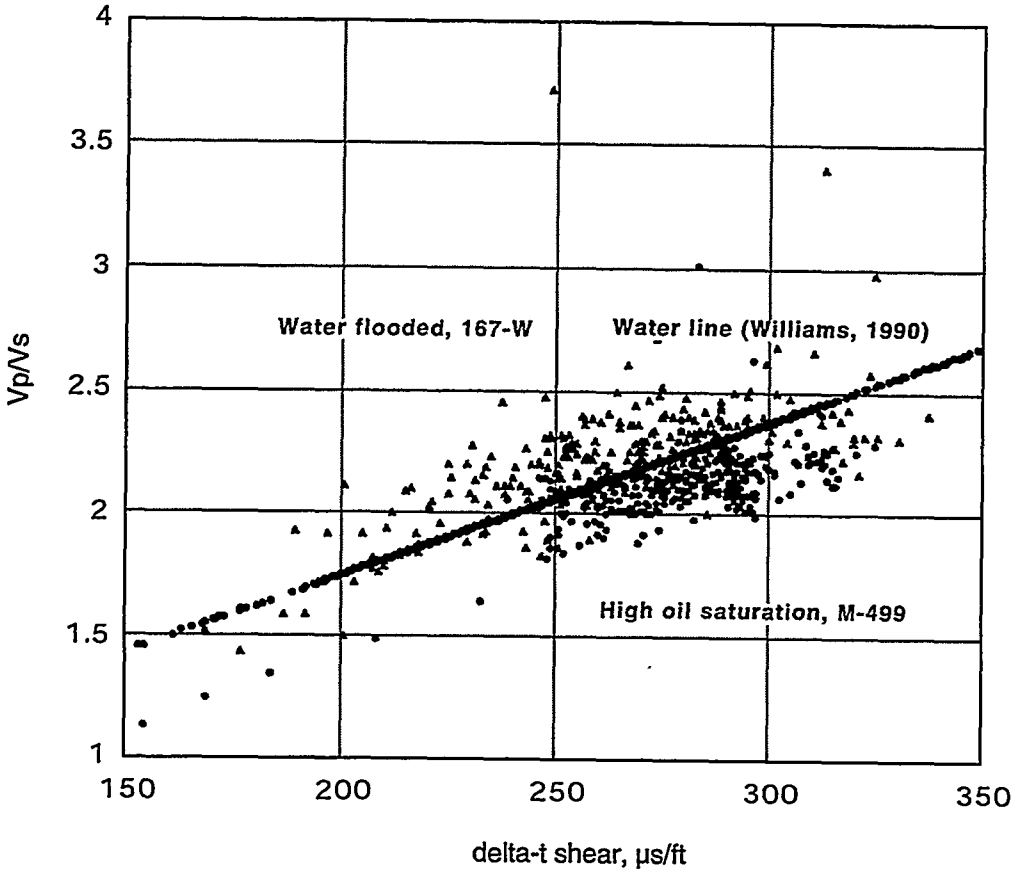

Based on theory and empirical results of Williams (1990), sands with high oil saturation should plot below the "ALHI water line", and sands with high water saturations should plot at or above the line. Data from Wilmington show this trend, with waterflooded sands above the line (red) and oil-bearing sands below the line (green).

FIGURE 1

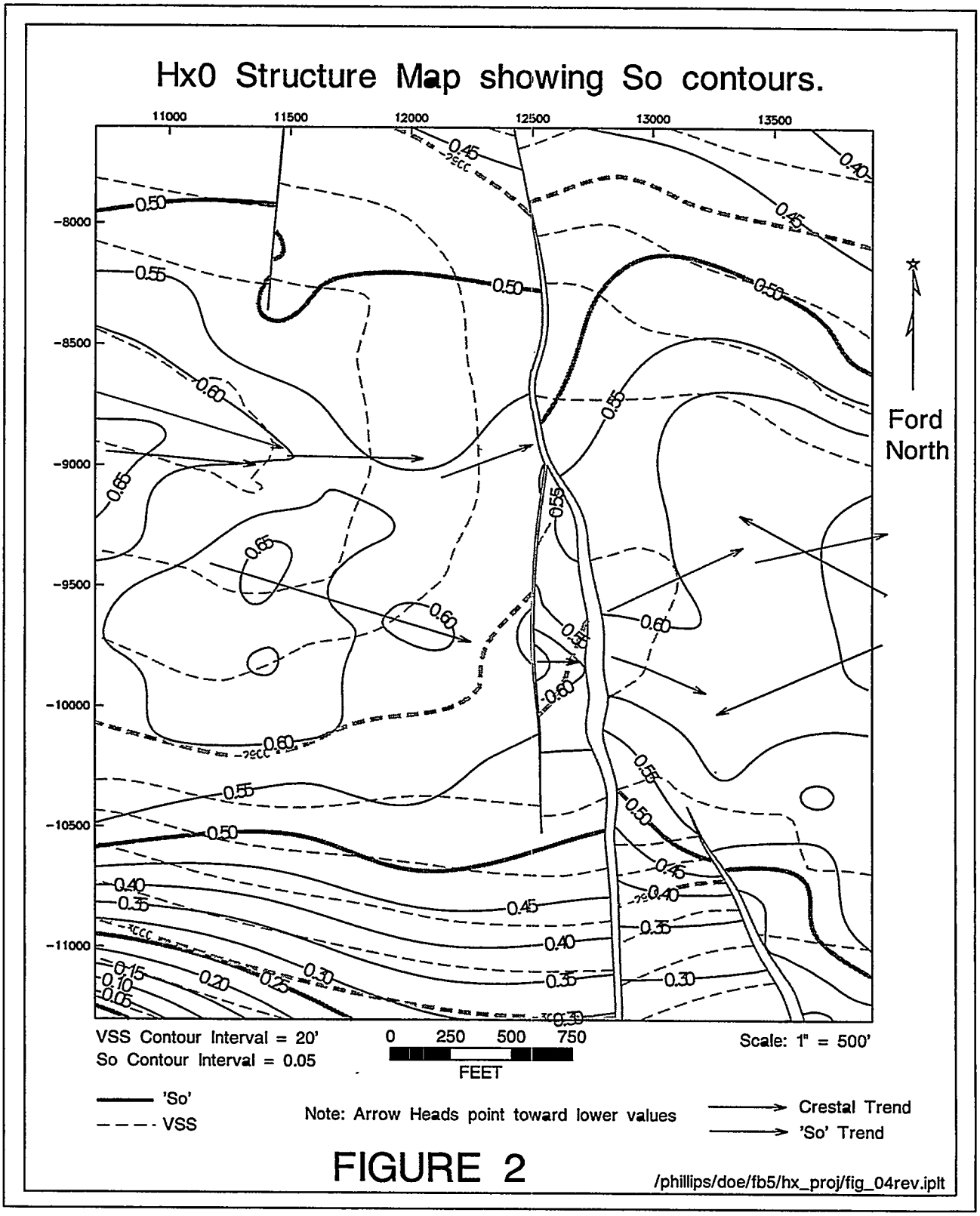
Hx0 Structure Map showing So contours.
11000
11500
12000
12500
13000
13500
-8000
-8500
-9000
-9500
-10000
-10500
-11000
Ford
North
VSS Contour Interval = 20'
So Contour Interval = 0.05
0 250 500 750
FEET
Scale: 1" = 500'
'So'
VSS
Note: Arrow Heads point toward lower values
Crestal Trend
'So' Trend
/phillips/doe/fb5/hx_proj/fig_04rev.iplt

FIGURE 2

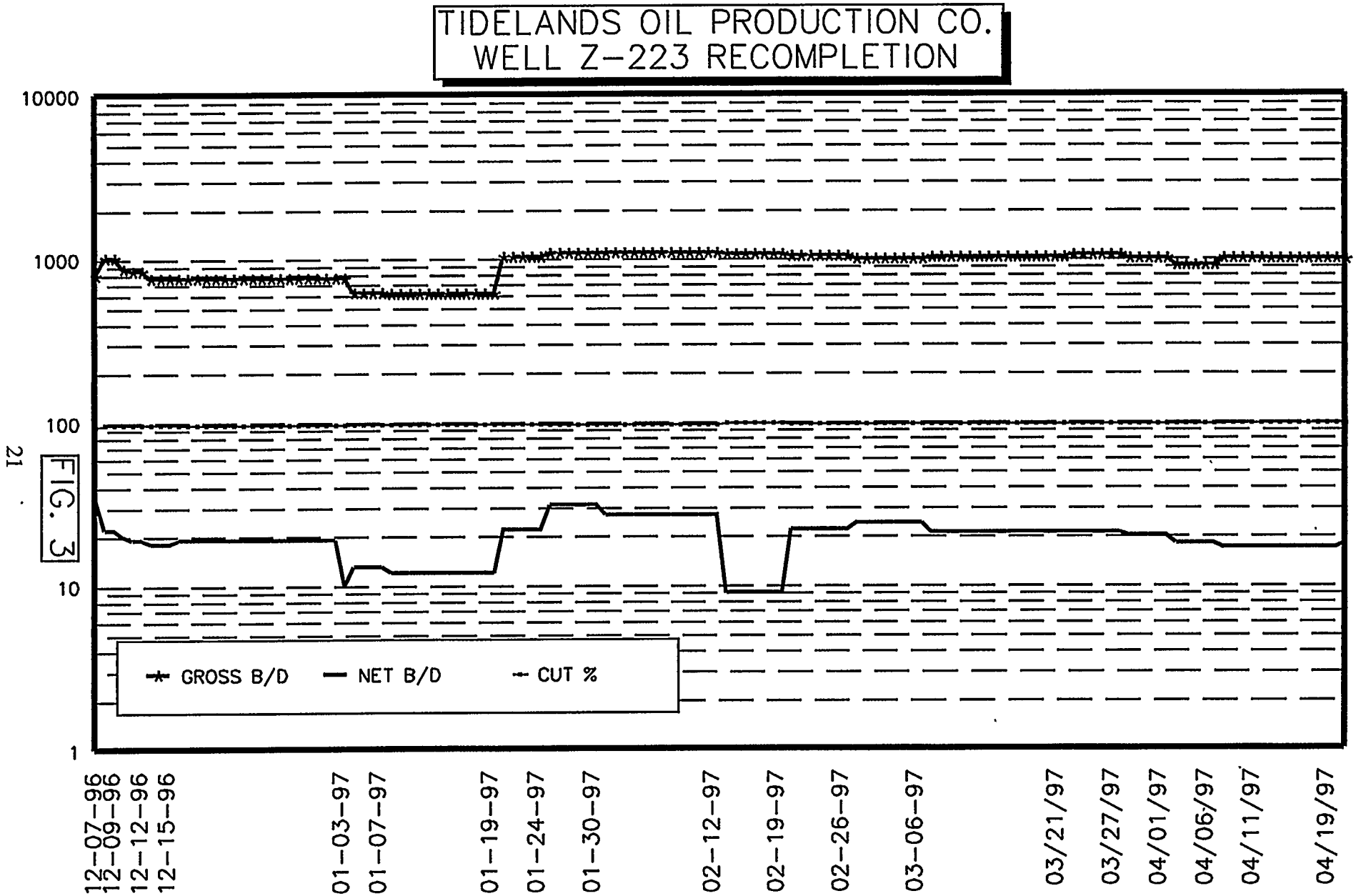
TIDELANDS OIL PRODUCTION CO.
WELL Z-223 RECOMPLETION
10000
1000
100
10
1
GROSS B/D
NET B/D
CUT %
12-07-96
12-09-96
12-12-96
12-15-96
01-03-97
01-07-97
01-19-97
01-24-97
01-30-97
02-12-97
02-19-97
02-26-97
03-06-97
03/21/97
03/27/97
04/01/97
04/06/97
04/11/97
04/19/97

FIG. 3

TIDELANDS OIL PRODUCTION CO.
WELL Y-063 RECOMPLETION
1000
100
10
GROSS B/D
NET B/D
CUT %
12-23-96
12-25-96
01-12-97
01-20-97
02-20-97
03/21/97
03/25/97
03/30/97
04/06/97
04/12/97

FIG. 4

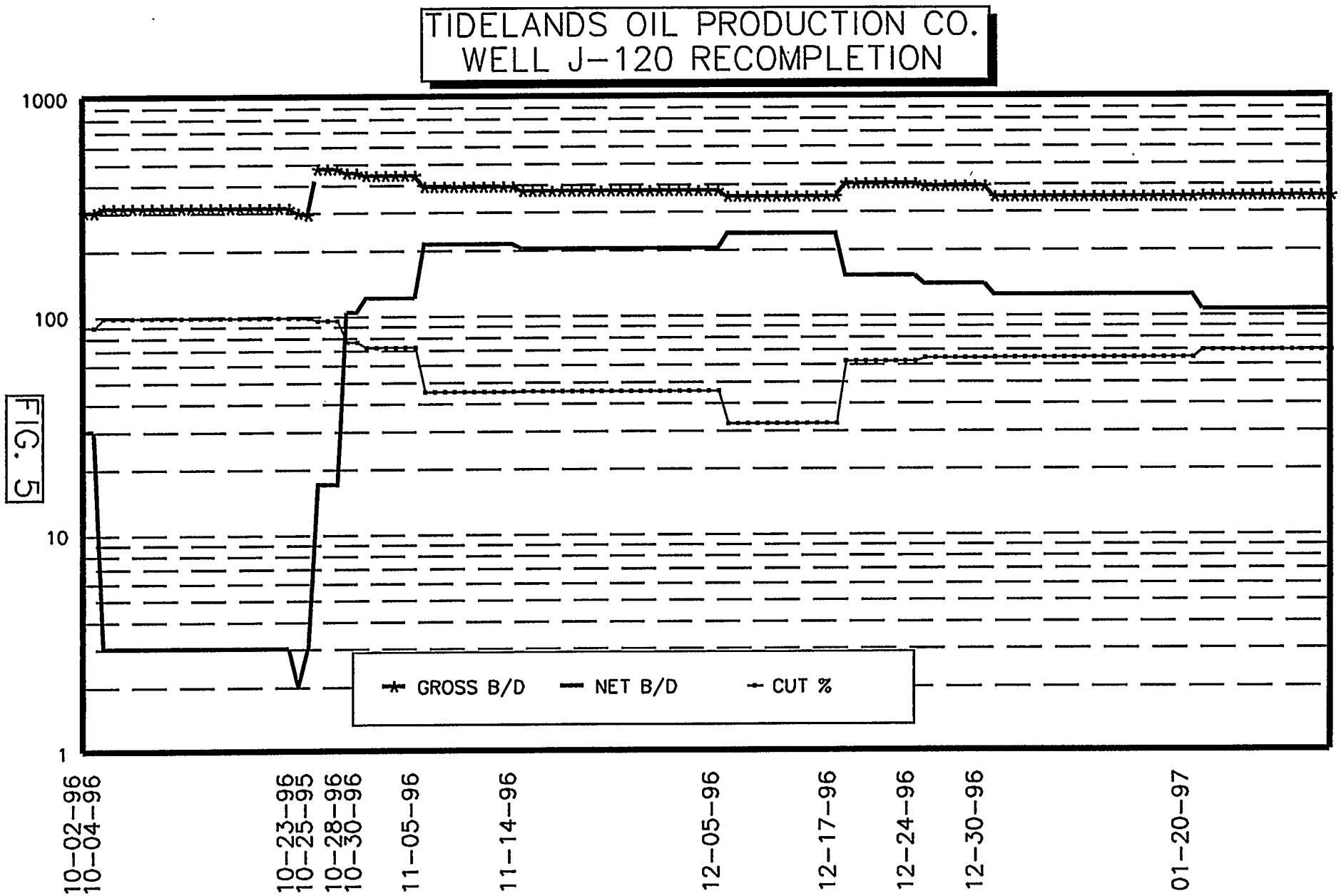
TIDELANDS OIL PRODUCTION CO.
WELL J-120 RECOMPLETION
1000
100
10
1
GROSS B/D
NET B/D
CUT %
10-02-96
10-04-96
10-23-96
10-25-95
10-28-96
10-30-96
11-05-96
11-14-96
12-05-96
12-17-96
12-24-96
12-30-96
01-20-97

FIG. 5

TIDELANDS OIL PRODUCTION CO.
WELL J-015 RECOMPLETION
1000
100
10
1
10-31-96
11-06-96
11-13-96
11-19-96
12-20-96
12-18-96
01-02-97
12-31-96
01-09-97
01-07-97
01-17-97
01-22-97
01-30-97
02-03-97
02-19-97
03-04-97
03/21/97
04/01/97
04/08/97
04/10/97
04/16/97
* GROSS B/D
— NET B/D
+ CUT %

FIG. 6

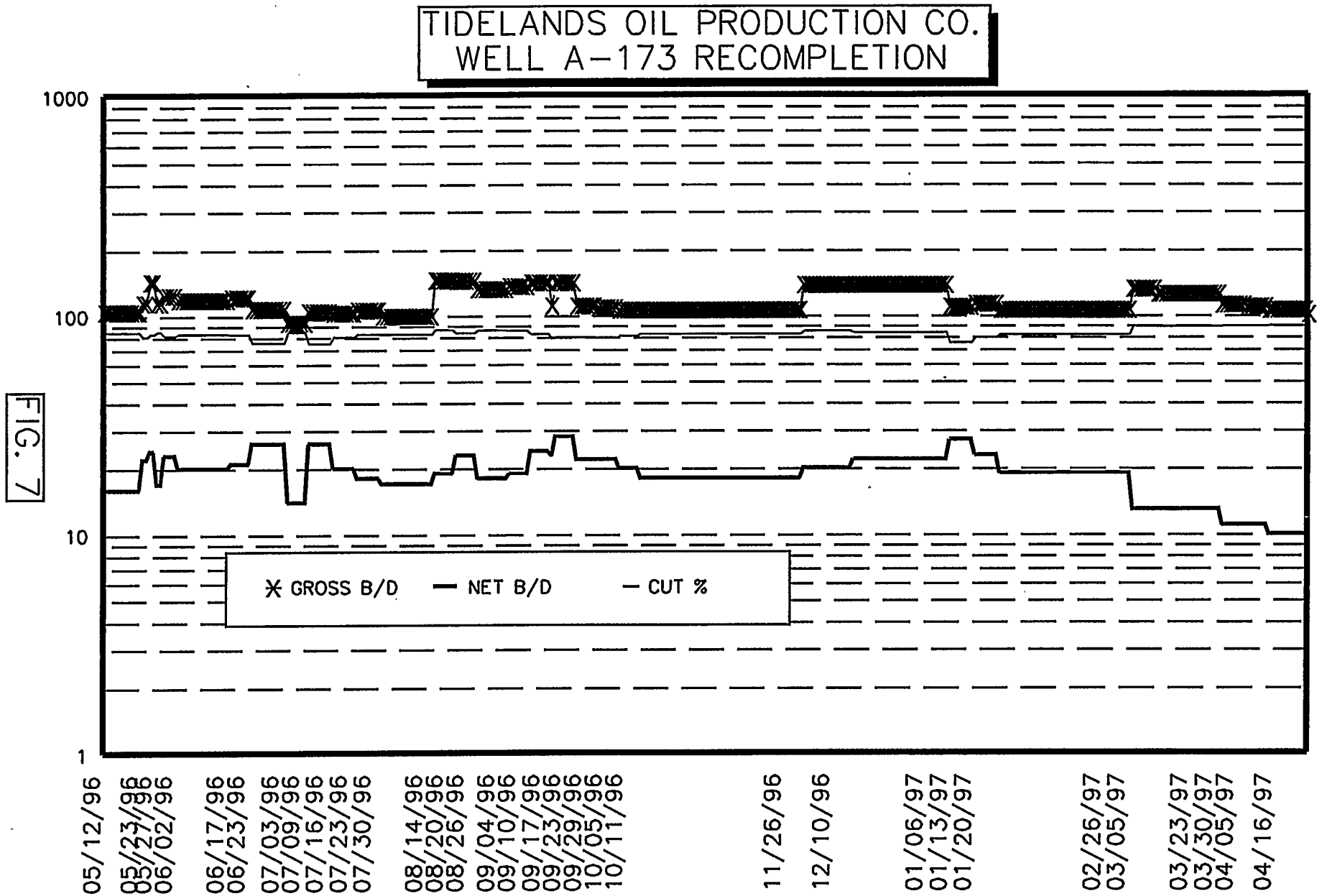
TIDELANDS OIL PRODUCTION CO.
WELL A-173 RECOMPLETION
1000
100
10
1
GROSS B/D
NET B/D
CUT %
05/12/96
05/23/96
06/02/96
06/17/96
06/23/96
07/03/96
07/09/96
07/16/96
07/23/96
07/30/96
08/14/96
08/20/96
08/26/96
09/04/96
09/10/96
09/17/96
09/23/96
09/29/96
10/05/96
10/11/96
11/26/96
12/10/96
01/06/97
01/13/97
01/20/97
02/26/97
03/05/97
03/23/97
03/30/97
04/05/97
04/16/97

FIG. 7

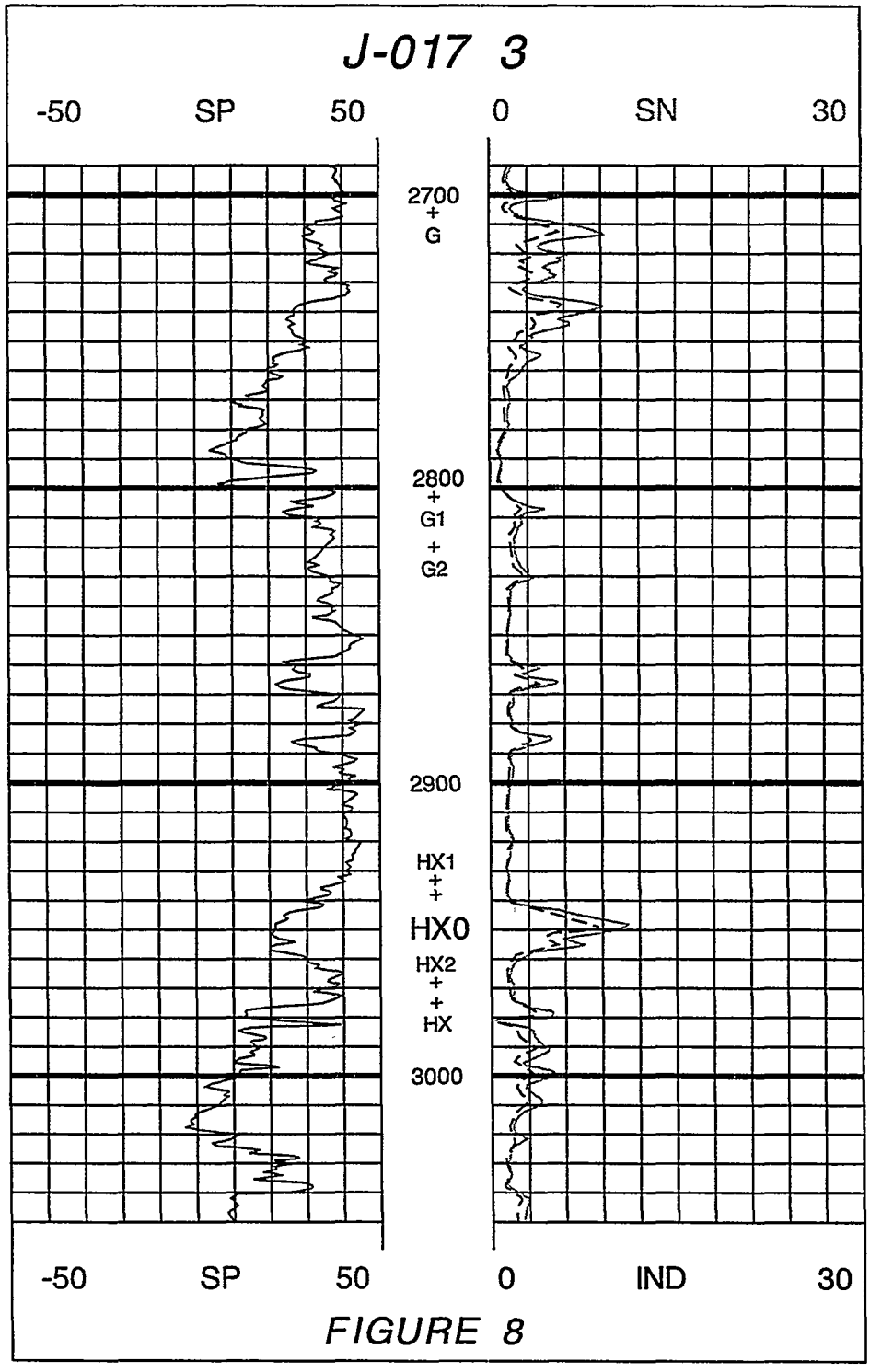
J-017 3
-50
SP
50
0
SN
30
2700
+
G
2800
+
G1
+
G2
2900
HX1
+
+
HX0
HX2
+
+
HX
3000
-50
SP
50
0
IND
30

FIGURE 8

Appendix #1

GEOLOGICAL REVIEW OF HX0 SANDS

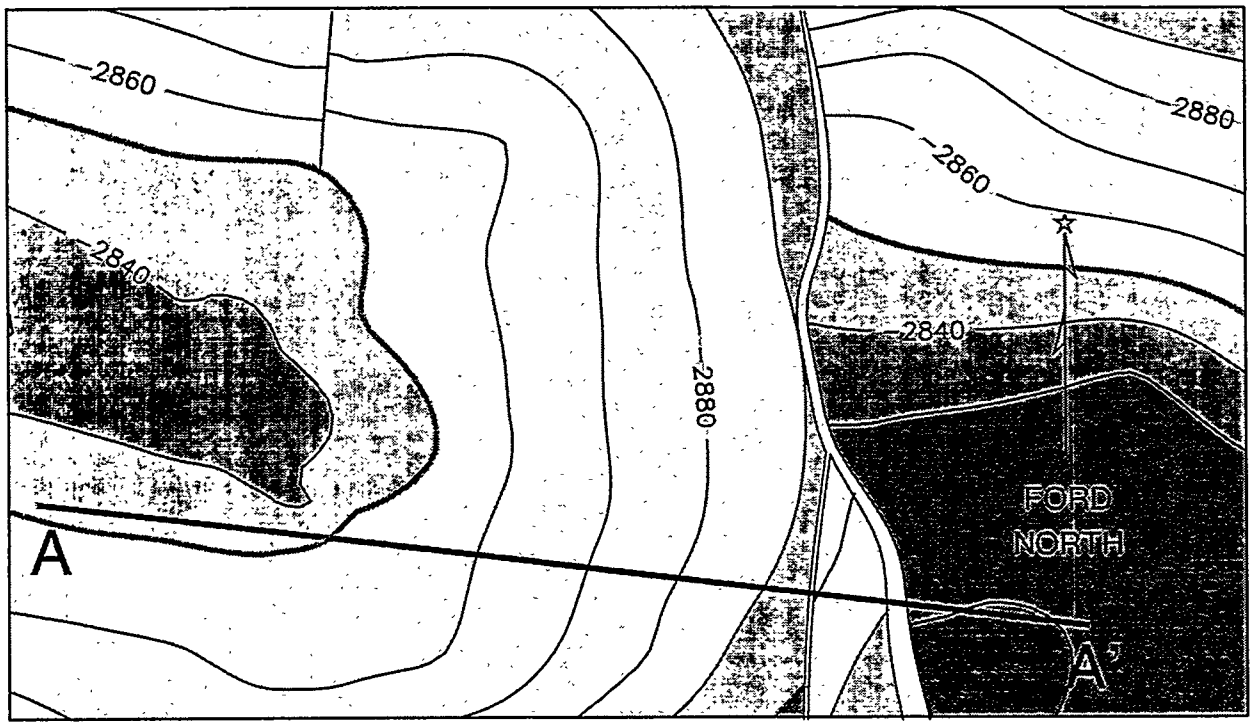

0 250 500
FEET

TIDELANDS
OIL PRODUCTION COMPANY
LONG BEACH, CALIFORNIA

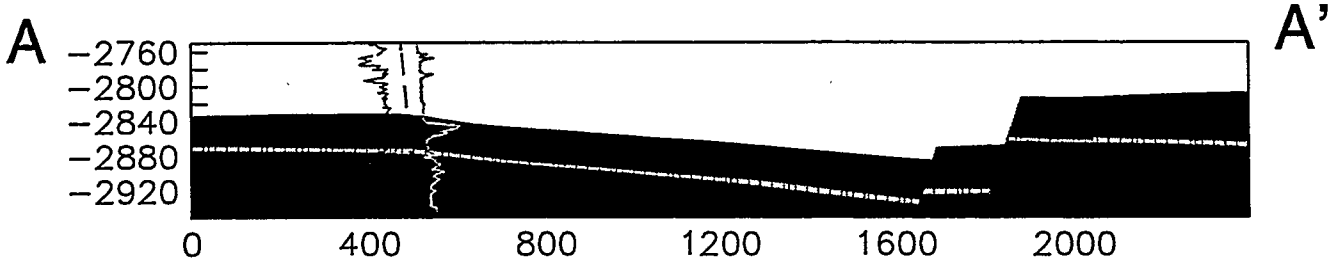

TIDELANDS OIL PRODUCTION COMPANY

GEOLOGICAL REVIEW OF HX0 SANDS

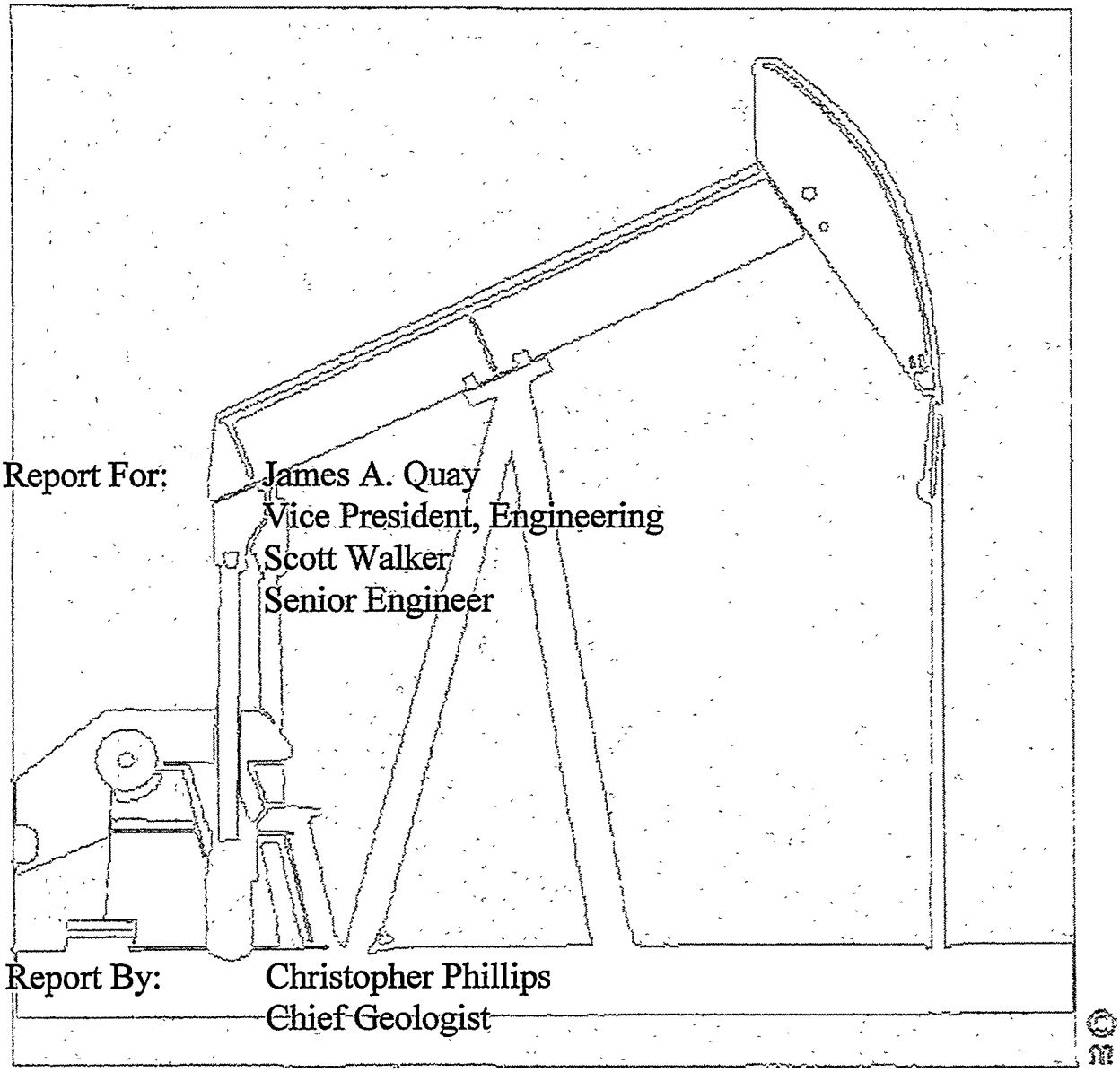

Report For: James A. Quay
Vice President, Engineering
Scott Walker
Senior Engineer

Report By: Christopher Phillips
Chief Geologist

DATE: October 30, 1996

PURPOSE OF THIS REPORT

The purpose of this report is to organize and model the existing geological data for a selected area of the Hx0 sand in Fault Blocks 5 and 6 of the Wilmington Oil Field, California. The study is part of a United States Department of Energy (DOE) cost share research development and demonstration project to increase reserves using advanced reservoir characterization techniques. Included in this report are examples of the utility and capabilities of the geological modeling software used for the three dimensional reservoir characterization and volumetric calculations.

TABLE OF CONTENTS

LIST OF FIGURES

LIST OF TABLES

INTRODUCTION

The Hx0 sands of Fault Blocks 5 and 6 were reviewed as part of the Department of Energy (DOE) short term project. Increasing Waterflood Reserves in the Wilmington Field through Improved Reservoir Management, proposed using new reservoir characterization tools to locate bypassed oil. The EarthVision™ software and the Silicon Graphics (SGI™) workstation were the primary reservoir modeling tools used. Scott Walker determined that the Hx0 sand was not fully exploited and requested a study to organize the existing available geological data. It should be noted that Scott selected Well J-120 as the first test well. Well J-120 is shown on all the 'block diagrams' for reference. The following tasks were assigned:

Scott Walker:

- Select a well to test effectiveness of thermal stimulation, sand consolidation and productivity of Hx0 sand.

Chris Phillips:

- Cull NEWILMA database for existing non-abandoned wells to assist in finding potential recompletion wells. Select all penetrating wells in defined area for Hx0 identification. Create initial maps to organize data.

- Define fault planes in area of study, create deterministic 3-D geological model. Expand model as necessary for accurate depiction of geological features. Define oil-water limits within the modeled area.

- Research methods and determine variables for qualitative oil saturation. Model qualitative oil saturation and percent sand as parameters within the Hx0 layer of the 3-D model.

- Determine volumes of original oil saturated sands and estimate current oil saturation based on review of newer logs.

- Create appropriate figures and write report.

Mike Henry:

- Review logs in area. Sub-sub zone the oil sands immediately above the Hx marker. Quality control sand tops for input into database (original defined area). Count net sand thickness.

Results:

EarthVision™ was used to create a deterministic 3-D geological model. After the stratigraphy was defined, the scattered data for the Hx1, Hx0, Hx2 and Hx sands were used to define the model layers (Figures 1 & 2). The model area was expanded so the horizon surfaces on the east side of the Daisy Avenue faults could be more accurately represented. Figure 3 shows the color contoured structure map on top of the Hx0 horizon. The grid for this map was pulled directly from the 3-D model. The structural highs were determined from the grid and are noted by the red arrows (arrow heads point toward anticlinal plunge). In addition, structural control points were added in areas of little or no data (red dots). A composite of the Hx0 structure map and an initial oil saturation (Soi) contour map is shown in Figure 4. The high saturation trends are noted with blue arrows and they point toward lower saturation. The arrow tails suggest higher saturation to both the east and west of the modeled area.

The 3-D model initially showed discrepancies to the west of the Daisy Avenue fault. A fault splay is proposed and is evident by the distribution of the scattered data for the four horizons studied. None of the wells showed missing section within the Hx0 interval, so the fault definition was estimated. The fault splay could also be a slump block. Both slump blocks and fault splays are structurally consistent with other parts of the field. The proposed fault is included in the model and provides good consistency for all the layers. The data show a vertical offset of approximately 15' in the faulted area.

Once the deterministic 3-D geological model was created, it became possible to model parameters within the layers. The Hx0 layer is the primary focus and Figure 5 shows a qualitative initial oil saturation model. Figure 5 shows that the two newer wells in Fault Block 6 have current oil saturation (Soc) values of only 0.14 and 0.36 within an area defined by Soi at least equal to 0.6. This indicates that the oil was successfully produced from the Hx0 sand. Sand percentage was also modeled (Figure 6). The x, y, z location for the data points were the same as the 'Soi' model but the percent sand was used as the modeling parameter. The 3-D grids created for the percent sand model are necessary for the volumetric calculations.

Oil in place calculations were restricted to that volume west of the Daisy Avenue Fault (Fault Block 5). Fault Block 6 was not considered because the newer wells to the east of the Daisy Avenue Fault show lower oil saturations. The 'original' estimated oil volume of the remaining Fault sub-blocks is approximately 3.4 million stock tank barrels (STB - see details on page 5, Table A). This estimated value should be reduced based on the difference between the 1980's well saturation and the gridded values. It can be seen from Figure 5 that this difference is about 0.065. The Soi data were reduced by subtracting 0.065, the "new" wells were included in the data set and the Soc was then modeled (Figure 7). The adjusted volume for the modeled portion of Fault Block 5 is then approximately 2.8 million STB (see details on page 6, Table B). Recovery factor is not included. Subsidence was also not considered and is not believed to be a significant factor.

As an example of the functionality of the EarthVision™ software, it is possible to determine a volume based on oil saturation limits. In the past, 40% oil saturation was used as a cutoff based on the Allen (Earlougher, 1972) chart which indicates the Upper and Lower Terminal zones are flooded out below Soc = 0.40. Although Fault Block 6 clearly shows water flood residual oil saturations between 0.14 and 0.36, this is just an example. Figure 8 is a 3-D rendering of the Fault Block 5, Hx0 sand where Soi >= 0.40. The oil volume was calculated to be 3 million STB (for details see page 6, Table C). Figure 9 is the 3-D visualization where the Soc >= 0.40 and the volume was calculated to be 2.3 million STB (for details see page 7, Table D).

Well J-120 was selected to test the effectiveness of the thermal stimulation and productivity of the Hx0 sand. As of the date of this report, the average of the last two production tests indicate the well is producing 446 bbls/day gross fluid, 112 bbl/day net oil (75% water cut) with 2279' of fluid over the pump.

Recommendations:

The model should be expanded east and west beyond where the oil saturation in the Hx0 falls below economic limits to establish the volume of recoverable oil. If through casing reservoir evaluation logs are run in other wells in Fault Block 5, they should be extended to include logging the Hx0 sand to determine saturation and porosity.

Investigate economics for drilling horizontal steam injector(s) along the crest of the anticline and horizontal steam producer(s) approximately 500' down dip along the crest of the oil saturation. If the economics are favorable, calculate reserves for the 'box' defined by the drainage areas of the proposed horizontal wells to determine viability of a horizontal well project.

Methodology:

The initial area was defined by Scott Walker and then expanded by Chris Phillips as follows (Ford Coordinates):

	Initial Area	Expanded Area
X	10,700 to 12,950	10,700 to 13,900
Y	-7,600 to -11,300	-7,600 to -11,300

Mike Henry reviewed those wells that have Hx picks in the initial area. He noted that there was saturation in three sand units above the Hx sand. He defined those as the Hx1, Hx0 and Hx2. Mike then correlated all the logs and determined the location and sand count for those sands. He also correlated the Hx marker (Typical log shown in Figure 10).

For modeling purposes and to better see trends, the model (Figures 1 & 2) was expanded to the East. The four markers were correlated and the sands counted. Rudy Payan was responsible for entering the data into the NEWILMA database (See Table 1 for data).

Since there are no porosity log suites in the modeled area, the porosity was established by using Fault Block 5 Well FZ1-062 neutron-density logs (drilled 1993, 800' from south-west model boundary). The neutron porosity for the Hx0 sand is 33.5% and the density porosity is 31.5% (Figure 11). The estimated porosity used in all the calculations for the Hx0 sand is 32 percent. The 32% porosity agrees well with the 1978 Williams Brothers Engineering report for well FT-1 (Report to Department of Oil Properties from Godsey-Earlougher Division comparing E-log and core). The report states that the Hxa porosity for 14 samples compacted to 2000 psi was found to be 33 percent. In addition the average compensated density porosity for those Hxa samples was found to be 33.2 percent. The Hxa sand (below Hx2) porosity should be higher as indicated by the SP, gamma ray and porosity logs (Figures 10 & 11). In addition, Well Z-223 (approximately 2300' to the west) recently had a Schlumberger RST™ log run and the porosity was calculated to be 29%.

Selected electric logs, predominantly SP and induction, from wells drilled between 1949 and 1966 were used to determine the "original" oil saturation. A simple Archie relationship was used because there were not enough clay data to determine the bound water correction for a dual-water model calculation. The logs were reviewed and the Hx0 sand showed two lobes consistently with differing resistivities. Either sand could show higher resistivity. The short normal was used for bed boundary definition and the deep tool used to define the measured resistivity. An average resistivity (Rt) was determined and the Archie formula was used to determine oil saturation. The values determined were as follows:

Est. Rw f/ Z-223 study:	0.21
Porosity f/ FZ1-062:	0.32
Resistivity of wet sand:	1.23
F Factor (0.81/phi^2):	7.91
R0 (F * Rw):	1.66
So (1 - Sw):	1 - Sqrt(R0/Rt)

It should be noted that logs as old as 1944 were reviewed but not used in the calculation of So. This is because the induction log was not developed until 1947 (Schlumberger, 1986) and was not used widely on the west coast until 1949 (pers. comm. Terry Woods, Schlumberger). As a test, two contour maps were made, one including the older data and one without. The 'So' map with the post 1949 data was more consistent.

A contour map was created by gridding the initial oil saturation (Soi). This was overlaid on the Hx0 structure contour map and the high saturation trends noted with blue arrows (Figure 4). The Blue arrows point toward lower saturation. It should be noted that the arrow heads are pointing inward toward the center of the model. This suggests a review of the wells outside the model range is necessary to determine additional reserves. The 'Soi' map was created using the Hx0 coordinate (x, y) instead of a point in space between the Hx0 and Hx2 sands as was the case for the property models subsequently created.

The EarthVision™ formula processor was used to locate a point (Z) halfway between the top of the Hx0 sand and the top of the Hx2 sand by back interpolating the X, Y location of the Hx0 scattered data onto the Hx2 horizon to determine the Hx2(z). The 'Z' location was determined by finding the average of the difference between Hx2(z) and Hx0(z) and then summing with Hx0(z). These calculated 'Z' values were then assigned corresponding 'Soi' values and modeled in 3-D (Figure 5). The tops of the Hx0 and Hx2 horizons and the Fault planes were used for boundary conditions.

The percent sand is calculated by the NEWILMA database application from sand counts extracted from the electric logs. The calculation method is to determine the difference in the measured depths for the Hx0 and next marker (Hx2) and then dividing into the footage reported as the sand count. This value was assigned to the 'Z' location determined above and modeled as a parameter within the Hx0 layer (Figure 6). The three variables for finding the volume of oil are then defined; porosity of sand, oil saturation and sand percentage. The steps to achieve this goal using EarthVision™ are are shown on page 8. The Bulk Volume is determined and then 'reduced' to find the Fluid Volume. The area of interest is shown in Figure 7. The Fault sub-blocks are depicted on Figure 8. A summary is shown below.

The estimated Original Oil in Place of the Hx0 sand based on log analysis (logs dated between 1949 and 1966) is as follows:

TABLE A

Fault Block (Sub-Block)	Area (sq. ft.)	Volume (cf)	Res. Bbls (vol/5.61)	STB (res/1.06)
FB5B1	4,654,813	14,052,644	2,504,928	2,363,139
FBA2	505,730	1,664,688	296,736	279,939
FB5B	2,084,554	4,455,649	794,233	749,277
		20,172,981	3,595,897	3,392,355

The last step was to attempt to find the existing oil saturation based on the newer electrical logs. Figure 5 shows that the modeled oil saturation is approximately 0.065 higher than the newer wells shown in the vicinity of Well J-120 2. The data were modified by subtracting 0.065 from the oil saturation of the older wells and the newer wells* were included in the data set. The revised model is shown in Figure 7. Comparing Figures 5 and 7 it appears the colors of the areas have shifted down on the color key. This color shift is the visual cue that the saturation numbers are lower in Figure 7 than in Figure 5. Volumetrics were calculated and are shown below (no recovery factors included).

The estimated Current Oil in Place of the Hx0 sand after modifying the data for resistivity decrease observed in the newer logs and adding data from the newer logs to the data set is given below.

TABLE B

Fault Block (Sub-Block)	Area (sq. ft.)	Volume (cf)	Res. Bbls (vol/5.61)	STB (res/1.06)
FB5B1	4,654,813	11,788,707	2,101,374	1,982,428
FBA2	505,730	1,214,575	216,502	204,247
FB5B	2,084,554	3,945,668	703,328	663,517
		16,948,950	3,021,204	2,850,192

It should be noted that the oil saturations calculated were of a semi-quantitative nature and should be taken into account when evaluating economics. The averaging of the resistivities may have been less accurate than the technique of using Rm and correcting for thin bed effects. Data from old logs as well as porosities established in the area outside the model limits were used. If it was believed the porosity was 29% instead of 32% then only 29/32 = 91% of the volume of oil in place should be used for economic evaluations.

For the example mentioned in the 'Results' section the following tables were generated. Estimated Original Oil in Place of the Hx0 sand based on log analysis - **40% Soi cutoff** (logs dated between 1949 and 1966):

TABLE C

Fault Block (Sub-Block)	Area (sq. ft.)	Volume (cf)	Res. Bbls (vol/5.61)	STB (res/1.06)
FB5B1	4,654,813	12,382,695	2,207,254	2,082,315
FBA2	505,730	1,207,745	215,284	203,098
FB5B	2,084,554	4,319,877	770,032	726,445
		17,910,317	3,192,570	3,011,858

Visualization shown in Figure 8.

Estimated Current Oil in Place of the Hx0 sand after modifying data for resistivity decrease observed in the newer logs and adding data from the newer logs to the data set less the **40% Soc cutoff** is summarized as follows:

TABLE D

Fault Block (Sub-Block)	Area (sq. ft.)	Volume (cf)	Res. Bbls (vol/5.61)	STB (res/1.06)
FB5B1	4,654,813	9,646,640	1,719,544	1,622,211
FBA2	505,730	646,197	115,187	108,667
FB5B	2,084,554	3,574,998	637,255	601,184
		13,867,835	2,471,985	2,332,062

Visualization shown in Figure 9.

* The exception to the data was Well FJ-091 2. An estimated Soi=0.37 was used for the first map as a control point and the Soc was calculated for the log to be Soc=0.18.

References:

Earlougher, 1972 Dennis Allen Chart in the Internal report for Department of Oil Properties - Subject: Saraband Analyses of LBOD wells Z-46B, Z-77A and FHS-9A. Earlougher Engineering, Tulsa, Oklahoma, p. 33.

Schlumberger, 1986, Prospecting with Old E-Logs, Schlumberger Educational Services, Houston, Texas, p 2.

Williams Bros., 1978, Internal report for Department of Oil Properties - Subject: FT-1 Hxa Sand Porosity and Saturation Values from Core and Electrical Log Analyses. Godsey-Earlougher Division, Resource Sciences Center, Tulsa, Oklahoma.

The steps to determine oil volume using EarthVision™ are listed below.

Bulk Volume:

1. 3-D Grid = Percent sand 3-D grid
    a. Modify the sand grid so there are no non sense values. In this case the maximum percent sand was extrapolated to 1.01. Use the formula processor to replace 1.01 with 1.00.
    b. Set the primary isovalue limits between 0.0 and 1.0.

2. Restriction Grid = Oil saturation 3-D grid
    a. Set the isovalue minimum and maximum to the appropriate values. In this case So > 0.40 was required so the minimum value was set at 0.40.

3. Set the Lateral and Vertical Volume Limits
    a. Vertical Limits. Use horizon grids for upper and lower surfaces (ev_combine the Hx0.htbl and Hx2.htbl).
    b. Lateral Limits. Use appropriate .vply file. Hint - copy cpf_xxx.ply file from the /surf directory. To find appropriate file, check the .htbl file and choose from text editor.

Fluid Volume (reduction of Bulk Volume):

1. Multiply all Bulk Volume grid nodes by So values > 0.4
    a. Under 'Limits', choose 'Zone Limits' and set Yield Factor 'by grid' equal to the oil_saturation.3grd. All grid nodes with So values > 0.4 will be used.
    b. Under 'Limits', chose 'Yield Factor' and set Global Yield factor (3-D yield grid) equal to the percent_sand.3grd. All grid nodes will be multiplied by the percent sand.
    c. Under 'Report', choose parameters and set output units to 'user conversion factor' and set to porosity value (in this case = 0.32). It is possible to bundle multiplying factors say 0.32 * 1/5.61 to determine bbls. All grid nodes will be multiplied by the selected value.

Example 3-D Volumetrics Output for 3 Fault Sub Blocks:

Run by: Phillips
Version: 3.0
Date: 10/24/96
Report file: fb5b1_coip.3vrpt

3-D grid file: /disk5/Phillips/doe/fb5/hx_proj/prop/
FB5B1_z_3_pctsand.3grd
3-D grid region: X - 10,895.9003 to 12,593.90039
Y - -11,300. to -7,600.
Z - -3,079.31 to -2,831.03003
Isovalue ranges specified: Shell 1 0.0 to 1
Restriction grid(s) specified: /disk5/Phillips/doe/fb5/hx_proj/prop/
FB5B1_z_3_curr_oip.3grd
-- 0.0 to .89999997616
Polygon file: fb5b1.vply
Zone definition: Operational
Deposition operation: hx0.2grd
Deposition operation: hx2.2grd
Global 3-D yield grid: /disk5/Phillips/doe/fb5/hx_proj/prop/
FB5B1_z_3_pctsand.3grd
Primary ordering by: Polygon order
Secondary ordering by: Polygon Class
Input units: feet square by feet
Volumetrics conversion factor: .32
Output units: User specified
Global minimum thickness: 0.0

---------- Zone name: hx0 ----------
Minimum z: none
Maximum z: none
Minimum thickness: 0.0
Layer 3-D yield grid: /disk5/Phillips/doe/fb5/hx_proj/prop/
FB5B1_z_3_curr_oip.3grd

3-D Volumetrics Report
Zone name: hx0

Isovalue Shell	Area	Volume	Positive Area
T:HX0			
Shell 1	4,654,813.2384	11,788,706.752	4,612,374.4834

Report file: fba2_coip.3vrpt

3-D grid file: /disk5/Phillips/doe/fb5/hx_proj/prop/
FBA2_z_3_pctsand.3grd
3-D grid region: X - 12,398. to 12,855.09961
Y - -11,300. to -8,950.
Z - -3,079.31 to -2,851.71997
Isovalue ranges specified: Shell 1 0.0 to 1
Restriction grid(s) specified: /disk5/Phillips/doe/fb5/hx_proj/prop/
FBA2_z_3_curr_oip.3grd

-- 0.0 to .89999997616
Polygon file: fba2.vply
Zone definition: Operational
Deposition operation: hx0.2grd
Deposition operation: hx2.2grd
Global 3-D yield grid: /disk5/Phillips/doe/fb5/hx_proj/prop/
FBA2_z_3_pctsand.3grd
Primary ordering by: Polygon order
Secondary ordering by: Polygon Class
Input units: feet square by feet
Volumetrics conversion factor: .32
Output units: User specified
Global minimum thickness: 0.0

---------- Zone name: hx0 ----------
Minimum z: none
Maximum z: none
Minimum thickness: 0.0
Layer 3-D yield grid: /disk5/Phillips/doe/fb5/hx_proj/prop/
FBA2_z_3_curr_oip.3grd

3-D Volumetrics Report

Zone name: hx0

Isovalue Shell	Area	Volume	Positive Area
T:HX0			
Shell 1	505,730.081303	1,214,575.4289	394,849.476756

Report file: fb5b_coip.3vrpt

3-D grid file: /disk5/Phillips/doe/fb5/hx_proj/prop/
FB5B_z_3_pctsand.3grd
3-D grid region: X - 10,700. to 11,483.7002
Y - -11,300. to -7,600.
Z - -3,079.31 to -2,810.34009
Isovalue ranges specified: Shell 1 0.0 to 1
Restriction grid(s) specified: /disk5/Phillips/doe/fb5/hx_proj/prop/
FB5B_z_3_curr_oip.3grd
-- 0.0 to .89999997616
Polygon file: fb5b.vply
Zone definition: Operational
Deposition operation: hx0.2grd
Deposition operation: hx2.2grd
Global 3-D yield grid: /disk5/Phillips/doe/fb5/hx_proj/prop/
FB5B_z_3_pctsand.3grd
Primary ordering by: Polygon order
Secondary ordering by: Polygon Class
Input units: feet square by feet
Volumetrics conversion factor: .32
Output units: User specified
Global minimum thickness: 0.0

---------- Zone name: hx0 ----------
Minimum z: none
Maximum z: none
Minimum thickness: 0.0
Layer 3-D yield grid: /disk5/Phillips/doe/fb5/hx_proj/prop/
FB5B_z_3_curr_oip.3grd

3-D Volumetrics Report
Zone name: hx0

Isovalue Shell	Area	Volume	Positive Area
T:HX0			
Shell 1	2,084,554.0786	3,945,667.7685	2,084,554.0786

CCP:C:\EDRIVE\PROJECTS\DOE\FB5\HX0_NESTE.RPT

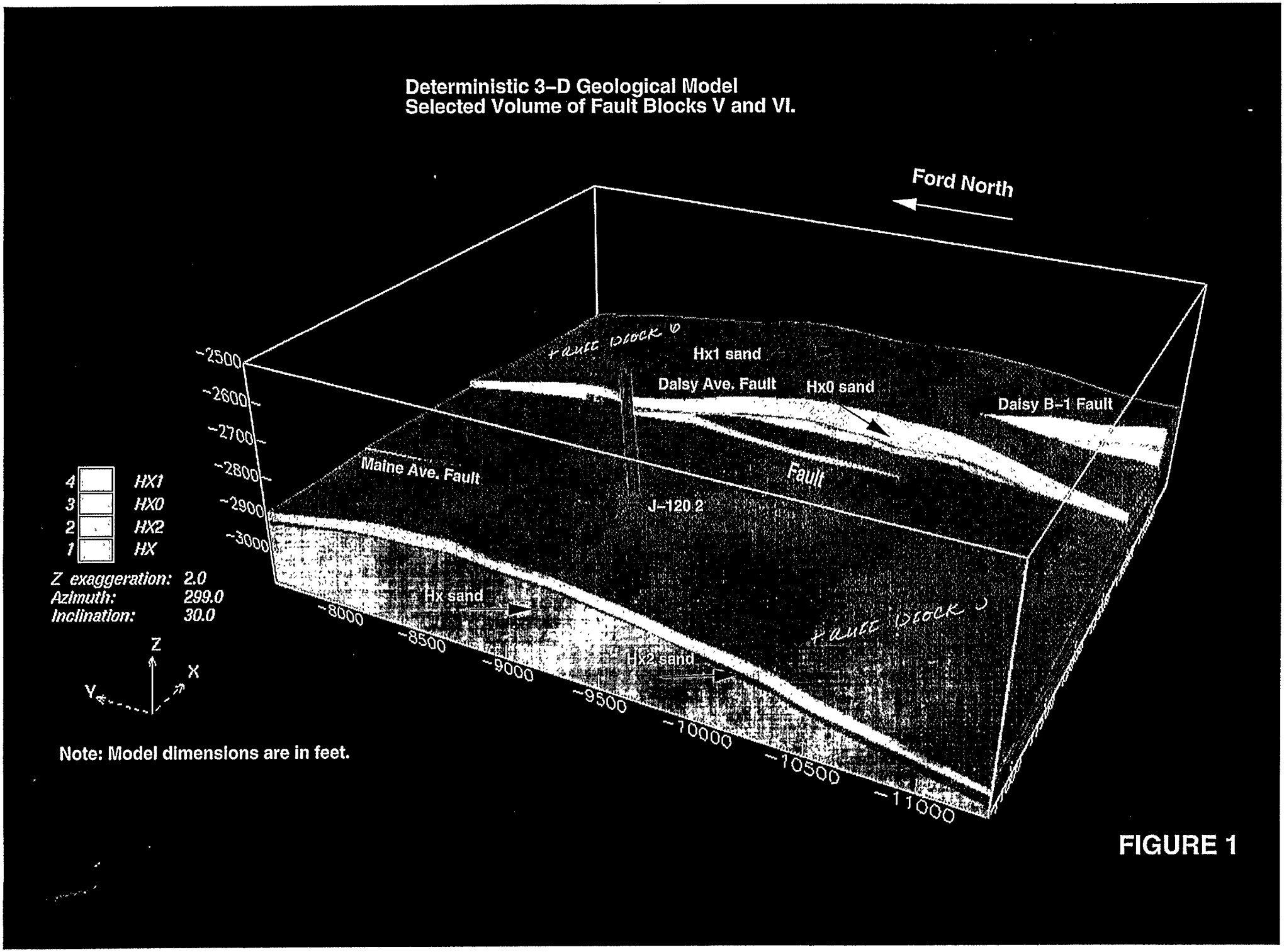
Deterministic 3-D Geological Model
Selected Volume of Fault Blocks V and VI.
Ford North
Fault Block V
Hx1 sand
Daisy Ave. Fault
Hx0 sand
Daisy B-1 Fault
Maine Ave. Fault
Fault
J-120 2
Hx sand
Fault Block J
Hx2 sand
-2500
-2600
-2700
-2800
-2900
-3000
-8000
-8500
-9000
-9500
-10000
-10500
-11000
4 HX1
3 HX0
2 HX2
1 HX
Z exaggeration: 2.0
Azimuth: 299.0
Inclination: 30.0
Z
X
Y
Note: Model dimensions are in feet.

FIGURE 1

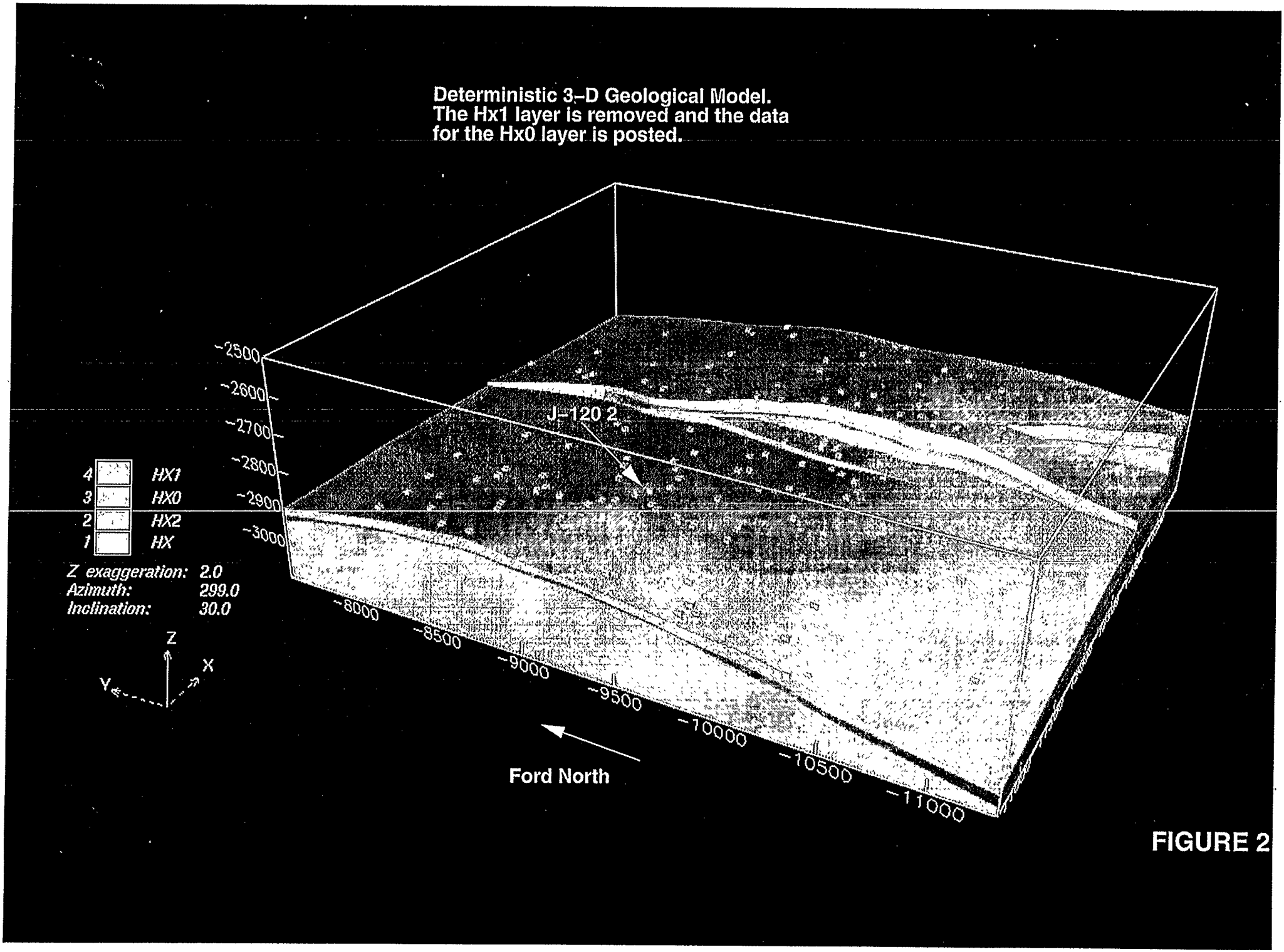
Deterministic 3-D Geological Model.
The Hx1 layer is removed and the data
for the Hx0 layer is posted.
J-120 2
-2500
-2600
-2700
-2800
-2900
-3000
4 HX1
3 HX0
2 HX2
1 HX
Z exaggeration: 2.0
Azimuth: 299.0
Inclination: 30.0
Z
X
Y
-8000
-8500
-9000
-9500
-10000
-10500
-11000
Ford North

FIGURE 2

Structure Map on top of Hx0 sand.

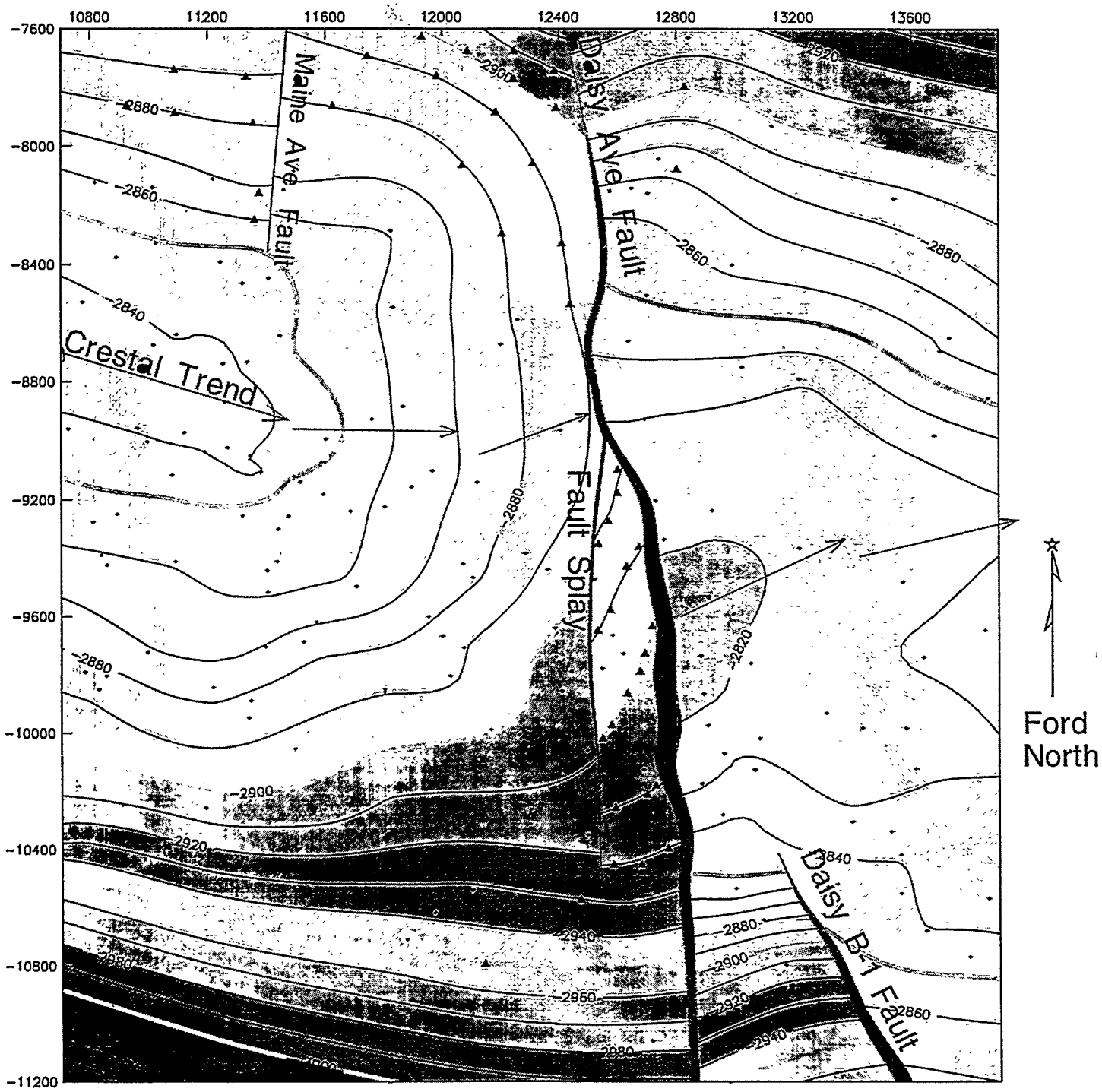

Contour Interval = 10'

0 250 500 750

FEET

Scale: 1" = 500'

· Data Point

▲ Control Point

FIGURE 3

phillips/doe/fb5/fig_03rev.iplt

Hx0 Structure Map showing So contours.

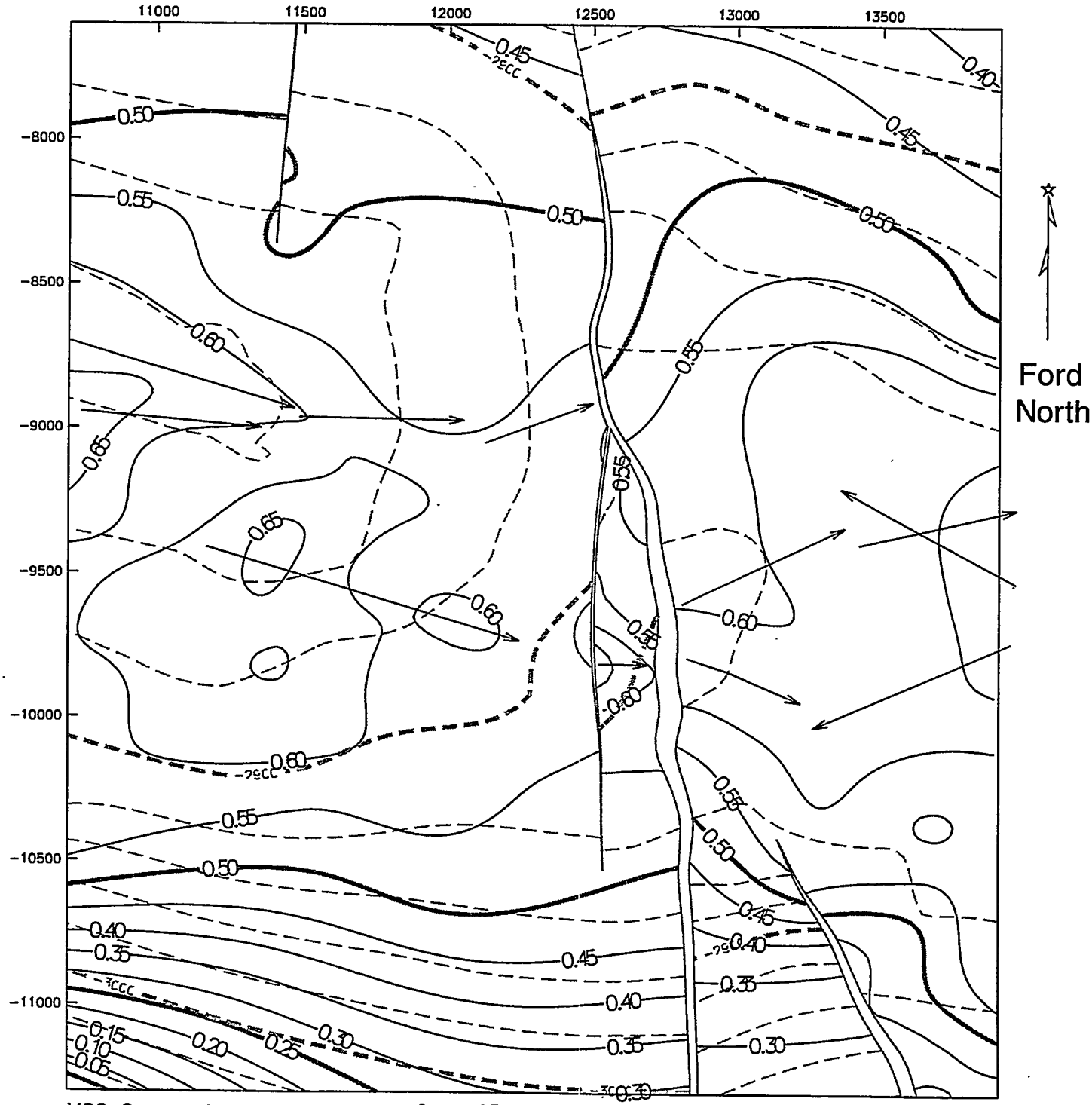

FIGURE 4

/phillips/doe/fb5/hx_proj/fig_04rev.iplt

Qualitative Oil Saturation modeled as a parameter within Hx0 sand.

Wells drilled in the 1980's shown with oil saturation posted.
Future recompletes labeled with light blue lettering.

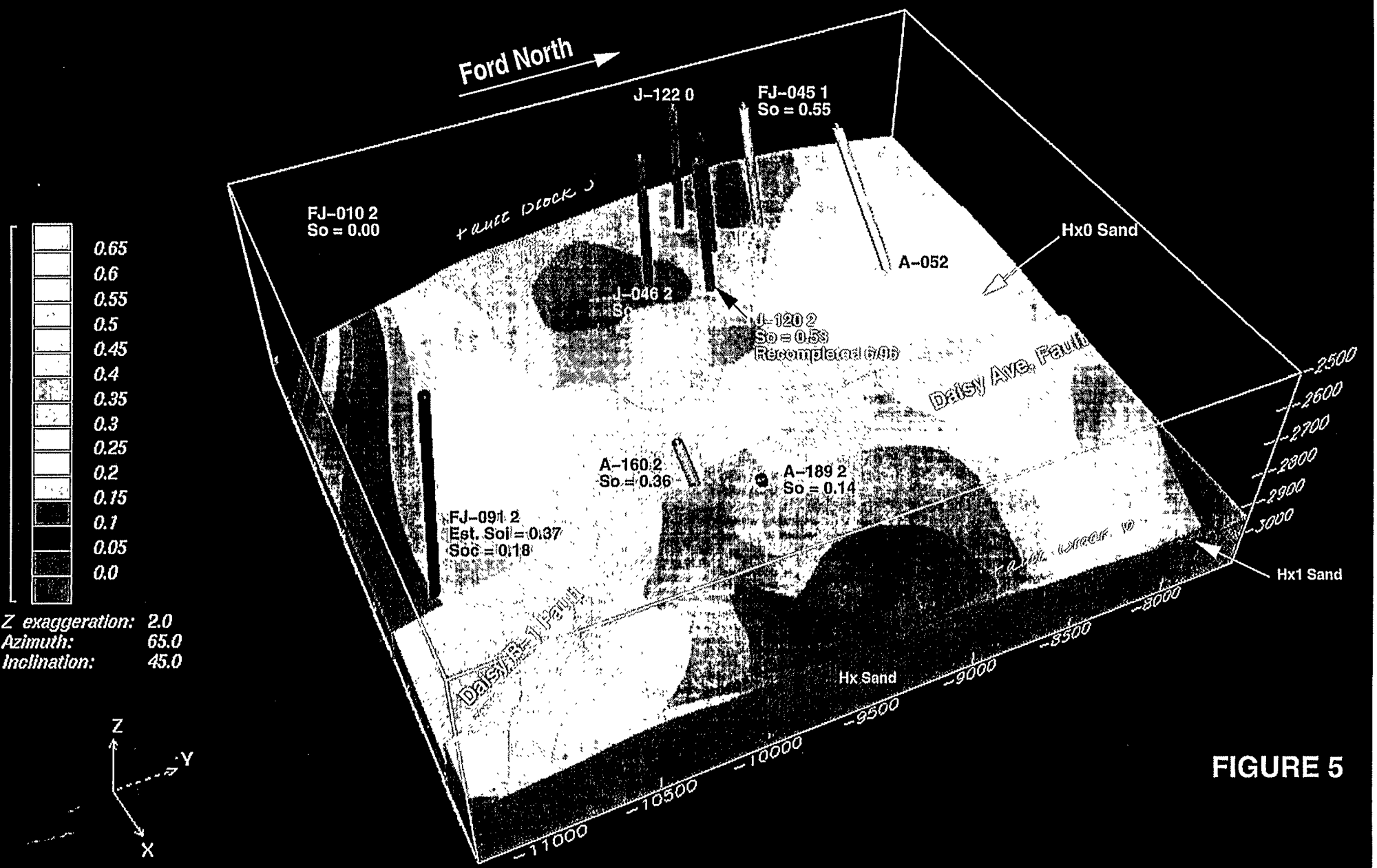

FIGURE 5

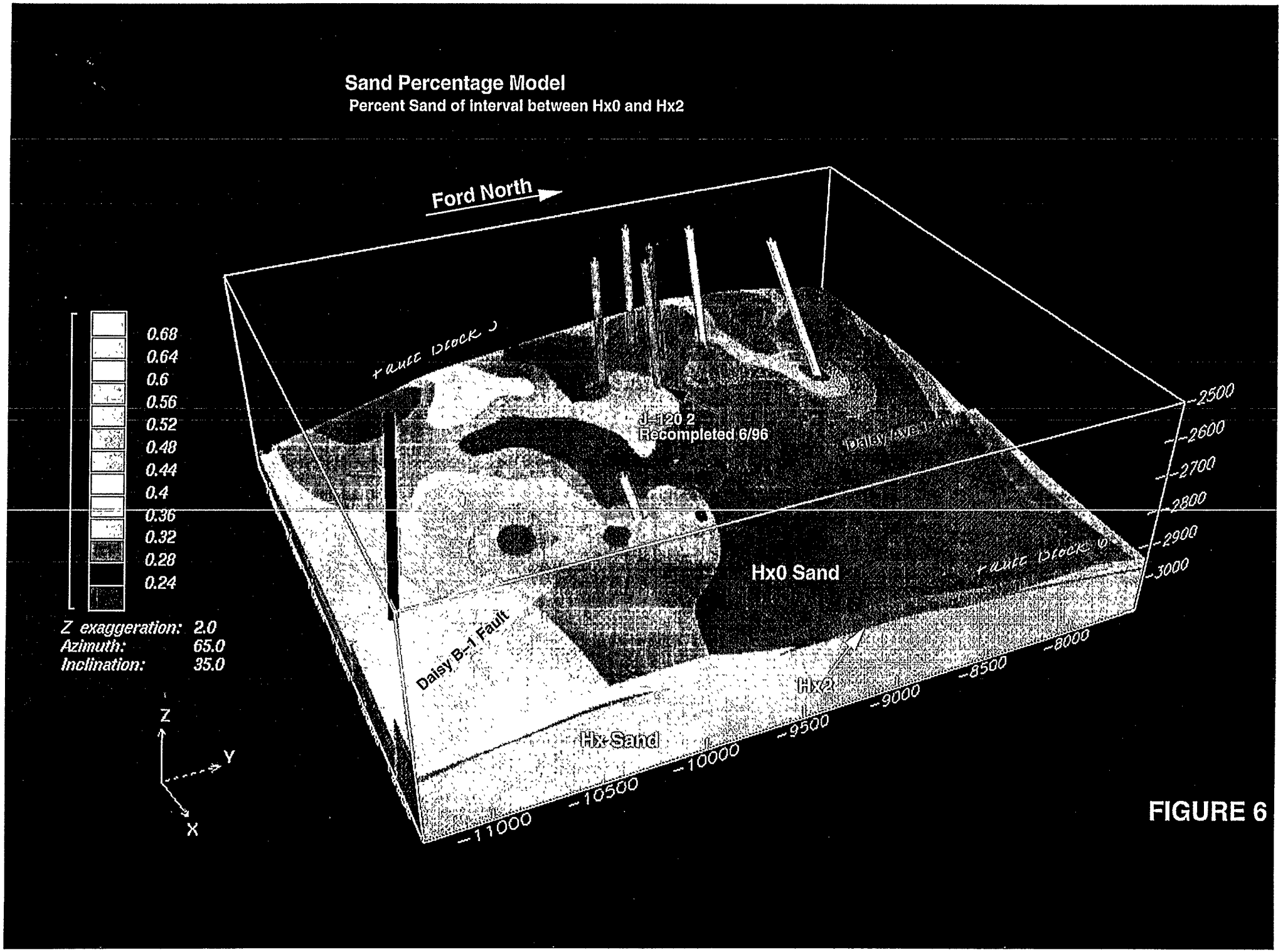
Sand Percentage Model
Percent Sand of interval between Hx0 and Hx2
Ford North
0.68
0.64
0.6
0.56
0.52
0.48
0.44
0.4
0.36
0.32
0.28
0.24
Z exaggeration: 2.0
Azimuth: 65.0
Inclination: 35.0
Z
Y
X
J-120 2
Recompleted 6/96
Hx0 Sand
Daisy B-1 Fault
Hx2
Hx Sand
-2500
-2600
-2700
-2800
-2900
-3000
-8000
-8500
-9000
-9500
-10000
-10500
-11000

FIGURE 6

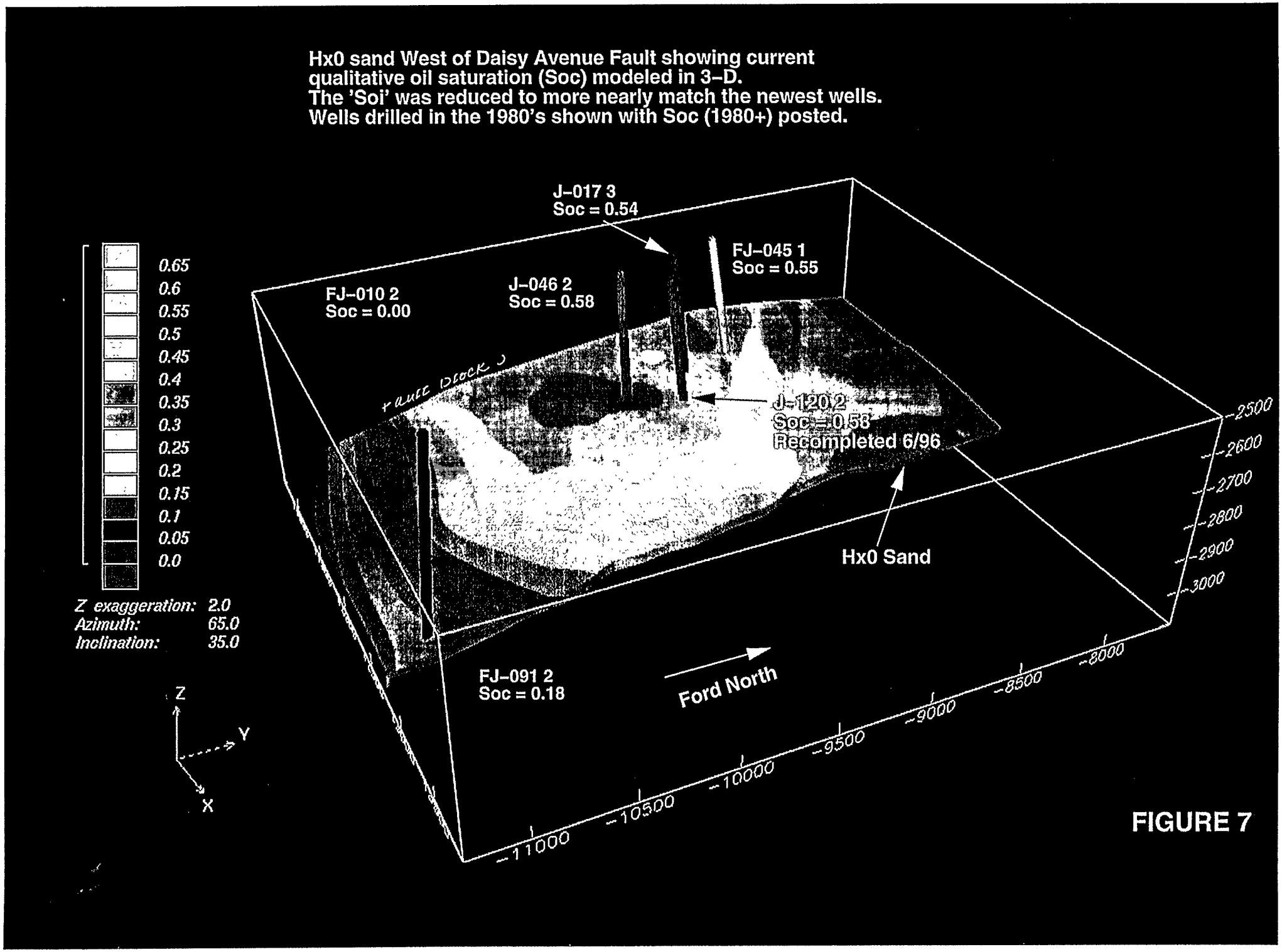
Hx0 sand West of Daisy Avenue Fault showing current qualitative oil saturation (Soc) modeled in 3–D.
The 'Soi' was reduced to more nearly match the newest wells.
Wells drilled in the 1980's shown with Soc (1980+) posted.
J–017 3
Soc = 0.54
FJ–045 1
Soc = 0.55
FJ–010 2
Soc = 0.00
J–046 2
Soc = 0.58
fault block J
J–120 2
Soc = 0.58
Recompleted 6/96
Hx0 Sand
FJ–091 2
Soc = 0.18
Ford North
0.65
0.6
0.55
0.5
0.45
0.4
0.35
0.3
0.25
0.2
0.15
0.1
0.05
0.0
Z exaggeration: 2.0
Azimuth: 65.0
Inclination: 35.0
Z
Y
X
2500
2600
2700
2800
2900
3000
8000
8500
9000
9500
10000
10500
11000

FIGURE 7

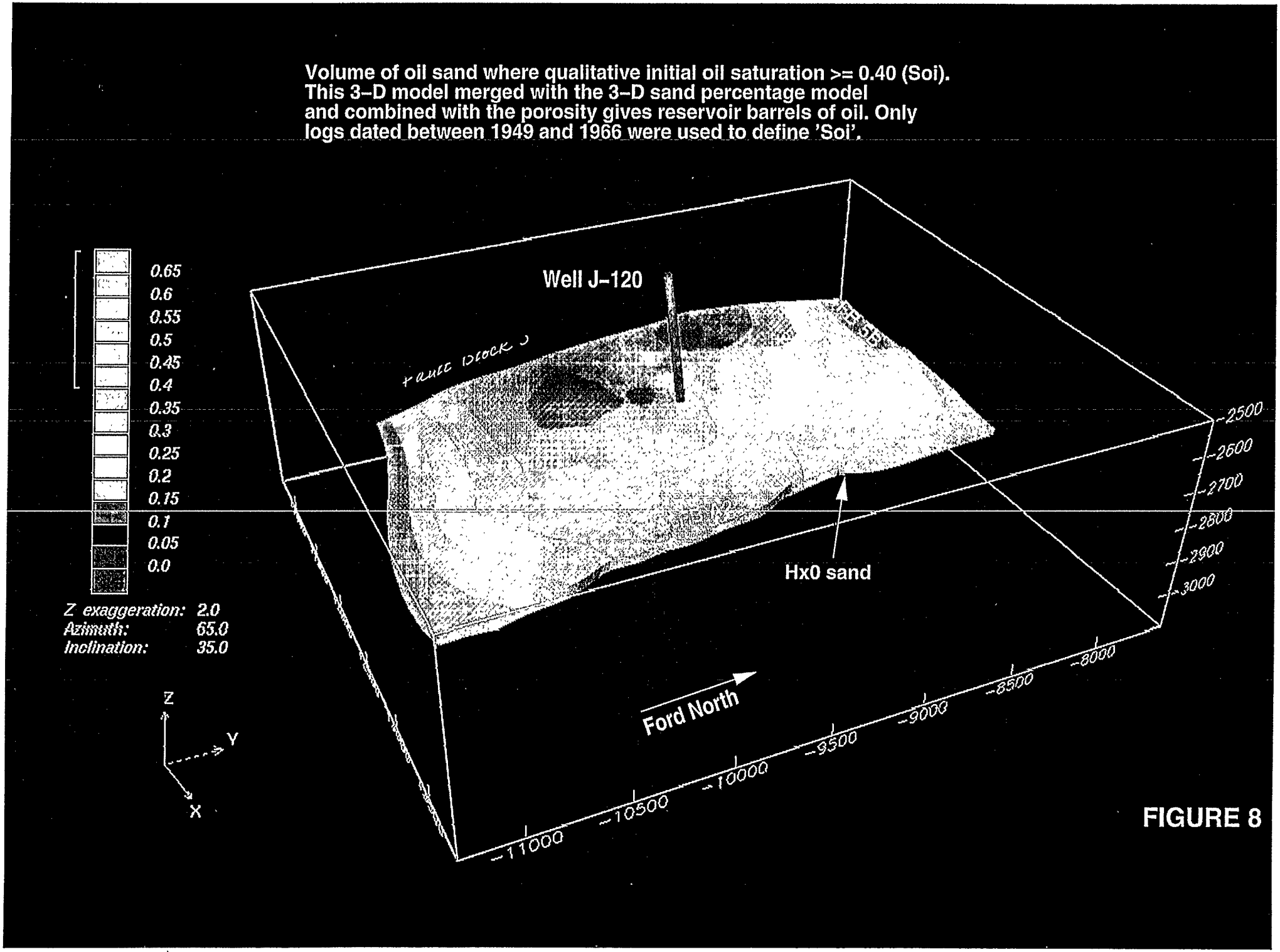
Volume of oil sand where qualitative initial oil saturation >= 0.40 (Soi).
This 3–D model merged with the 3–D sand percentage model
and combined with the porosity gives reservoir barrels of oil. Only
logs dated between 1949 and 1966 were used to define 'Soi'.
0.65
0.6
0.55
0.5
0.45
0.4
0.35
0.3
0.25
0.2
0.15
0.1
0.05
0.0
Z exaggeration: 2.0
Azimuth: 65.0
Inclination: 35.0
Z
Y
X
Well J–120
Fault block J
Hx0 sand
Ford North
-2500
-2600
-2700
-2800
-2900
-3000
-8000
-8500
-9000
-9500
-10000
-10500
-11000

FIGURE 8

Volume of Oil Sand where qualitative current oil saturation (Soc) > 0.40.
The 'Soc' was reduced to more nearly match the new wells.
Wells drilled in the 1980's shown with Soc (1980+) posted.

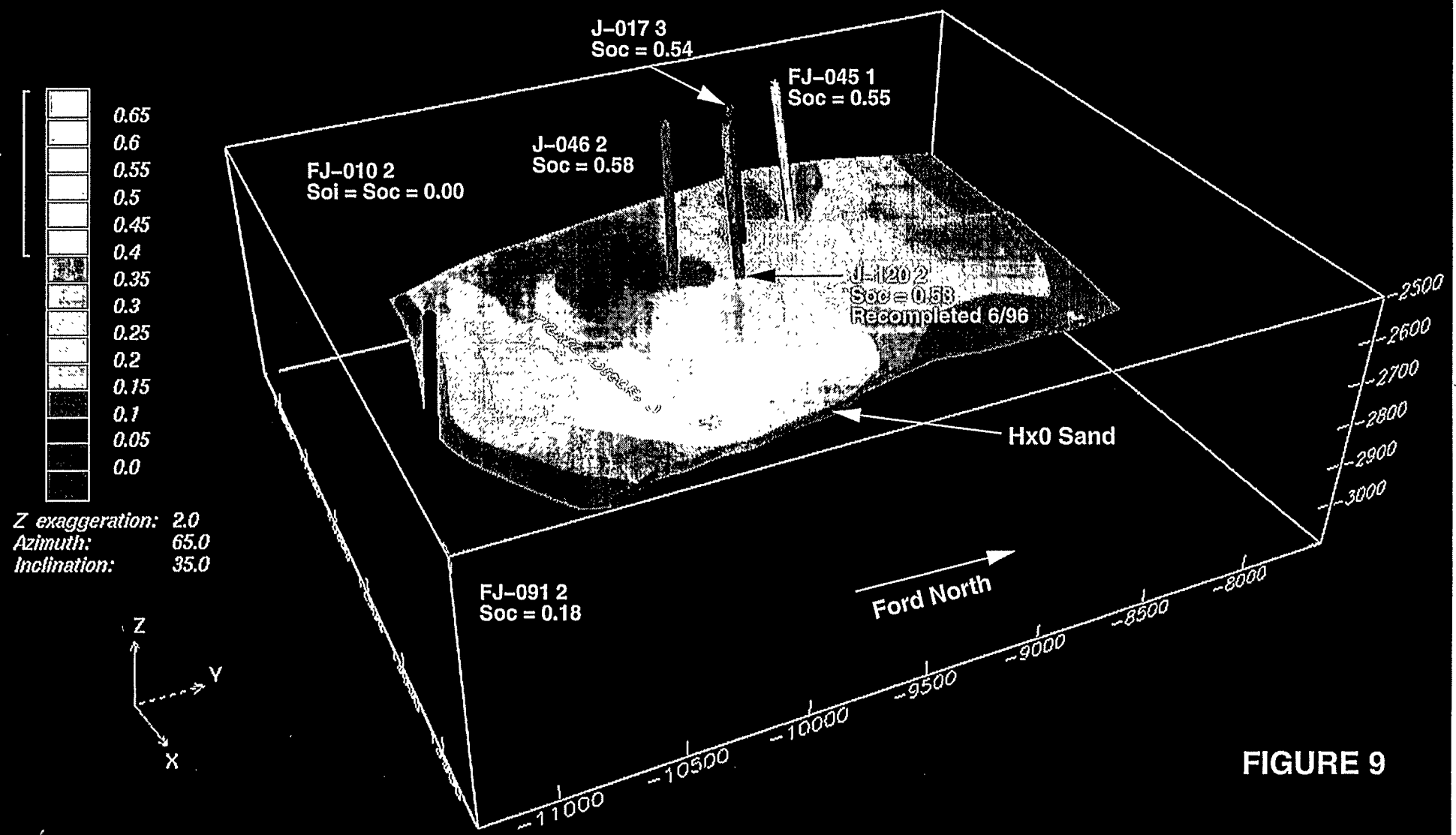

FIGURE 9

J -017 3

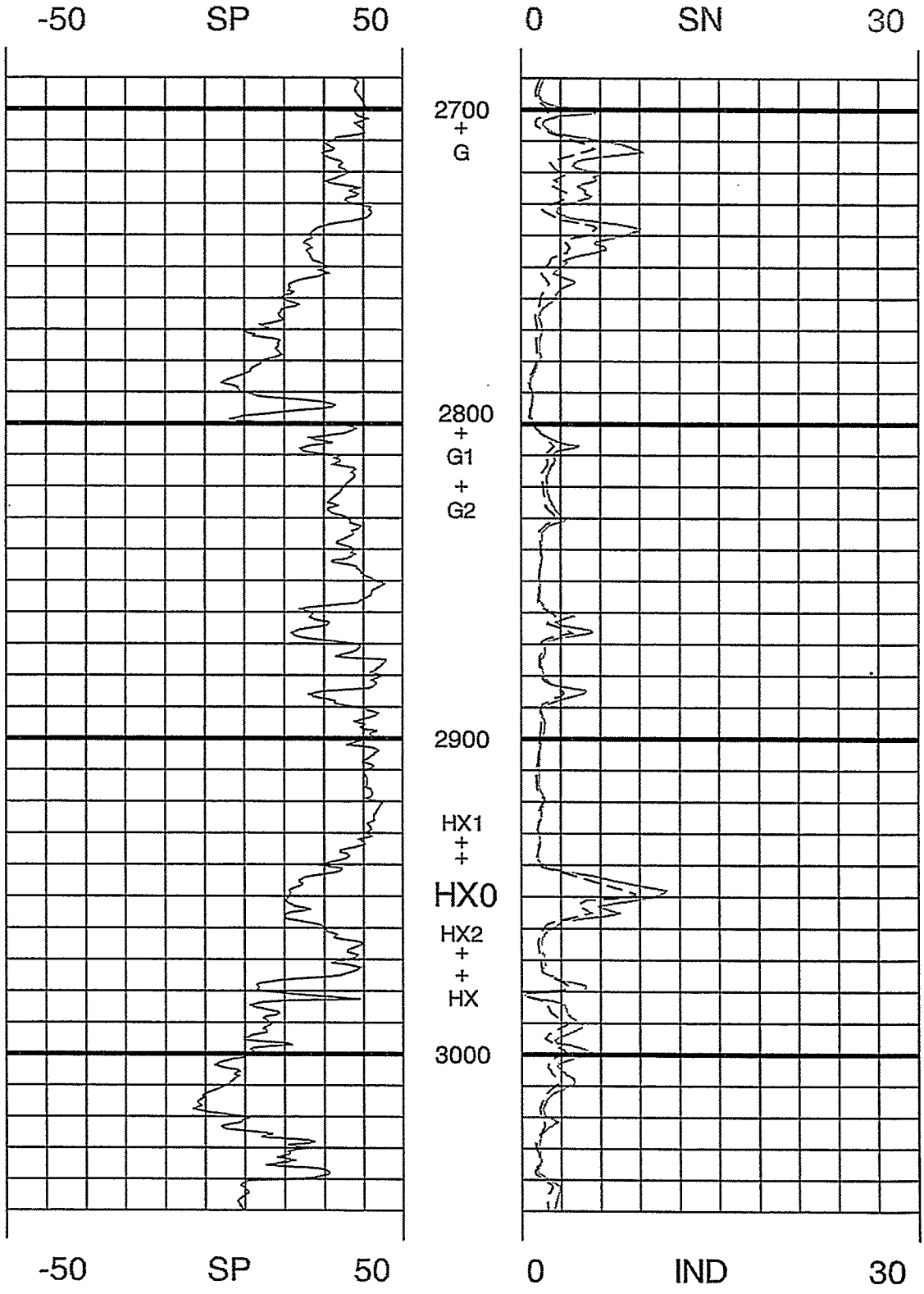

FIGURE 10

Hx0 Structure Map showing So contours.

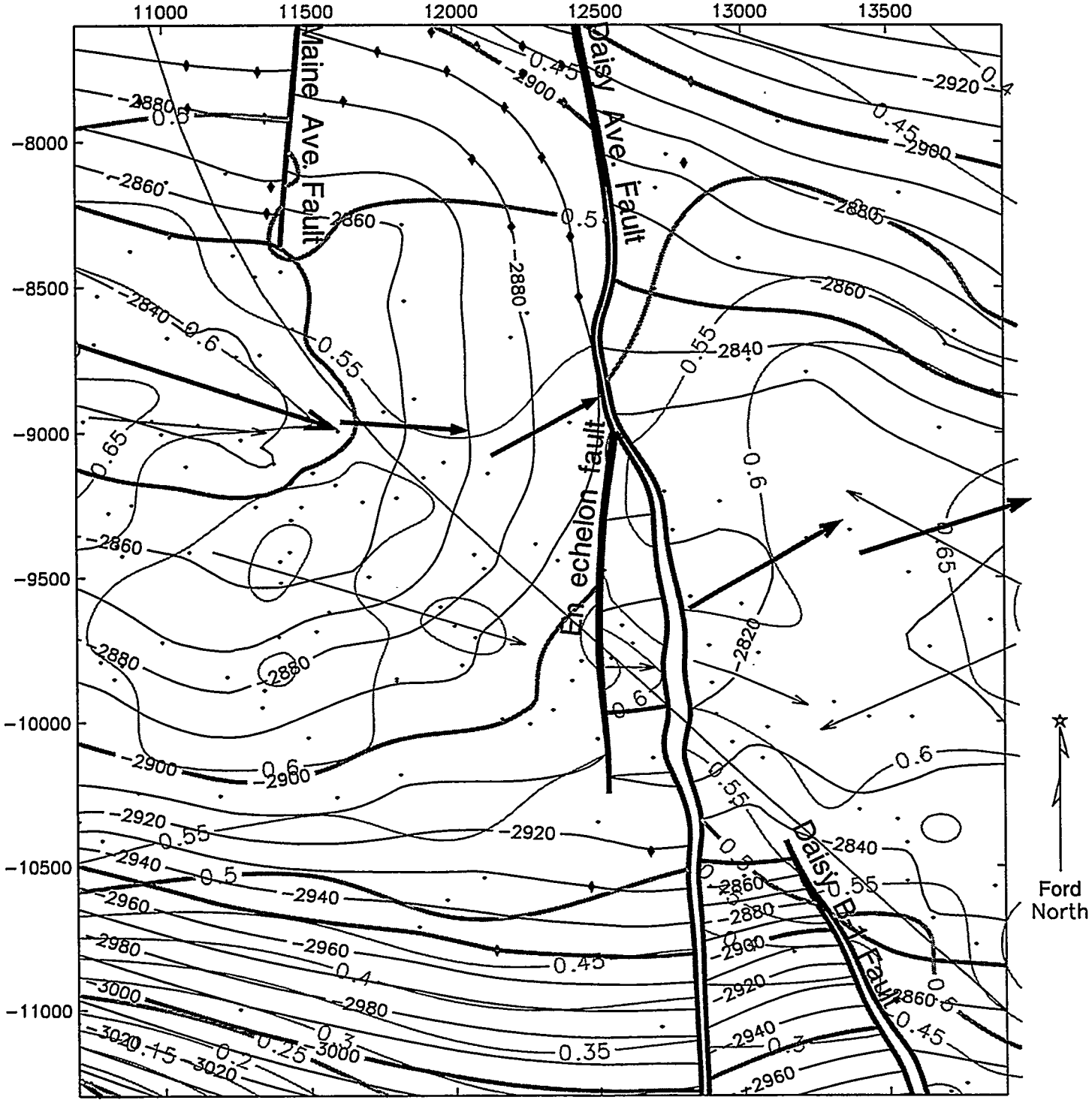

Contour Interval = 10'

0 250 500 750
FEET

Scale: 1" = 500'

• Data Point
♦ Control Point

Note: Arrow Heads point toward lower values.

→ Crestal Trend
→ 'So' Trend

FIGURE 4

/phillips/doe/fb5/hx_proj/fig_04.iplt

TABLE 1

Wellid	Rd	X	Y	TVD	MD	Sand Count	Net Thick	Oil Thick	Spud Date	Feet	Ohm-m	Feet	Ohm-m	Average Rt	So		PCT ST
A -030	0	12480.2	-7870.9	2906.3	3713	17	12.10	12.10	1949	8.0	6.7	9.0	6.7	6.7	0.50	DEEP - 10'	
A -039	0	11218.6	-8108.0	2869.6	3080	11	9.47	9.47	1950	4.0	6.0	7.0	8.1	7.3	0.52	5FF40	60
A -039	1	11318.7	-8463.6	2841.8	2999	14	0.00	0.00	1961	5.0	5.3	9.0	8.0	7.0	0.51		36
A -040	0	11493.1	-8083.7	2873.2	3182	15	12.76	12.76	1950	7.0	6.0	8.0	7.0	6.5	0.50		
A -049	0	11242.7	-8390.8	2846.1	3014	14	12.42	12.42	1947	5.0	6.0	9.0	8.0	7.3	0.52		39
A -051	0	11407.2	-8446.6	2847.3	3072	14	11.31	11.31	1947	5.0	7.5	9.0	8.9	8.4	0.56		34
A -052	0	11823.5	-8285.9	2859.4	3302	13	9.42	9.42	1948	4.0	10.0	9.0	14.3	13.0	0.64	DEEP - 10'	33
A -066	0	11333.9	-8732.4	2843.6	2960	14	13.12	13.12	1947	5.0	7.0	9.0	9.0	8.3	0.55		48
A -073	0	12257.8	-8589.6	2882.1	3360	18	13.51	13.51	1948	8.0	7.0	10.0	9.0	8.1	0.55		43
A -075	0	13023.9	-8750.0	2838.3	3657	28	20.11	20.11	1948	7.0	7.2	21.0	10.3	9.5	0.58		
A -076	0	12689.9	-8926.9	2829.7	3450	24	17.24	17.24	1948	6.0	7.8	18.0	9.2	8.9	0.57		46
A -078	0	11513.5	-9138.6	2856.4	2953	18	17.05	17.05	1952	12.0	10.0	6.0	8.1	9.4	0.58	DEEP - 10'	56
A -079	0	11684.9	-9239.4	2859.1	2980	21	19.76	19.76	1952	14.0	10.8	7.0	10.4	10.7	0.61	DEEP - 10'	58
A -080	0	11266.2	-9023.5	2838.0	2918	16	15.42	15.42	1953	11.0	10.9	5.0	9.2	10.4	0.60	DEEP - 10'	51
A -085	0	11758.4	-8927.2	2854.9	3022	17	15.98	15.98	1947	17.0	8.0			8.0	0.54	DEEP - 12'	47
A -088	0	11965.2	-9102.8	2866.0	3082	18	15.58	15.58	1947	18.0	9.0			9.0	0.57		45
A -089	0	13678.7	-8983.0	2834.7	4052	32	22.83	22.83	1947	23.0	10.0	9.0	8.6	9.6	0.58	DEEP - 10'	
A -090	0	11801.7	-9225.2	2861.9	2992	20	18.98	18.98	1948	10.0	8.9	10.0	8.1	8.5	0.56	DEEP - 10'	60
A -092	0	13367.1	-9336.6	2823.0	3708	36	23.60	23.60	1948	23.0	10.3	13.0	7.3	9.2	0.58		
A -093	0	12698.3	-8506.4	2851.0	3561	25	16.92	16.92	1948	10.0	5.1	15.0	6.8	6.1	0.48		48
A -095	0	12408.5	-9856.4	2906.8	3283	25	17.28	17.28	1948	13.0	9.2	12.0	8.4	8.8	0.57		44
A -097	0	11445.3	-8643.5	2848.4	3120	15	12.39	12.39	1961	15.0	8.1			8.1	0.55	6FF40	42
A -098	0	11600.7	-8994.2	2845.8	2975	18	16.91	16.91	1961	18.0	10.8			10.8	0.61	6FF40	42
A -099	0	12756.6	-9336.7	2823.7	3424	28	17.01	17.01	1962	19.0	9.2	9.0	6.2	8.2	0.55	DEEP - 10'	51
A -100	0	12922.4	-9237.8	2821.2	3501	31	20.13	20.13	1962	19.0	11.1	12.0	6.9	9.5	0.58		43
A -110	0	13570.3	-9482.9	2823.4	3731	0	0.00	0.00	1962					ERR			
A -160	1	12892.6	-9865.0	2817.0	3106	30	21.59	21.59	1966	30.0	4.2			4.2	0.37		
A -160	2	12867.5	-9866.9	2817.1	3094	26	22.36	22.36	1982	26.0	4.0			4.0	0.36	OBM	
A -161	0	13309.1	-9931.2	2822.2	3151	37	31.96	31.96	1963	29.0	11.6	8.0	6.8	10.6	0.60		
A -162	0	12360.4	-9439.7	2891.1	3127	23	20.97	20.97	1961	23.0	9.5			9.5	0.58	DEEP - 10'	53
A -164	0	12283.4	-9384.2	2888.2	3155	21	17.81	17.81	1951	15.0	9.3	6.0	10.4	9.6	0.58	DEEP - 10'	39
A -165	0	12404.1	-8964.9	2886.1	3345	22	17.05	17.05	1951	22.0	9.2			9.2	0.58	6FF40	46
A -165	4	12520.5	-9474.3	2885.2	3113	22	19.38	19.38	1965	14.0	9.0	8.0	6.3	8.0	0.54	DEEP - 10'	
A -166	0	11830.7	-8547.7	2862.7	3516	16	13.66	13.66	1951	7.0	7.4	9.0	7.4	7.4	0.53	DEEP - 10'	50
A -167	0	12200.4	-8672.9	2876.4	3450	21	16.36	16.36	1951	8.0	7.4	13.0	7.4	7.4	0.53		55
A -168	0	12636.6	-8662.7	2843.4	3530	20	14.18	14.18	1951	10.0	6.0	10.0	7.4	6.7	0.50	DEEP - 10'	44
A -170	0	12727.6	-9203.5	2823.6	3230	23	18.37	18.37	1951	15.0	7.8	8.0	12.0	9.3	0.58	DEEP - 10'	47
A -171	0	13051.9	-9761.4	2822.7	3200	35	26.34	26.34	1951	20.0	9.8	15.0	12.7	11.0	0.61	DEEP - 10'	
A -172	0	13580.0	-9983.2	2818.9	3378	40	28.40	28.40	1951	28.0	16.1	12.0	8.4	13.8	0.65	DEEP - 10'	

TABLE 1

Wellid	Rd	X	Y	TVD	MD	Sand Count	Net Thick	Oil Thick	Spud Date	Feet	Ohm-m	Feet	Ohm-m	Average Rt	So		PCT ST
A -173	0	13217.8	-9366.2	2821.6	3409	33	22.73	22.73	1951	22.0	11.6	11.0	10.5	11.2	0.62		
A -174	0	12581.0	-9665.3	2891.8	3136	22	18.68	18.68	1951	14.0	9.7	8.0	7.8	9.0	0.57	DEEP - 10'	53
A -175	0	13219.0	-8791.4	2829.7	3568	34	23.91	23.91	1952	23.0	12.2	11.0	10.5	11.7	0.62		
A -176	0	12440.6	-9788.4	2906.6	3063	23	20.81	20.81	1952	14.0	8.6	9.0	7.3	8.1	0.55		48
A -177	0	13730.8	-8651.0	2858.2	3833	34	23.47	23.47	1952	9.0	5.8	25.0	7.7	7.2	0.52	DEEP - 10'	
A -178	0	12816.9	-9566.8	2809.6	3053	21	21.29	21.29	1952	12.0	10.9	9.0	8.4	9.8	0.59	DEEP - 10'	54
A -179	0	13862.3	-8856.8	2851.2	3853	36	23.45	23.45	1952	36.0	10.3	0.0	0.0	10.3	0.60		
A -180	0	12385.2	-9639.5	2899.9	3088	23	19.88	19.88	1953	13.0	9.2	10.0	7.8	8.6	0.56	DEEP - 10'	52
A -181	0	13065.4	-10125.7	2831.2	3033	28	25.47	25.47	1953	28.0	10.0			10.0	0.59	DEEP - 10'	
A -182	0	13851.1	-9648.5	2836.3	3477	37	27.80	27.80	1953	30.0	18.4	7.0	8.9	16.6	0.68		
A -188	0	12907.1	-9972.6	2823.8	3020	25	22.17	22.17	1950	13.0	10.9	12.0	9.6	10.3	0.60	DEEP - 10'	50
A -189	0	12994.8	-9592.6	2816.3	3161	22	18.01	18.01	1950	15.0	9.4	7.0	11.3	10.0	0.59	DEEP - 10'	
A -189	2	12997.0	-9590.0	2820.0	3168	24	20.82	20.82	1982	24.0	2.3			2.3	0.14	OBM	
A -190	0	13082.5	-10018.1	2828.2	3085	33	28.07	28.07	1950	20.0	10.5	13.0	11.9	11.1	0.61		
A -191	2	13613.4	-10121.6	2829.9	3274	35	27.95	27.95	1963	15.0	9.9	20.0	9.9	9.9	0.59	6FF40	
A -199	0	13641.3	-9740.6	2832.6	3352	41	29.05	29.05	1962	33.0	12.4	8.0	8.9	11.7	0.62	6FF40	
A -201	0	12617.4	-9728.3	2897.6	3098	23	21.05	21.05	1961	13.0	11.9	10.0	7.6	10.0	0.59	6FF40	57
A -202	0	13528.8	-10337.6	2833.9	3127	22	19.23	19.23	1961	13.0	9.2	9.0	7.2	8.4	0.55		
A -203	0	12886.0	-10172.5	2826.7	2955	27	24.70	24.70	1961	15.0	8.8	12.0	6.5	7.8	0.54	DEEP - 10'	53
A -204	0	13431.3	-9982.1	2821.8	3112	36	31.23	31.23	1954	28.0	13.8	8.0	6.2	12.1	0.63	DEEP - 10'	
A -206	0	13396.4	-10304.2	2831.3	3084	26	23.22	23.22	1954	26.0	10.5			10.5	0.60	DEEP - 10'	
A -210	0	13311.9	-10528.6	2846.5	3087	23	20.56	20.56	1954	23.0	9.0			9.0	0.57		
A -212	0	13137.2	-10478.9	2847.9	3022	19	16.97	16.97	1954	19.0	8.4			8.4	0.56	DEEP - 10'	
A -213	0	13795.5	-10769.7	2846.2	3285	31	26.35	26.35	1954	31.0	8.9			8.9	0.57		
A -214	0	13561.4	-10551.7	2840.8	3168	22	15.90	15.90	1955	22.0	9.0			9.0	0.57	6FF40	
A -214	1	13648.3	-10679.7	2838.5	3151	16	18.85	18.85	1971	10.0	6.3	6.0	7.2	6.6	0.50		
A -215	0	13862.2	-10569.3	2834.9	3212	29	27.07	27.07	1955	21.0	10.3	8.0	5.4	8.9	0.57	6FF40	
A -217	2	12955.3	-10278.9	2840.5	2988	26	21.92	21.92	1963	18.0	8.8	8.0	5.8	7.9	0.54	DEEP - 10'	
A -218	0	13561.6	-10417.9	2841.8	3199	32	23.69	23.69	1962	23.0	9.6	9.0	5.1	8.3	0.55	DEEP - 10'	
A -303	0	11567.4	-9618.9	2868.5	2985	24	20.17	20.17	1954	17.0	11.9	7.0	11.1	11.7	0.62	DEEP - 10'	55
A -304	0	11894.8	-9155.4	2866.5	3118	19	17.54	17.54	1955	11.0	10.2	8.0	10.2	10.2	0.60	?	52
A -305	0	11864.4	-8884.1	2863.5	3202	18	16.01	16.01	1955	18.0	6.8			6.8	0.51	DEEP - 10'	48
A -306	0	12070.0	-9420.2	2876.6	3091	21	19.31	19.31	1955	14.0	10.3	7.0	9.2	9.9	0.59	?	52
A -308	0	12118.9	-9141.1	2871.7	3223	21	18.36	18.36	1955	21.0	9.6			9.6	0.58		53
A -310	0	12104.2	-9468.1	2876.8	3096	23	21.48	21.48	1955	14.0	10.3	9.0	7.8	9.3	0.58	DEEP - 10'	57
A -318	0	12026.5	-9803.6	2886.7	3039	21	18.74	18.74	1954	10.0	10.3	11.0	9.7	10.0	0.59		47
A -321	0	12544.2	-9779.3	2892.6	3242	26	20.69	20.69	1955	15.0	26.0	10.3			0.67		54
A -322	0	12883.3	-9735.1	2817.4	3266	26	22.51	22.51	1955	15.0	12.8	11.0	9.1	11.2	0.62		59
A -323	0	12165.0	-9988.7	2899.2	3053	27	24.27	24.27	1955	12.0	8.9	15.0	8.4	8.6	0.56	DEEP - 10'	59

TABLE 1

Wellid	Rd	X	Y	TVD	MD	Sand Count	Net Thick	Oil Thick	Spud Date	Feet	Ohm-m	Feet	Ohm-m	Average Rt	So		PCT ST
FJ-010	2	10736.8	-11250.9	3044.7	3357	15	13.62	0.00	1984	15.0	1.7			1.7	0.00	DEEP - 10'	57
FJ-029	0	11190.5	-10254.4	2904.7	3057	19	17.03	17.03	1950	10.0	9.7	9.0	9.0	9.4	0.58	DEEP - 10'	65
FJ-030	0	11811.9	-10182.2	2908.6	3194	27	23.01	23.01	1950	8.0	9.7	19.0	9.7	9.7	0.59	DEEP - 10'	55
FJ-036	0	11873.0	-10709.5	2948.7	3312	32	26.48	26.48	1950	12.0	7.3	18.0	5.4	5.8	0.48		52
FJ-045	0	11228.4	-8840.2	2841.1	2980	15	14.31	14.31	1951	12.0	11.9	3.0	8.9	11.3	0.62		
FJ-045	1	11251.7	-8737.9	2831.9	2968	15	14.13	14.13	1983	11.0	9.4	4.0	5.2	8.3	0.55	DEEP - 10'	40
FJ-049	0	11592.7	-10259.8	2905.1	3131	22	18.42	18.42	1951	8.0	7.3	14.0	9.6	8.8	0.56	DEEP - 9'	47
FJ-051	0	10781.1	-9790.0	2882.6	2907	17	16.81	16.81	1951	4.0	4.3	13.0	12.2	10.3	0.60		53
FJ-053	0	10703.3	-10344.0	2922.8	3000	17	16.44	16.44	1951	17.0	10.0			10.0	0.59	DEEP - 12'	58
FJ-060	0	11971.2	-10616.2	2936.3	2970	34	34.00	34.00	1953	21.0	7.2	13.0	6.9	7.1	0.52		70
FJ-080	0	11494.6	-10053.2	2893.8	3002	25	24.09	24.09	1953	18.0	14.0	7.0	8.1	12.3	0.63	MED - 5'	50
FJ-091*	2	12710.3	-11059.4	2976.3	3170	26	22.47	22.47	1982	14.0	4.6	12.0	3.6	4.1	0.37	MED - 5'	63
FJ-107	0	12261.2	-10006.6	2903.5	3356	28	25.34	25.34	1954	11.0	10.0	17.0	8.1	8.8	0.57	MED - 5'	54
FJ-107	1	12341.7	-9957.1	2898.9	3414	28	26.04	26.04	1957	8.0	8.9	20.0	10.5	10.0	0.59	DEEP - 12'	61
FJ-112	0	12494.5	-10347.7	2917.3	3555	22	19.28	19.28	1955	13.0	8.2	9.0	6.5	7.5	0.53	MED - 5'	45
FJ-114	0	12099.7	-10539.6	2932.0	2986	26	25.03	25.03	1958	13.0	9.1	13.0	6.2	7.7	0.53		61
FJ-116	0	10890.1	-8374.9	2844.2	2985	10	9.19	9.19	1960	4.0	4.9	6.0	12.2	9.3	0.58		37
FR-101	0	12648.0	-8141.3	2866.2	3579	20	16.34	16.34	1956	9.0	5.7	11.0	6.8	6.3	0.49	MED - 64"	46
FR-309	0	12703.2	-8159.0	2865.6	3878	23	15.04	15.04	1959	9.0	5.5	14.0	7.1	6.5	0.49		43
FR-324	0	12999.2	-10534.3	2853.0	3303	22	19.76	19.76	1959	22.0	6.2			6.2	0.48		
FRA-025	0	12842.5	-7629.9	2915.5	4023	27	16.87	16.87	1949	14.0	4.9	13.0	6.2	5.5	0.45		
FRA-027	0	12739.7	-8042.7	2876.4	3824	23	16.03	16.03	1949	7.0	4.5	16.0	7.2	6.4	0.49		
FRA-031	0	11014.1	-8137.6	2862.2	2972	9	8.39	8.39	1947	4.0	4.7	5.0	7.5	6.3	0.48	DEEP -10'	34
FRA-044	0	13127.3	-7930.6	2898.9	4087	32	19.98	19.98	1949	13.0	5.1	19.0	6.7	6.1	0.48	DEEP -10'	
FRA-072	0	12991.1	-8401.0	2863.1	3802	26	16.56	16.56	1948	12.0	7.3	14.0	7.3	7.3	0.52		
FRA-081	0	11704.4	-9497.5	2860.7	2996	22	20.30	20.30	1953	12.0	9.6	10.0	9.4	9.5	0.58		59
FRA-209	1	12961.7	-10069.6	2828.4	2986	33	30.28	30.28	1960	18.0	11.9	15.0	7.8	10.0	0.59	DEEP - 10'	
FRA-311	0	13542.8	-8175.5	2886.4	4209	36	21.50	21.50	1955	25.0	6.9	11.0	4.5	6.2	0.48		
FRA-316	0	13699.0	-8696.4	2863.7	4064	42	26.09	26.09	1955	42.0	9.5	0.0	0.0	9.5	0.58		
J -004	0	10993.7	-9003.2	2841.7	2879	14	13.79	13.79	1944	14.0	16.7			16.7	0.68	6FF40	56
J -005	0	11438.4	-9301.0	2852.3	2955	19	17.95	17.95	1950	14.0	16.2	5.0	12.2	15.1	0.67		57
J -006	2	11189.2	-9036.9	2840.9	2953	15	14.96	14.96	1966	10.0	12.3	5.0	5.4	10.0	0.59	OBM	51
J -014	0	11799.6	-9850.0	2890.9	3133	23	20.82	20.82	1945	11.0	12.3	12.0	10.5	11.4	0.62	DEEP -10'	48
J -014	1	11799.7	-9858.7	2888.3	3135	21	18.60	18.60	1955	21.0	9.5			9.5	0.58	MED - 5'	51
J -016	1	10763.2	-8694.9	2830.5	2899	12	12.00	12.00	1955	8.0	12.8	4.0	8.6	11.4	0.62	40"	42
J -017	0	11433.8	-9410.6	2859.2	2960	18	17.32	17.32	1949	13.0	14.3	5.0	14.8	14.4	0.66	DIL	54
J -017	2	11379.4	-9106.1	2839.9	2936	16	15.52	15.52	1964	16.0	9.1			9.1	0.57		50
J -017	3	11344.9	-9051.3	2840.5	2938	15	14.65	14.65	1983	11.0	8.9	4.0	5.4	8.0	0.54		50
J -018	0	10909.3	-10243.9	2909.7	2980	17	16.64	16.64	1947	7.0	6.1	10.0	9.9	8.3	0.55	DEEP -10'	58

TABLE 1

Wellid	Rd	X	Y	TVD	MD	Sand Count	Net Thick	Oil Thick	Spud Date	Feet	Ohm-m	Feet	Ohm-m	Average Rt	So		PCT ST
J -020	0	11317.6	-9255.7	2852.3	2952	17	16.21	16.21	1947	13.0	9.9	4.0	8.1	9.5	0.58	?	53
J -023	0	10829.3	-9850.0	2889.9	2911	16	16.00	16.00	1950	16.0	9.7			9.7	0.59	DEEP -10'	55
J -031	0	10810.5	-9275.7	2854.5	2924	6	5.86	5.86	1950	6.0	4.3			4.3	0.38	DEEP -10'	37
J -032	0	11952.0	-9602.2	2876.9	3231	22	18.78	18.78	1950	15.0	11.3	7.0	10.8	11.1	0.61	DEEP - 10'	51
J -033	0	11345.2	-9888.5	2883.4	3026	22	20.96	20.96	1950	17.0	13.5	5.0	15.6	14.0	0.66	DEEP - 10'	56
J -034	0	10783.9	-10408.4	2935.7	3017	15	14.54	14.54	1950	15.0	9.0			9.0	0.57		45
J -035	0	11255.7	-10996.7	2992.4	3304	16	13.40	13.40	1950	16.0	3.3	0.0	0.0	3.3	0.29	DEEP -10'	53
J -037	0	11015.8	-8674.0	2836.8	2923	12	11.68	11.68	1951	4.0	7.6	8.0	13.5	11.5	0.62		44
J -038	0	11524.3	-9685.9	2877.2	3010	22	17.79	17.79	1951	15.0	13.8	7.0	13.8	13.8	0.65	DEEP -10'	53
J -039	0	10994.8	-9722.6	2870.4	2892	17	17.00	17.00	1951	14.0	14.3	3.0	5.9	12.8	0.64	MED - 5'	54
J -040	0	11216.4	-9842.8	2876.0	2914	22	22.00	22.00	1951	16.0	12.0	6.0	15.0	12.8	0.64	DEEP -10'	61
J -044	0	11024.6	-8326.9	2849.6	2991	10	9.23	9.23	1951	4.0	8.4	6.0	9.5	9.1	0.57	DIL	24
J -046	0	11402.8	-9517.2	2860.2	2947	18	17.62	17.62	1951	10.0	14.1	8.0	14.2	14.1	0.66	DEEP -10'	37
J -046	2	11400.2	-9441.7	2855.3	2940	19	18.60	18.60	1982	19.0	9.5			9.5	0.58	DEEP -10'	57
J -047	0	12000.8	-9667.2	2888.3	3195	20	17.83	17.83	1951	13.0	10.3	7.0	10.8	10.5	0.60		46
J -048	0	12073.2	-9708.5	2890.0	3172	23	19.49	19.49	1951	13.0	10.8	10.0	12.0	11.3	0.62	MED -5'	48
J -052	0	11337.8	-9947.1	2884.9	2950	23	22.25	22.25	1951	17.0	13.8	6.0	8.6	12.4	0.63	MED -5'	53
J -066	0	10857.7	-9422.2	2858.6	2879	10	10.00	10.00	1952	10.0	10.5			10.5	0.60	MED -5'	40
J -067	0	10891.2	-9248.9	2852.8	2950	12	11.30	11.30	1952	6.0	10.8	6.0	10.8	10.8	0.61		42
J -079	0	11395.7	-9703.8	2869.4	2945	21	20.07	20.07	1953	15.0	13.8	6.0	11.1	13.0	0.64	MED -5'	55
J -109	0	12495.3	-10058.4	2909.0	3078	29	28.74	28.74	1954	17.0	8.6	12.0	7.3	8.1	0.55		67
J -115	0	10838.2	-9387.3	2862.6	2885	10	9.89	9.89	1960	5.0	9.7	5.0	9.7	9.7	0.59		43
J -115	1	11089.0	-9410.6	2859.8	2893	15	15.00	15.00	1965	15.0	10.2			10.2	0.60	MED - 5'	51
J -117	0	10855.3	-9803.1	2880.6	2902	16	15.95	15.95	1960	9.0	10.5	7.0	9.2	9.9	0.59		48
J -118	0	10775.2	-8528.2	2838.7	2910	11	10.03	10.03	1960	11.0	10.9			10.9	0.61		36
J -119	0	11119.6	-8971.9	2835.8	2920	15	14.68	14.68	1961	15.0	11.5			11.5	0.62	DIL	51
J -120	0	11473.9	-9256.2	2855.1	3000	19	17.14	17.14	1961	19.0	11.9			11.9	0.63	40"	54
J -120	2	11591.9	-9181.2	2850.1	2985	19	17.90	17.90	1983	19.0	7.5			7.5	0.53		
J -121	0	11093.8	-8638.7	2844.2	3007	12	10.35	10.35	1961	12.0	10.3			10.3	0.60	6FF40	38
J -122	0	11077.8	-9116.4	2846.6	2925	12	11.73	11.73	1961	8.0	8.2	4.0	6.3	7.6	0.53		46
J -123	0	11257.9	-8868.5	2832.2	2969	14	13.46	13.46	1961	14.0	10.9			10.9	0.61	6FF40	46
J -124	0	12685.8	-10124.6	2905.8	3095	24	23.72	23.72	1961	24.0	8.5			8.5	0.56	6FF40	55
J -130	0	10960.6	-8957.0	2839.0	2893	14	14.00	14.00	1962	9.0	16.8	5.0	7.0	13.3	0.65	6FF40	53
L -310	0	13092.1	-10642.2	2880.4	3168	25	21.03	21.03	1964	25.0	6.0			6.0	0.47	806M-191	
L -314	0	13167.8	-10795.9	2912.9	3278	29	22.33	22.33	1964	29.0	4.5			4.5	0.39		
L -320	0	13541.9	-10964.9	2861.0	3339	25	19.67	19.67	1964	11.0	5.4	14.0	6.3	5.9	0.47	6FF40	
L -341	0	13761.0	-11256.4	2873.2	3428	23	18.85	18.85	1964	12.0	3.9	11.0	6.9	5.3	0.44	MED - 5'	
L -343	0	13705.0	-11286.8	2878.8	3414	20	16.01	16.01	1964	8.0	4.8	12.0	8.1	6.8	0.51		
SFJ-113	0	10817.4	-8119.5	2859.4	2993	9	8.46	8.46	1958	3.0	7.4	6.0	7.4	7.4	0.53		36

TABLE 1

Wellid	Rd	X	Y	TVD	MD	Sand Count	Net Thick	Oil Thick	Spud Date	Feet	Ohm-m	Feet	Ohm-m	Average Rt	So	PCT ST
#A -035	0	11410.7	-8091.2	2861.4	3147	0	0.00	0.00	1947						ERR	
#A -056	0	12053.2	-8671.8	2873.6	3258	19	16.10	16.10	1948						ERR	
#A -068	0	11919.9	-8647.6	2855.7	3178	18	15.03	15.03	1947						ERR	
#A -070	0	11641.8	-8866.1	2853.6	3031	17	14.99	14.99	1948						ERR	
#A -091	2	13583.5	-9118.6	2823.4	3912	0	0.00	0.00	1958						ERR	
#A -094	0	12240.5	-9118.3	2886.2	3215	23	17.22	17.22	1948						ERR	
#A -160	0	13261.2	-9760.1	2831.2	3218	25	19.78	19.78	1963						ERR	
#A -163	0	12804.1	-9852.6	2827.6	3055	24	21.25	21.25	1961						ERR	
#A -168	2	12858.0	-9294.7	2803.3	3186	0	0.00	0.00	1963						ERR	
#A -169	0	12776.3	-9744.4	2818.0	3095	22	17.08	17.08	1951						ERR	
#A -191	0	13485.2	-9208.9	2837.8	3468	0	0.00	0.00	1951						ERR	
#FRA-074	0	12532.8	-8656.5	2860.5	3467	16	11.48	11.48	1948						ERR	
#J -016	0	10791.6	-8195.2	2861.1	3033	10	8.90	8.90	1950						ERR	
#J -050	0	10724.3	-8958.8	2844.3	2877	0	0.00	0.00	1951						ERR	
#L -312	0	13024.4	-10600.8	2893.5	3088	0	0.00	0.00	1964						ERR	
				2863.1	Average		18.5								0.6	49.8
				2803.3	Minimum		0.0								0.0	24.0
				3044.7	Maximum		34.0								0.7	70.0

* The FJ-091 2 oil saturation for Soi was fabricated to provide for a control point. The Hx0 is at the bottom of the well and may not be reliable. The calculated Soc is 0.18 and was used for the Soc models.

Appendix #2

Sonic Logging to Detect Bypassed Hydrocarbons in the Wilmington Field, CA

reprinted from
Clark, D.D., Otott, G.E., and Phillips, C.C. (eds.),
Old Oil Fields and New Life: A Visit to the Giants of the Los Angeles Basin, AAPG/SPE, Bakersfield, CA, 57-65, 1996.

Daniel Moos
Stanford University
Department of Geophysics
Stanford, CA 94305-2215

F. Scott Walker
Tidelands Oil Production Company
Long Beach, CA

Donald D. Clarke,
Department of Oil Properties
Long Beach, CA

INTRODUCTION

Theoretical relationships, confirmed by laboratory and field data, suggest that hydrocarbon-bearing rocks in situ can be differentiated from rocks containing brines using sonic velocity measurements. A project to test this technique has been undertaken in the Wilmington Field, California, with co-funding from the Department of Energy (DOE cooperative agreement no. DE-FC22-95BC14934). Models, using values of fluid and formation properties typical of the Miocene-age turbidites within the target interval, confirmed that it should be possible to differentiate between hydrocarbon and non-hydrocarbon bearing sands in this field using compressional and shear wave sonic velocity logs. To date six wells (ranging in age up to 50 years) have been logged through casing with a multipole sonic logging sonde. Velocities measured in the open hole agreed with those measured after casing was installed in the most recently drilled well. Although compressional velocities have been determined in all but one case, shear-wave velocities have been obtained in only two of the six wells. Predictions of oil saturation are in qualitative agreement with models and prior measurements. However, one surprising result is that porosity can be determined from shear-wave velocity logs through casing. This may prove to be important in the future when through-casing resistivity logs become commercially available.

THE WILMINGTON FIELD

The Wilmington field is located within a NW-SE trending faulted anticline beneath and immediately offshore of Long Beach, CA (Figure 1). The first successful well was drilled in 1936. As of 1967, more than 1.2 bbls of oil and 840 Tcf gas had been produced, and it was believed that more than 1.8 bbls of oil still remained. Initial production was enhanced by a waterflood started in the 1950's primarily to mitigate surface subsidence which had reached more than 29 feet in the center of the bowl directly overlying the region of greatest production. Injection wells are located at the margins of the field, and production continues from the center.

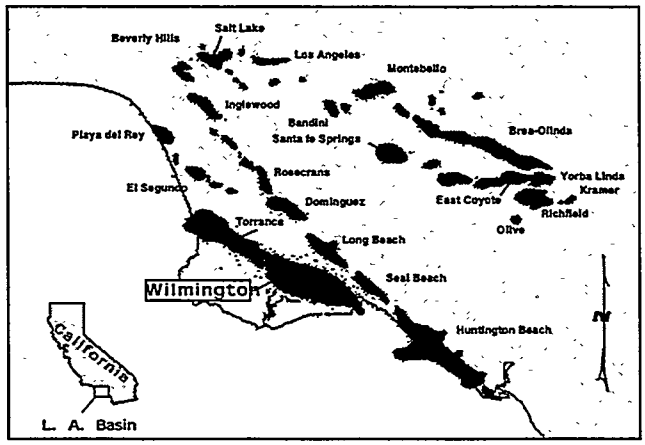

Figure 1: Location map, showing the Wilmington Field and other oil fields within the Los Angeles Basin (after Mayuga, 1968).

Production at Wilmington is from a thick sequence of clastic slope sediments (unconsolidated, low maturity, turbiditic arenites and clean arenites with porosities exceeding 25% and permeabilities of 100's of millidarcys, interlayered with sandy clays (wackes) containing 50% or more detrital smectite). The producing horizons lie between depths of 2350 and about 6000 feet. The hydrocarbons produced at Wilmington range from API gravity 12 (Tar zone) to API gravity 18-19 (Ranger and Upper Terminal Zones) to API gravity 27 (Lower Terminal). API gravities as high as 30 are produced from deeper sections of the field (the Union Pacific, Ford, and 238 zones).

THEORETICAL BASIS OF THE SONIC DETECTION TECHNIQUE

Generally, when a rock is loaded under an increment of compression, such as from a passing seismic wave, an

increment of pore pressure change is induced, which resists the compression and therefore stiffens the rock. The low-frequency Gassmann (1951) - Biot (1956) theory predicts the resulting increase in effective bulk modulus, K_{sat}, of the saturated rock:

$$\frac{K_{sat}}{K_0 - K_{sat}} = \frac{K_{dry}}{K_0 - K_{dry}} + \frac{K_f}{\phi(K_0 - K_f)} \qquad (1)$$

where ϕ is the porosity and K_0, K_f, and K_{dry} are the bulk moduli of the mineral material, the pore fluid, and the dry rock, respectively. Gassmann predicted no change for the isotropic shear modulus with saturation, $\mu_{sat} = \mu_{dry}$. The bulk and shear moduli are related to the compressional wave velocity, V_P, shear wave velocity, V_S, and density, , through the familiar equations:

$$V_P = \sqrt{\frac{K + \frac{4}{3}\mu}{\rho}} \qquad V_S = \sqrt{\frac{\mu}{\rho}} \qquad (2)$$

Equation (1) assumes a homogeneous mineral modulus and statistical isotropy of the pore space, but is free of assumptions about the pore geometry. Most importantly, it is valid only at sufficiently low frequencies such that the induced pore pressures are equilibrated throughout the pore space (i.e., that there is sufficient time for the pore fluid to flow and eliminate wave-induced pore pressure gradients).

These theoretical predictions have been confirmed qualitatively by a number of field studies. For example, seismic detection of free gas exploits this fluid effect, because the abrupt increase in fluid compliance due to the gas generates a very large P-wave impedance contrast, producing a "bright spot" on a reflection seismic record. More recently, bright spots have also been observed to occur at oil/water interfaces(Clark, 1990). Using sonic P- and S-wave velocity logs, Williams (Williams, 1990) demonstrated an Acoustic Log Hydrocarbon Indicator (ALHI) which was based on the difference between measured V_P/V_S and that predicted for a water-saturated rock from the shear-wave velocity. More recent results indicate that elastic properties may vary systematically with saturation (Hornby, et al., 1992).

Predictions for Wilmington

The ability to detect hydrocarbons using elastic waves depends both on the amount by which their properties differ from those of brines and the degree to which those properties control the velocities of the saturated rock. Several factors influence the properties of the fluids at reservoir conditions. In general, density, bulk modulus and viscosity all decrease with increasing API number (decreasing density) and temperature and increase slightly with increasing pressure. Gas in solution has a large effect, even in comparison to that of temperature, in reducing density and bulk modulus. Using equations presented in Batzle and Wang (1992), it is straightforward to determine the properties of reservoir fluids.

These can then be applied, using the Biot-Gassmann relations, to predict the elastic-wave velocities as a function of depth. Figure 2 shows the predicted shear and compressional velocities and the velocity ratios as a function of depth and pore fluid for an assumed porosity of 30%. These results suggest that, for basin clastics such as those found at Wilmington, seismic velocities are quite sensitive to the properties of the pore fluids. And, for the expected properties of the actual pore fluids, the sonic detection technique should be quite successful at differentiating between sands with high saturations and those in which the hydrocarbons have largely been replaced with water.

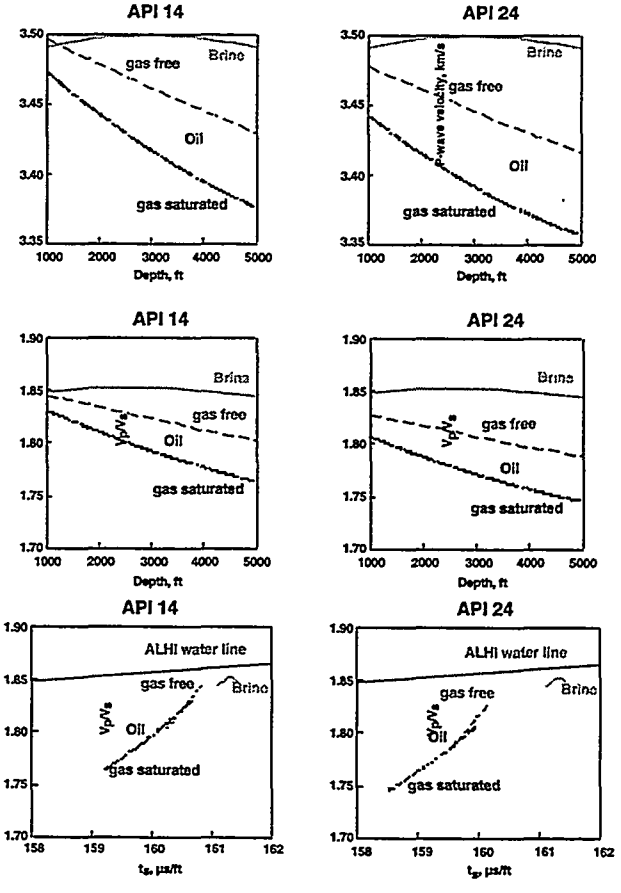

Figure 2: Elastic-wave velocities predicted for a 30% porosity Wilmington sand saturated with various pore fluids (after Moos, et al., 1995). Also shown are cross plots of V_P/V_S vs. dt_S, including the Williams (1990) ALHI water line for comparison.

RESULTS IN M-499

Well M-499 was completed in the Upper Terminal Zone of Fault Block IV in an area previously considered to be watered out. To evaluate the production potential from selective recompletion of an existing well, M-499 was selectively perforated only in sands with oil saturations above 40%, based on the analysis of open-

hole well logs. New high power, low frequency (1.2-2.5 kHz) monopole and dipole sonic logs (Chen and Eriksen, 1991) were recorded to evaluate their ability to measure formation porosity and oil saturation through casing as a guide in carrying out selective recompletions in existing wells. Compressional-wave velocities were determined from analysis of monopole waveforms. Shear-wave velocities were determined through analysis of the dipole waveforms.

The very high energy and low center frequency of the source results in a depth of investigation which is more than ten times that of typical sonic logs, allowing data to be recorded in both open and cased holes. By exciting dipole modes in the wellbore, shear-wave velocities can be determined even in "slow" formations (that is, with shear-wave velocity below 1.5 km/s or shear-wave slowness (dt_S) above 200 μs/ft). And, by separately recording the waves on opposite sides of the tool, one can differentiate between true dipole modes, which provide information on the shear-wave velocity, and tube waves, which can interfere with the dipole mode in cased holes.

Sonic data were recorded in M-499 both before and after the installation of casing (Moos, et al., 1995). The velocity data presented here were determined from the cased-hole measurements. A comprehensive suite of open-hole logs was also recorded in the well to guide in completion decisions and for comparison to analyses of porosity and saturation using the sonic data.

Porosity

It is generally accepted that in hard rocks conventional (compressional-wave) sonic logs can be used to determine porosity through the use of the Wyllie time-average equation or Raymer's relationship. However, experience has demonstrated that these techniques cannot be used to determine porosity in fields such as Wilmington. This is largely because of the unconsolidated nature of the rocks in these fields (Moos, et al., in press). Furthermore, dt_P is affected both by porosity and by other factors such as fluid properties. Because the shear wave is (theoretically) relatively unaffected by the fluid, it should be possible to derive a porosity log from dt_S, provided an appropriate model is used to relate porosity to velocity.

A further benefit of using shear-wave velocity to determine porosity is that such logs can be run through casing in most instances. And, they have a much greater radius of investigation than nuclear logs (Westaway, et al., 1981), making the result from shear-wave analysis a more reliable predictor of formation properties away from the near-wellbore zone.

Figure 3 shows porosity derived from shear-wave velocity using techniques described in Moos et al. (in press) for the entire logged interval in M-499. Also shown are porosities derived from empirical relationships (Moos, et al., 1995) and from the density log. There is excellent agreement throughout most of the logged interval between the different porosity measures, with the exception of washed-out sections within which the density log reads anomalously small values leading to overly large porosity estimates.

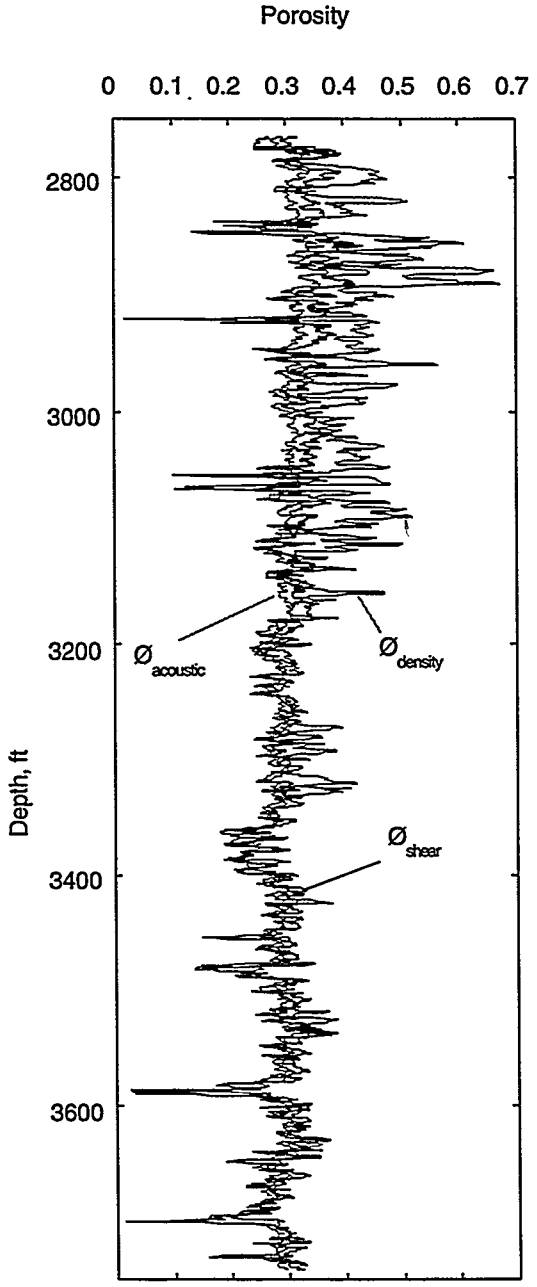

Figure 3: Porosity determined from a density log ($Ø_{density}$), from an empirical relationship developed using other data ($Ø_{acoustic}$) (Moos, et al., 1995), and from the theoretical relationship described in Moos et al. (in press); ($Ø_{shear}$). In general, there is excellent agreement between the two sonic porosity measures, whereas the density porosity is generally slightly greater, likely due in shallow sections to poor pad contact in the rugose hole.

Saturation

Figure 4 compares the ALHI water lines of Williams (1990) to data from the Upper Terminal section

of M-499. Based on William's analysis and Biot-Gassmann, oil-bearing units are predicted to lie below the water lines. As can be seen, a significant percentage of the depth interval logged is predicted to be oil-bearing.

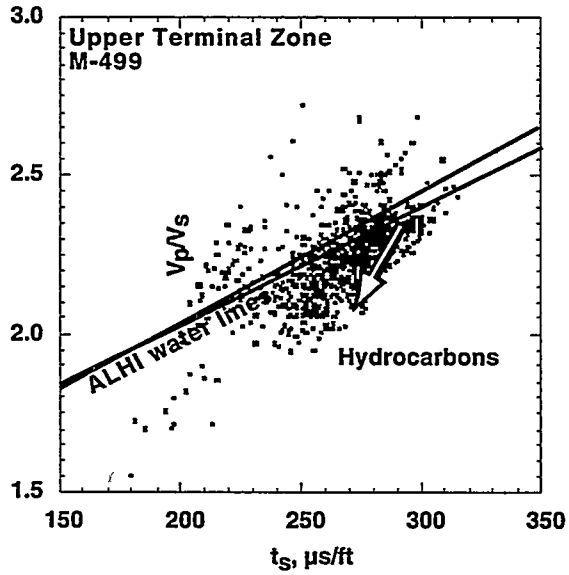

Figure 4. Crossplot of V_P/V_S vs. dt_S showing the ALHI water lines of Williams, compared to data from the Upper terminal of Hole M-499.

In Figure 5 the normalized distance from the water line is compared to saturation determined using Archie's Law for the Upper Terminal Zone. There is qualitative agreement between the two curves, with the exception of some intervals which are predicted to have high oil saturations based on the sonic data, but which do not appear to have high oil saturation based on the conventional log analysis. These zones can largely be eliminated from consideration for recompletion using geological constraints, data from recent offset wells, and production experience. Of more import is the observation that the intervals chosen for completion based on the conventional analysis are also predicted to have high oil saturation based on the sonic results.

RESULTS IN OTHER WELLS

Although the results from M-499 are promising, it is necessary to demonstrate first that it is possible to routinely obtain the sonic data necessary for this analysis, and second that the sonic technique can accurately differentiate between watered-out and potentially productive zones. To accomplish this the sonic logs were run in five more holes as summarized in Table I. Prior to running these additional logs the tool was modified to improve receiver characteristics and to allow independent recording of wave arrivals on opposite sides of the tool.

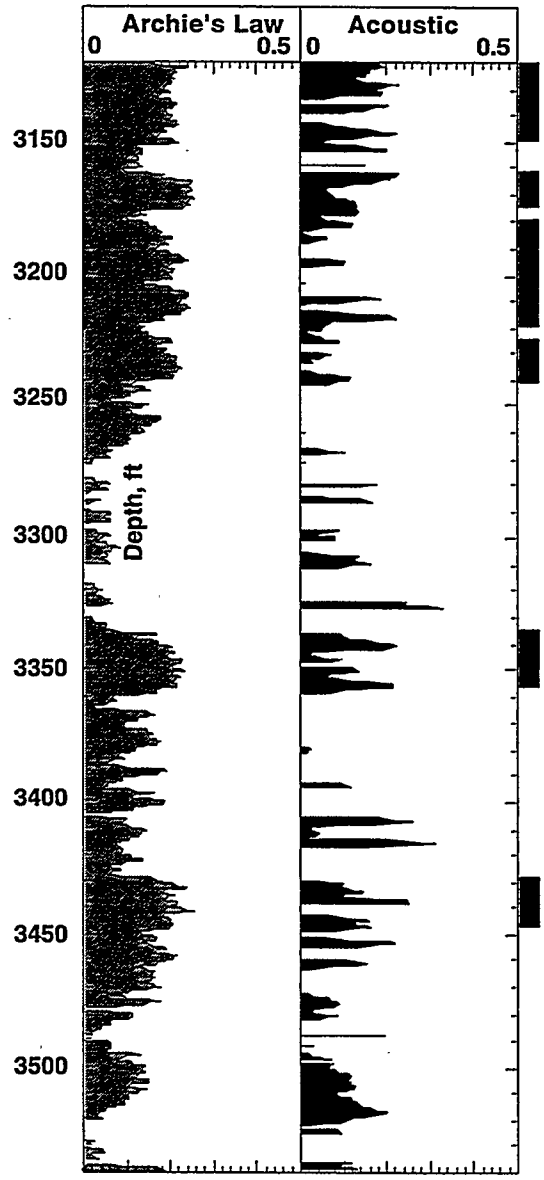

Figure 5. Saturation predictions based on Archie's Law and on the sonic data. Also shown are the intervals chosen for completion based on the Archie's Law analyses.

Table I: Summary of hole characteristics.

Hole	Depth Interval, kft	Deviation	Year Drilled	Well Type
M-499	2.8-3.7	43°	1993	Prospect
167-W	2.5-4.5	30°	1983	Water flood
FY-67	1.6-3.7	17°	1948	Water flood
Y-63	1.6-3.2	17°	1948	Prospect
X-32	3.0-5.6	-	1946	Prospect
J-15	1.2-2.9	vertical	1942	Prospect

Compressional-wave velocities were determined in all of these wells except in Y-63. In contrast, shear-wave velocities could be determined only in M-499 and in the uppermost few hundred and lowermost several hundred feet of hole 167-W. In the intermediate depth range within 167-W (from about 2900 to 3300 feet) the shear wave arrived at the same time and was characterized by the same frequency content as the interfering tube wave. In 167-W, the ability to record independently the wave arrivals on opposite sides of the tool was essential in differentiating between tube wave and the dipole mode.

Thus it appears that the critical determinants of the success of shear-wave logging are: (1) the age of the well, and (2) the shear-wave velocity. Deviation, leading to eccentering of the tool in the casing, and the casing in the hole, does not appear to be a problem in spite of the inevitable additional generation of tube-wave energy by the dipole source. Further study is needed to determine if factors such as the casing diameter and the cement thickness and bonding to the formation affect the quality of the dipole data.

Neither standard casing bond logs nor specialty logs which measure the azimuthal variation of bond using acoustic techniques provided unambiguous predictions of the quality of the sonic logs.

CONCLUSIONS

Based on the results so far, three conclusions can be reached. First, porosity can be determined accurately using shear-wave velocity in reservoirs such as Wilmington, provided the appropriate model for their relationship is used. Second, cased-hole shear-wave logging in formations such as the Wilmington sands is extremely difficult, due both to wellbore conditions and to the similarity of the dipole mode moveout and that of the tube wave. Furthermore, discrimination between these two modes, even where their moveout is different, requires separate recording of arrivals on opposite sides of the tool to verify wave mode symmetry. However, it is clear that if the data can be recorded it is possible to discriminate between watered out and potentially productive zones. Additional analysis of the data so far recorded and of new data will help to refine these preliminary conclusions.

REFERENCES CITED

Batzle, M., and Wang, Z., 1992, Seismic properties of pore fluids: Geophysics, v. 57, p. 1396-1408.

Biot, M.A., 1956, Theory of elastic waves in a fluid-saturated porous solid, II. Higher frequency range: J. Acoust. Soc. Am., v. 28, p. 179-191.

Chen, S.T., and Eriksen, E.A., 1991, Compressional and shear-wave logging in open and cased holes using a multipole tool: Geophysics, v. 56, p. 550-557.

Clark, V.A., 1990, The effect of oil under in situ conditions on the seismic properties of rocks: Geophysics, v. 57, p. 894-901.

Gassmann, F., 1951, Uber die elastizität poroser medien: Vierteljahrsschr. Naturforsh. Ges. Zuerich, v. 96, p. 1-23.

Hornby, B.E., W. F. Murphy, I., Liu, H.-L., and Hsu, K., 1992, Reservoir sonics: A North Sea case study: Geophysics, v. 57, p. 146-160.

Mayuga, M.N., 1968, Geology and Development of California's Giant - The Wilmington Oil Field, AAPG 53rd Ann. Meeting, Oklahoma City, OK, p. 47.

Moos, D., Dvorkin, J., and Hooks, A., in press, Application of Theoretically Derived Rock Physics Relationships for Clastic Rocks to Log Data - Example from the Wilmington Field, CA: Geophys. Res. Lett.

Moos, D., Hara, S., Phillips, C., Hooks, A., and Tagbor, K., 1995, Field test of acoustic logs for measuring porosity and oil saturation in a mature waterflood in the Wilmington Field, CA, SPE 29655, SPE Western Regional Meeting, Bakersfield, CA.

Westaway, P., Wittmann, M., and Rochette, P., 1981, Application of nuclear techniques to reservoir monitoring: Journal of Petroleum Technology, Jan 1981, p. 46-54.

Williams, D.M., 1990, The acoustic log hydrocarbon indicator *in* SPWLA 31st Annual Logging Symposium, June 24-27, Paper W.

Appendix #3

PAPER G7

VISCOELASTICITY AND DISPERSION IN UNCONSOLIDATED RESERVOIR ROCKS FROM THE WILMINGTON FIELD, CALIFORNIA

Carl T. Chang
Mark D. Zoback
Dan Moos

Stanford Borehole Geophysics Laboratory

ABSTRACT

Dry turbidite sand samples from the Wilmington field, Long Beach, California, exhibited creeping behavior in load controlled creep tests. Creep occurred at hydrostatic loads of 10 - 30 MPa, and axial loads of 4 MPa with 20 MPa confinement. Creeping time constants were approximately 10 hours. Ottawa sand samples tested in a similar manner do not exhibit creep. A standard linear solid model was fitted to the turbidite creep test data to determine if the difference between static and dynamic moduli measured in Paper G6 could be attributed to viscoelasticity, and to calculate the frequency dependent modulus. Based on the model, the crossover point from high to low frequency response came at .001 Hz, which reflects the high viscosity of these dry rocks. The close fit to the experimental data suggests that viscoelasticity may be responsible for the dispersion detected in the Wilmington Upper Terminal zone turbidite samples.

INTRODUCTION

Although viscoelasticity has been extensively documented in soil mechanics, the phenomenon has been traditionally associated with dewatering of saturated soils (Terzaghi, 1936). Terzaghi established that the reduction of void ratio in a saturated clay soil results in a transient pore pressure that carries the load. This pressure, known as the hydrostatic excess pressure, is dissipated at a rate which depends on the permeability of the soil mass and the load is eventually transferred to the soil structure in the consolidation process. Soil engineers use the oedometer consolidation test (El Refai, 1978) to study this time

dependent deformation. This simple test is a step load uniaxial strain (i.e., laterally constrained) test on a cylindrical sample in the drained state. This behavior is dependent on fluid saturation. Thus, it is unusual to observe time dependent consolidation oedometer tests on a dry and highly permeable sand. Dry sand creep is peculiar and unexpected in our pressure and temperature ranges since there is no hydrostatic excess pressure. Since creep is a manifestation of viscoelasticity, an alternate mechanism besides poroelasticity must be responsible for dry creep.

Viscoelasticity is clearly an important mechanism responsible for dispersion in saturated cemented rocks (Bourbie, 1987). Previous results investigating frequency dependent moduli in cemented rocks (Winkler, 1983) have established a relationship between the presence of pore fluids and matrix stiffness. The resulting dispersion is believed to be caused by inertial effects of the fluid moving in the pore volume (Biot, 1956, Mavko and Nur, 1979). Higher frequencies result in higher elastic stiffnesses. It is not obvious why a dry sample would display viscoelasticity, since it is generally understood to result from fluid saturation.

Dry rock creep is a crystalplastic flow mechanism. Creep has been detected experimentally (Robertson , 1960) in dry chalk samples compressed hydrostatically. Calcareous sediments will deform in crystalplastic flow at low temperatures unlike terrigenous clastics consisting of quartz grains. Pressures high enough to cause crystalplastic flow in quartz sandstones usually result in grain crushing and cataclastic flow leading to plastic deformation (Zhang et al, 1990). Zhang et al (1990) did not report detectable creep in their triaxial compression tests on Berea sandstone.

To describe creep and viscoelasticity, many phenomenological models have been developed (e.g., Bourbie et al, 1987). These consist of idealized mechanical components to represent linear viscosity and elasticity. The standard linear solid model is a simple example of an idealized viscoelastic material consisting of two springs and dashpot. This model, like all viscoelastic models, will have a stiff response for high frequency strains, and a compliant response for low frequency strains depending on the relative magnitudes of the elastic and viscous part of the modulus. Given the deformation response to a ramp force, the values of viscosity and elasticity can be extracted from the creep time constants. These parameters will roughly describe the mechanical behavior of the rock. By finding the frequency dependent moduli of the standard linear solid, one can estimate the frequency dependence of the rock sample.

EXPERIMENTAL PROCEDURE

In paper G6 we describe stress cycles on a sample of dry turbiditic sand in a pressure vessel. During one of the many runs, a series of axial compressions under confinement were performed. In all of the experiments, we observed creep during hydrostatic loading and axial loading. To keep this creep from superimposing itself on the unloading response of the rock during stress cycling, we let the samples sit for 5 to 10 hours after reaching peak stress. During these waiting periods, we recorded the strain on the samples. These were basically creep curves resulting from a constant stress rate ramp. The ramp was 4 MPa in 1 hour, under confining pressure varying from 10 to 25 MPa.

Our tests also included three creep tests on Ottawa sand samples. The first sample was clean Ottawa sand. The second sample was tested with 15% dry Montmorillonite clay mixed into the sand. The third sample was a 15% Montmorillonite clay sample with the clay premoistened, then air dried before compression. These tests investigated the possibility of clay content being responsible for creep.

RESULTS AND ANALYSIS

Data for the creep tests is shown below in Figure 1. A 4 MPa axial loading ramp test on a sample of Upper Terminal turbidite under 20 MPa of confining stress is shown. For approximately 5 hours, the sample was allowed to creep. The axial stress of 4 MPa and confining pressure of 20 MPa was maintained while the sample was monitored. The data shown shows the transient behavior after the pressure is shut in at t=0. We observed creep in hydrostatic tests as well (Figs. 1b, 1c). These tests show less creep than the axial case. They were performed under lower stresses and they had no shear stress. The clean Ottawa sand sample did not creep, nor did the mixture of dry Montmorillonite clay and Ottawa sand. The mixture of moistened then air dried Montmorillonite clay and Ottawa sand did show a creeping behavior (Fig. 1c) with approximately the same amount of strain as the hydrostatically tested Upper Terminal zone turbidite. The two Figures 1b and 1c show approximately the same amount of strain although over different times;

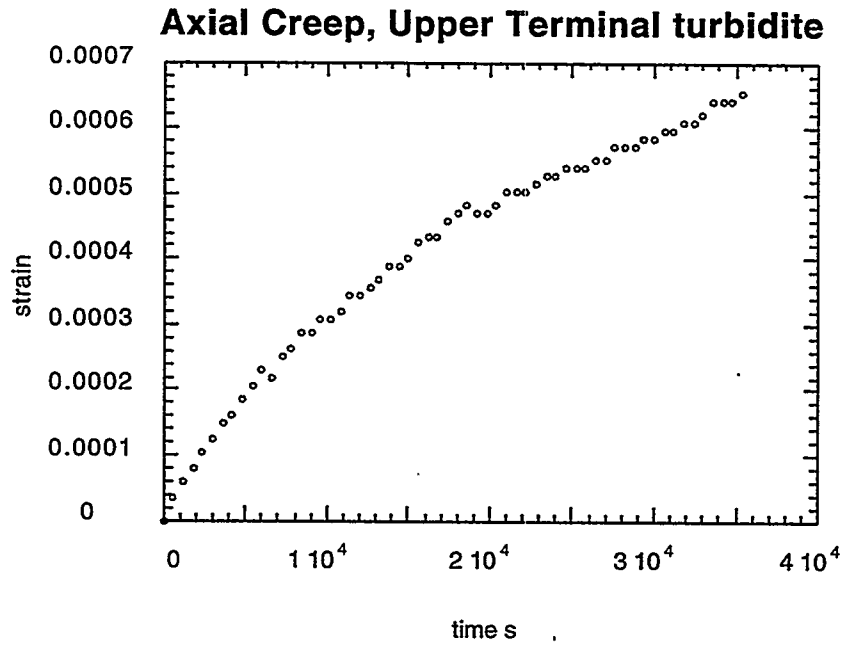

Figure 1a: Strain vs. time after loading to 4 MPa of axial stress in an Upper Terminal zone turbidite. The sample was under 20 MPa of confining pressure.

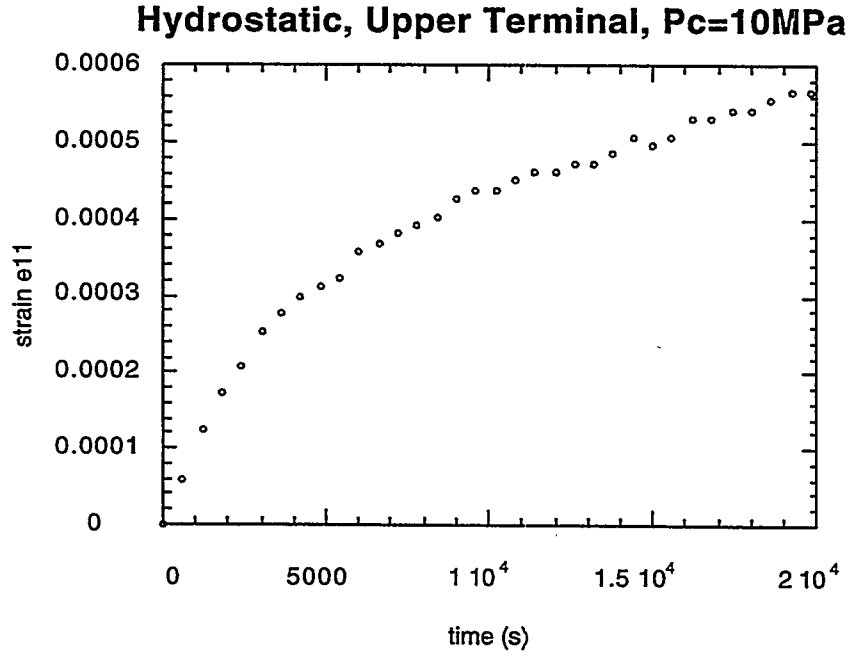

Figure 1b: Strain vs. time after loading to 10 MPa of confining stress in an Upper Terminal zone turbidite. Note the creeping is the same order of magnitude as in the axial case.

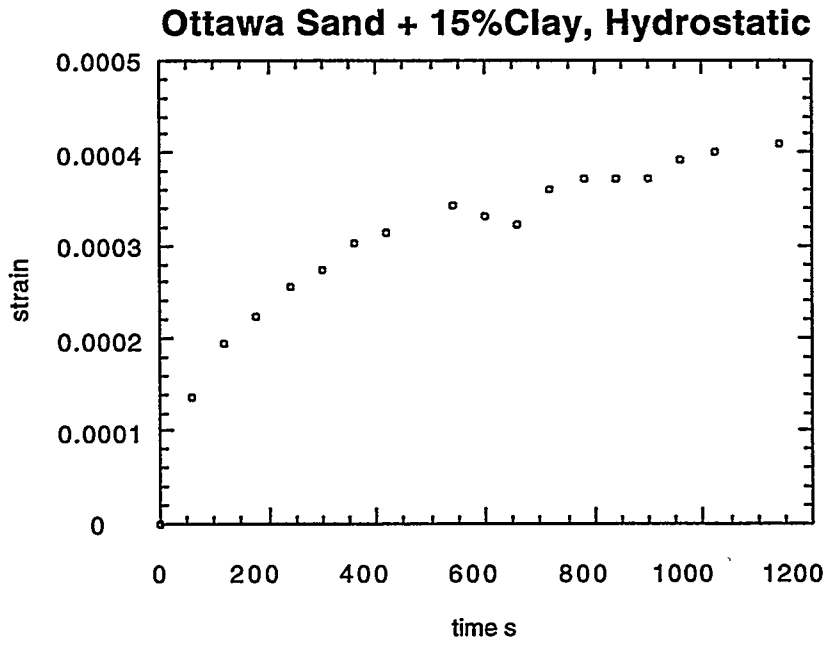

Figure1c: Strain vs. time after loading to 10 MPa of confining stress on an Ottawa sand sample mixed with 10% Montmorillonite clay. Although clean Ottawa samples showed no creep, adding Montmorillonite clay to a sample of Ottawa sand induced creep.

Using the standard linear solid viscosity model (Fig. 2), we attempted to modeled the mechanical behavior of our rock sample . The model is a combination of Hookean springs and a Newtonian dashpot. The relative values of these components determines the crossover point from high to low frequency behavior.

A simple differential equation can be written to describe the behavior of the solid in one dimension (see equation 1): T

$$\eta\dot{\sigma}_{11} + (E_1+E_2)\sigma_{11}=E_2(\eta\dot{\varepsilon}_{11}+E_1\varepsilon_{11}). \quad (1)$$

where η is the dashpot, σ the stress, ε the axial strain, and E1 and E2 the spring stiffnesses. The free parameters are the viscosity, and two spring constants.

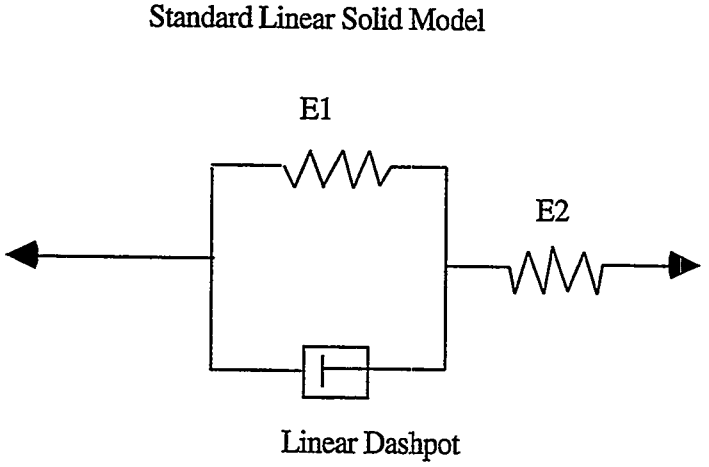

Figure 2: The standard linear solid viscoelastity model. The springs are Hookean and the dashpot is Newtonian.

Examining the behavior of these functions can relate the stress, strain, viscosity, elasticity, stress rate, and time for a model rock undergoing compression. We used Matlab, to calculate the creeping response given a 1 hour loading ramp (Fig. 3). The high frequency limit was calculated from the wave propagation experiments at high pressure (Paper G6). Initial estimates of the high and low frequency limits of the frame modulus E1 and were determined from lab data (Paper G6). The low frequency limit was approximated from the static bulk modulus and using the measured dynamic Poisson's ratio as .25. The data was fit by adjusting the viscosity. The raw axial data in Figure 1a was fit with the standard linear solid model to determine the parameters shown in table 1 resulting in Figure 3.

Viscosity (Pa.s)	1.85E+13
Spring 1 (Pa)	2.5E+9
Spring 2 (Pa)	1.0E+10

Table 1: Parameters determined by fitting the axial loading data.

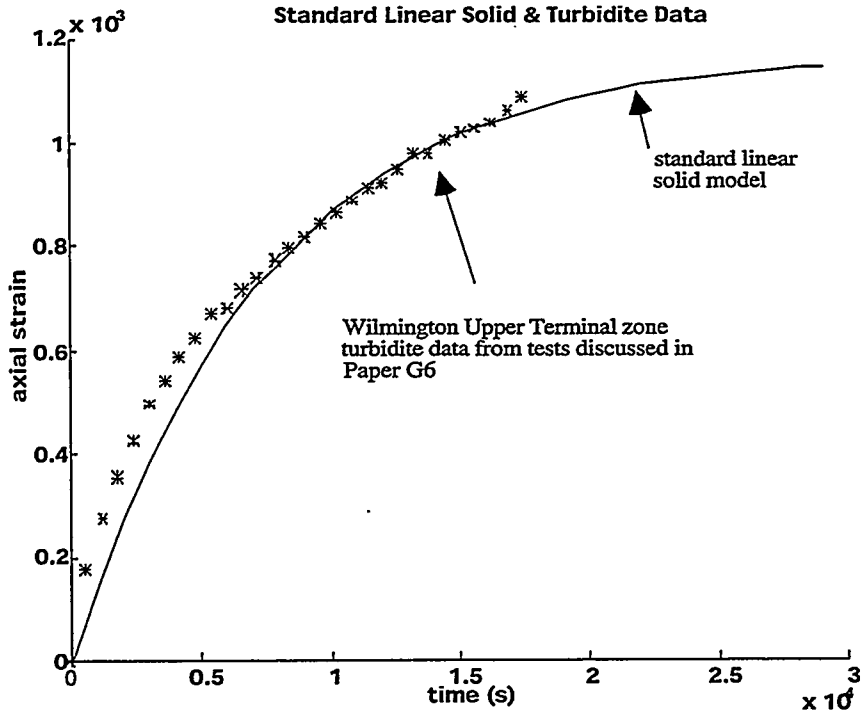

Figure 3: The fit of the axial loading data to the model.

After determining the model parameters, it is possible to determine the system's frequency dependence. The standard linear solid has a complex modulus of the form,

$$M(\omega)=\frac{E_2(E_1+i\omega\eta)}{E_1+E_2+i\omega\eta} \qquad (2)$$

By taking the magnitude of this complex number and plotting it as a function of frequency, we can determine the dispersive behavior of the system. As end members, the sample has the elasticity of the two springs in series at low frequency, and the second spring at high frequency.

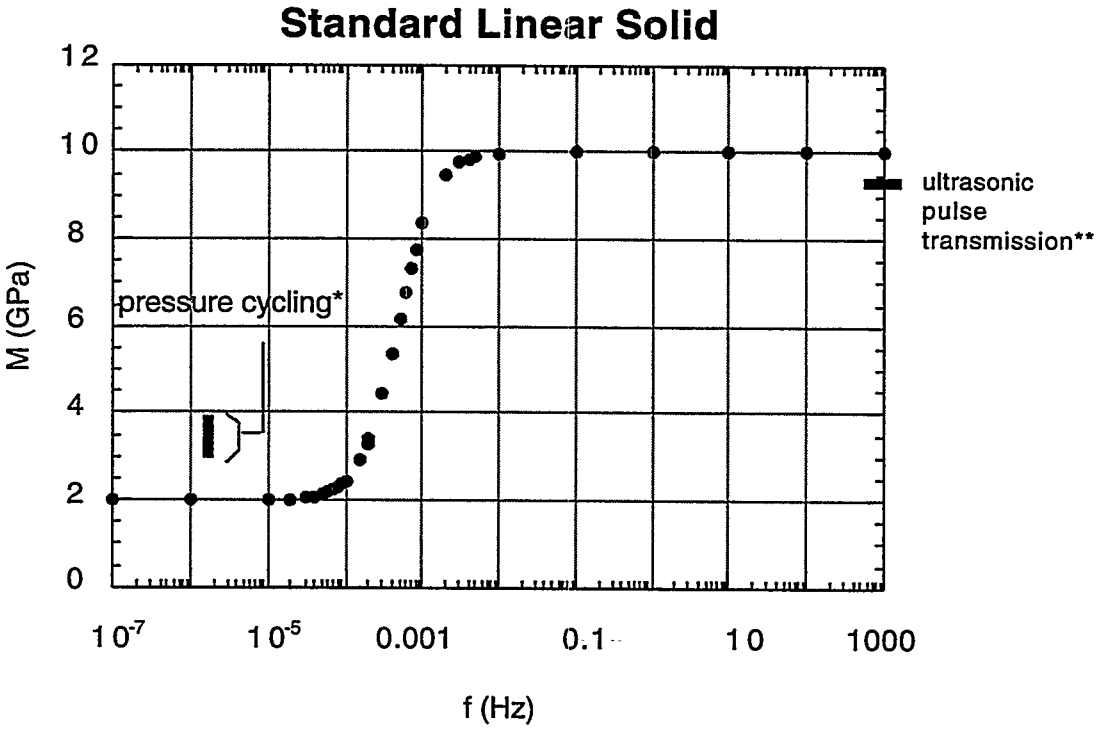

* using Kstat =2.5 GPa and (.25<Poisson's<.30).
**using Kdyn=5.5 GPa and (Poisson's=.25).

Figure 4: The magnitude of the modulus as a function of frequency. Note the low crossover point indicative of a highly viscous component in a compliant solid.

As expected from viscoelasticity, the model rock stiffens with loading rate. Also, there is a high frequency limit associated with high loading rates where the spring constant approaches the stiffness of spring #2.

DISCUSSION

The viscoelastic response of the sands tested may be an explanation for the relationship between static and dynamic modulus. The dispersion curve indicated that the sample was very viscous. Viscoelasticity is unusual in a dry sand, since we expect to find it associated with the discharge of pore fluids. We have several hypotheses, (1) microcracking could be leading to cataclasic flow of the grains, (2) strain amplitude differences between the high pressure loading of the sample and the ultrasonic measurement gives different moduli due to material nonlinearity, or (3) clay and mica between the grains may be affecting the overall modulus measurement for large

deformation. Given the amount of mechanical and microstructural evidence, hypothesis (3) appears to be the most likely mechanism.

Time dependent microcracking has been studied in fault mechanics to explain aseismic creep on faults (Costin, 1987). We may be looking at grain crushing and cataclasic flow (Zhang et al, 1990). This is improbable because cataclasis usually occurs at much higher pressures than we have gone to in the lab (Zhang et al, 1990). Grain angularity may get around this since stress concentrations can be quite large on a pointlike contact. However, at the temperatures and pressures of the experiment, this seems improbable.

Strain amplitude and sample nonlinearity is another possible reason for dispersion. The samples we deformed are nonlinear in both hydrostatic loading and triaxial loading. If the sample has a very nonlinear stress vs. strain response, a large amplitude strain may give a lower stiffness measurement since we are trying to describe the behavior with a single constant. The ultrasonic measurement is a small deformation that gives a more linear measurement since no inelastic deformation occurs. Tutuncu et al (1995) explained dispersive behavior of cemented sandstones with differences in strain amplitude. However, although this explains the large difference between static and dynamic modulus, it leaves the creeping behavior unaddressed.

Soft intragranular materials under high pressures could give rise to time dependent deformation. Analysis of thin sections reveals that of the samples indicated that much of the 20% mica fraction was placed between stronger grains of quartz, feldspar, and lithic particles. The mica was deformed during the natural consolidation process along the quartz boundaries and could dramatically affect the mechanical properties of the rock. Small amounts of clay in the matrix could give rise to a similar mechanical behavior, as suggested by the creep which occurred in the 15% Montmorillonite clay and Ottawa sand mixture, that exhibited creeping behavior. This seems to favor this mechanism as an explanation for the creeping behavior as well as the dispersion.

The relative values chosen for the viscosity and the elasticities in the model strongly suggest that the clay and mica hypothesis is correct. At low frequency, the turbidite is compliant, and very viscous. A well cemented sandstone saturated with water would represent a stiff set of springs and a very inviscid dashpot. A stiff rock matrix, represented by spring E1 in the model, combined with a smaller the viscous component, will result in less dispersion than a compliant matrix with the same viscous component. This was seen in Winkler (1983) where saturated experiments on fused glass beads showed less dispersion than saturated experiments on Massilon sandstone because of the glass beads' higher matrix stiffness. The turbidite dispersion results imply that the opposite is also true.

If the system is very compliant, represented by a weak spring E1, and highly viscous, represented by a large η, low frequency measurements such as creep tests will be dominated by the dashpot, while high frequency tests will be dominated by the spring E2 since the dashpot will be locked. This may explain the differences between the turbidite and Ottawa sand. It's possible that the micas and clays contribute the highly viscous term which dominates at low frequencies since the unconsolidated matrix is compliant. The Ottawa sand, although compliant, has no viscous mechanism and the high and low frequency elasticities E1 and E2 add in series resulting in a nearly linear response with no dispersion.

This phenomenological model along with the evidence from clay mixture tests and thin sections suggests that the intragranular clay and mica hypothesis is potentially a viable mechanism for dispersion in these samples.

CONCLUSION

The creep response of our Upper Terminal zone turbidite provides information about the mechanical behavior of the sample at high and low frequency. The experimental results suggested that the mica and clay content between the hard quartz grains may be the mechanism for responsible for viscoelasticity in dry sand. By modeling the mechanical behavior with a series of compliant springs to represent the poorly consolidated grains, and a very viscous dashpot, to represent the intragranular clays and micas, we determined the frequency dependent modulus of the rock. The combination of experimental data, thin section data, and modeling results, favor the soft intragranular mica and clay hypothesis as an explanation for the highly dispersive behavior.

ACKNOWLEDGMENTS

Special thanks to Tidelands Oil and The Department of Energy who funded this research. Also, thanks to New England Research, who constructed the pressure vessel and acquisition/control system for the apparatus. Thanks to Don Lowe of the Department of Geology, Stanford University for his help on the thin section analysis.

REFERENCES

Biot, M.A., 1956, "Theory of propagation of elastic waves in a fluid saturated porous solid." II. Higher-frequency range, J. Acoust. Soc. Amer., **28**, 168-178.

Bourbie, T., Coussy, O. and Zinser, B., 1987, "Acoustics of porous media", Gulf Publishing Company.

Costin, L.S. 1987, "Time -dependent deformation and failure", in "Fracture Mechanics of Rock", edited by B.K. Atkinson, Academic Press.

Dvorkin, J. and Nur, A., 1993, Dynamic poroelasticity: A unified model with the squirt and the Biot mechanism: Geophysics, **58**, 524-533.

El Refai, W.T.H, and Hsu, J.R., "Creep deformation of clays," Proc. ASCE J.Soil tech. Engng. Div., **104**, GT, 61-76, 1978.

Mavko, G. and Jizba, D., 1991, "Estimating grain-scale fluid effects on velocity disperion in rocks," Geophysics, **56**, 1940-1949.

Mavko, G., and A. Nur, 1979, "Wave attenuation in partially saturated rocks", Geophysics, **44**, p.161-178.

Robertson, E.C., 165) Robertson, Eugene C., et al. "Experimental consolidation of calcium carbonate sediment." 1962. U. S. GEOLOGICAL SURVEY PROFESSIONALPAPER ; P 0350, p. 82-83.

Tutuncu A.N.; Podio A.L.; Sharma M.M; "Nonlinear Viscoelastic Behavior of Sedimentary Rocks: I. Effect of Frequency", submitted to Geophysics, February 1995

Terzaghi, K., 1936, "The stability of slopes of natural clay," Proc. 1st Int. Conf. Soil Mech. Found.Engng., Cambridge, Mass., **1**, 161-165.

Winkler, K.W., 1983, Frequency dependent ultrasonic velocities of high porosity sandstones, Journal of Geophysical Research, **88**, 9493-9499.

Zhang, J., Wong, T.F., Davis, D.M., 1990, "High pressure embrittlement and shear-enhanced compaction of Berea Sandstone; acoustic emission measurement and microstructural observation", Rock mechanics; contributions and challenges; proceedings of the 31st U.S. symposium; Vol. **31**, p. 653-660.

PAPER G6

A COMPARISON OF DYNAMIC AND STATIC MODULI IN UNCONSOLIDATED RESERVOIR ROCKS FROM THE WILMINGTON FIELD, CALIFORNIA

Carl T. Chang
Dan Moos
Mark D. Zoback
Stanford Borehole Geophysics Laboratory

ABSTRACT

Measurements of the elastic properties of unconsolidated sand samples recovered from the Wilmington field, Long Beach, California have been made at pressures simulating in situ conditions. Dry samples were tested under hydrostatic loading to determine accurate values of the frame moduli for a related study on fluid detection from logs (see Paper G3). Dynamic shear and bulk moduli were calculated from P- and S-wave velocities determined during loading by pulse transmission. Both static and dynamic bulk moduli increase with pressure. However the dynamic bulk modulus is consistently three times higher than static bulk modulus. In the same experimental apparatus, a sample of dry Ottawa sand showed a nearly elastic strain response to hydrostatic pressure cycling, suggesting that constituents present in the turbidite and absent in the clean sand, such as micas and clays, were responsible for the anelasticity.

INTRODUCTION

In theory, static and dynamic modulus should be the same for an elastic material. This is observed in crystalline materials where both static deformations and deformation arising from wave propagation are small. However, this is not the case in sedimentary rocks. For example, in cemented sandstone, dispersion has been observed and attributed to the effects of fluid saturation in the pore space (Mavko & Nur, 1979). Wave attenuation and dispersion in saturated sandstone has been studied and documented (Murphy & Winkler 1982). Using simultaneous ultrasonic measurements and triaxial stress cycling, Tutuncu et al (1995) determined that apparent dispersion can also be a result of differences in strain amplitude between high and low frequency measurements.

Previous work on Upper Terminal zone turbidites from the Wilmington field, CA demonstrated that loading bulk moduli were more than six times smaller than moduli derived from simultaneous pulse transmission experiments. This is a consequence of irreversible pore compaction during loading, which was a result of plastic deformation associated with pore collapse (as suggested by Han, 1995, pers. comm.).

To compare dynamic and static moduli in a sample that yields plastically requires measurement of static modulus during unloading. Additionally, by simultaneously conducting pulse transmission experiments (e.g. Tutuncu et al, 1995), we can determine both the high-frequency small-strain modulus and the low-frequency large-strain modulus during elastic and elastoplastic limbs of each loading cycle. This isolates the loading and unloading moduli on two legs of the loading curve and yields a more realistic comparison of static and dynamic moduli.

EXPERIMENTAL PROCEDURE

As in last years' investigation of unconsolidated rock, core samples were obtained from the Wilmington field, Long Beach, California in well UP941b from a depth of 3233 feet. The samples were a fine grained turbidite sand from the Upper Terminal zone. Thin section analysis indicated that the sample consisted of approximately 20% quartz, 20% feldspar, 20% crushed metamorphic rocks, 20% mica, and 10% clay. The poorly sorted grains are highly angular with a mean grain size of 300 μm. After plunge cutting at room temperature with steel tubing we extruded the samples into soft polyolefin jacketing. The jacketed specimen was 1" in diameter and 2" long. Before testing, residual heavy oil was removed from the samples by flushing first with mineral spirits and then with air to dry the porespace. The samples were then wired to a transducer stack and placed in a pressure vessel for testing under room-dry conditions.

Cyclic loading was performed in the following manner (see Figure 1): the sample was initially pressurized to 10 MPa at a loading rate of 10^{-7}/s (the first loading leg). It was then allowed to sit for 5 hours to allow transient creep to subside (the creeping leg). Then the pressure was lowered to 5 MPa at 10^{-8}/s (the unloading leg). Similar cycles were repeated, with each cycle reaching a maximum confining pressure 10 MPa higher than the previous cycle, to a maximum confining pressure of 30 MPa. Simultaneous travel time measurements were made by propagating P- and S- waves along the axis of the cylinder using 1MHz quartz crystals as shown in Fig. 1. An automated data acquisition system recorded hydrostatic stress and axial deformation as well as the full waveforms transmitted through the sample. A sample of dry unsorted Ottawa sand was tested in a similar fashion.

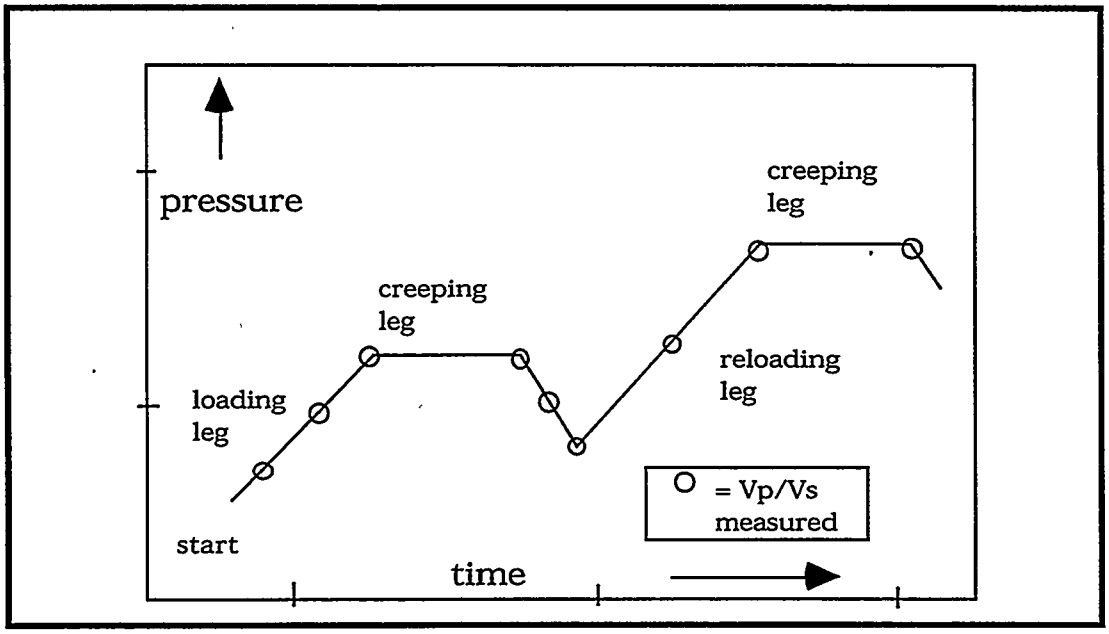

Figure 1: The loading process showing pressure vs. time. First the sample is loaded using a constant stress rate to a nominal pressure. The pressure is shut in and the sample is allowed to creep. The sample is then unloaded to an intermediate pressure then reloaded linearly to the next creeping leg.

RESULTS

Figure 2 shows the response of the turbidite and of the Ottawa sand to the loading history outlined above. The turbidite (Fig. 2a) shows a highly elastoplastic mechanical response; the difference in slope between a loading leg and the following unloading leg is due to irreversible plastic strain during loading. As in soil tests, the sample reloaded along the unloading curve until the previous maximum pressure was achieved, at which point the sample begins to yield plastically again and the loading curve continues along its previous path. When the loading was paused at the top of each cycle, the sample would creep for approximately 5 hours (see Paper G7). Therefore, we held the pressure constant before unloading the sample to allow transient creep to abate.

In the same experimental apparatus, the Ottawa sand sample showed a significantly different mechanical behavior. Although this sample had approximately the same mean grainsize, it behaved almost purely elastically, unlike the Upper Terminal zone turbidite. This is seen in the loading and unloading paths in Fig. 2b that nearly superimpose upon one another. The loading slope is greater than that of the turbidite sample, but the unloading slope is smaller. Nor did the Ottawa sand sample exhibit creeping behavior. Unfortunately, the return path from 30 MPa to 0 MPa wasn't recovered because of an acquisition failure towards the end of the test.

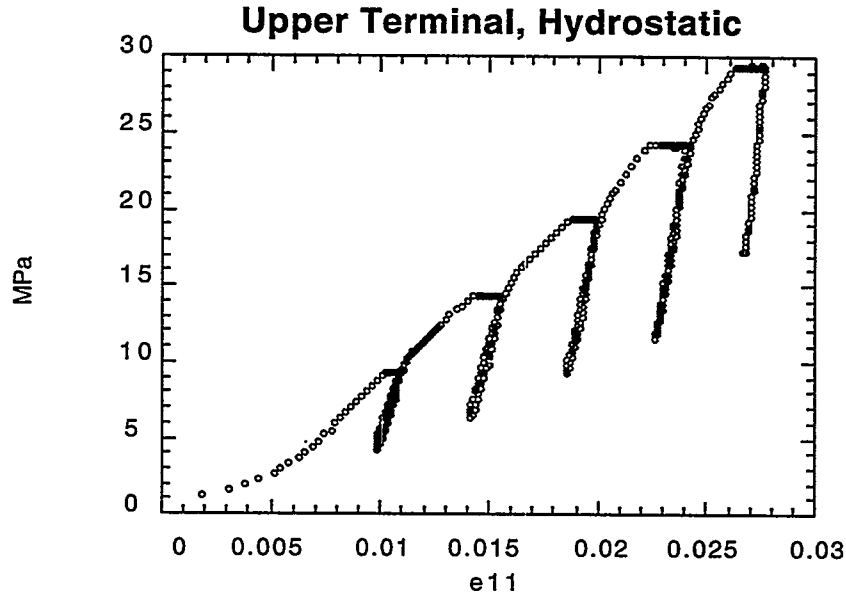

Figure 2a: The stress vs. strain response of the turbidite under hydrostatic loading. The curve shows a highly plastic response. Note that the unloading cycles have a higher slope than the loading cycles, yet, the successive loading cycle follows the previous loading curve.

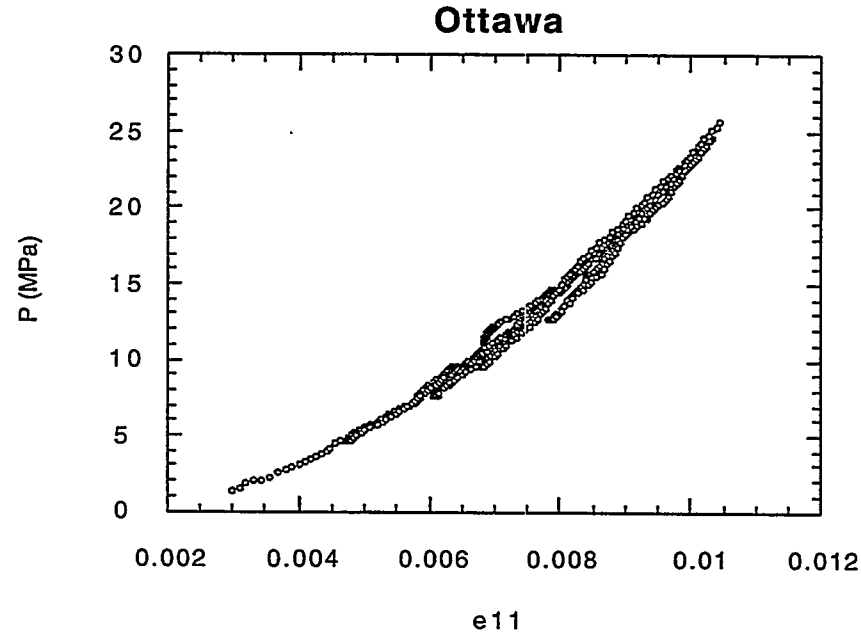

Figure 2b: The stress vs. strain curve for a similarly tested sample of dry Ottawa sand with approximately the same mean grain size, shows a significantly different elastic response. The final unloading curve is not shown here because of an acquisition failure at the end of the experiment.

Figures 3 and 4 show P - and S -wave velocities calculated from travel times of axially propagated waves and length corrected for strain. The velocities are consistent with results measured on other unconsolidated sand samples (Dominico, 1977, Estes et al, 1994). As with all sands, the velocity increases monotonically with pressure. Assuming linearity and isotropy, we calculated the dynamic elastic moduli for these velocities correcting for the deformed density from the volumetric strain. Velocity values are shown for the turbidite and Ottawa sand in Figure 5. The bulk moduli measured from velocity show the same increasing trend with increasing pressure. By calculating the slopes of the stress vs. strain curve during the unloading cycle exerted by the confining pressure we determined the static compressibility of the matrix. This value is plotted along with the dynamic moduli in Figures 6 and 7 for Upper Terminal turbidite and Ottawa sand respectively.

The dynamic Poisson's ratio is easily calculated from the Upper Terminal velocities (Figure 8). The value of 0.25 measured above about 5 Mpa is quite large, in comparison with data from clean sands reported in previous SRB volumes.

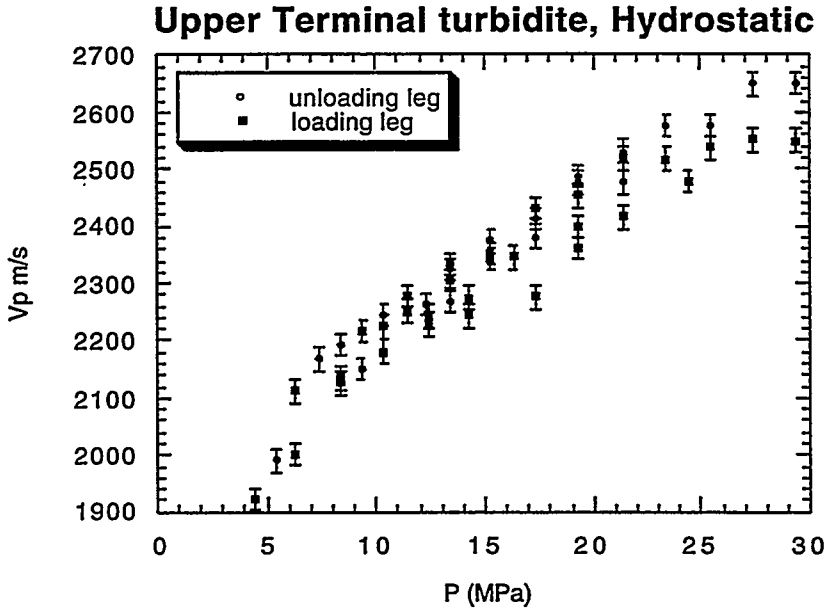

Figure 3: P- wave velocities in the turbidite calculated from the travel time along the axis of the sample corrected for axial strain.

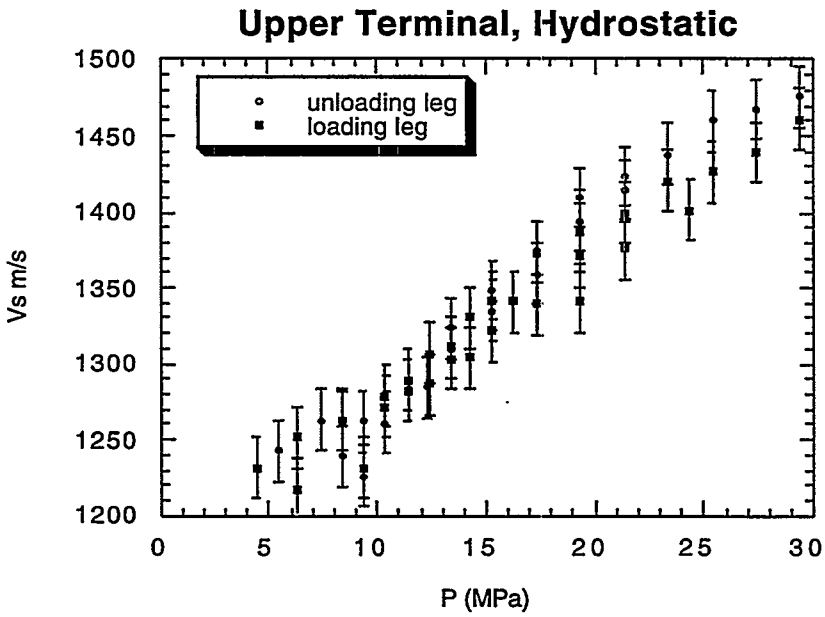

Figure 4: S-wave velocities in the in the turbidite calculated from the travel time along the axis of the sample corrected for axial strain.

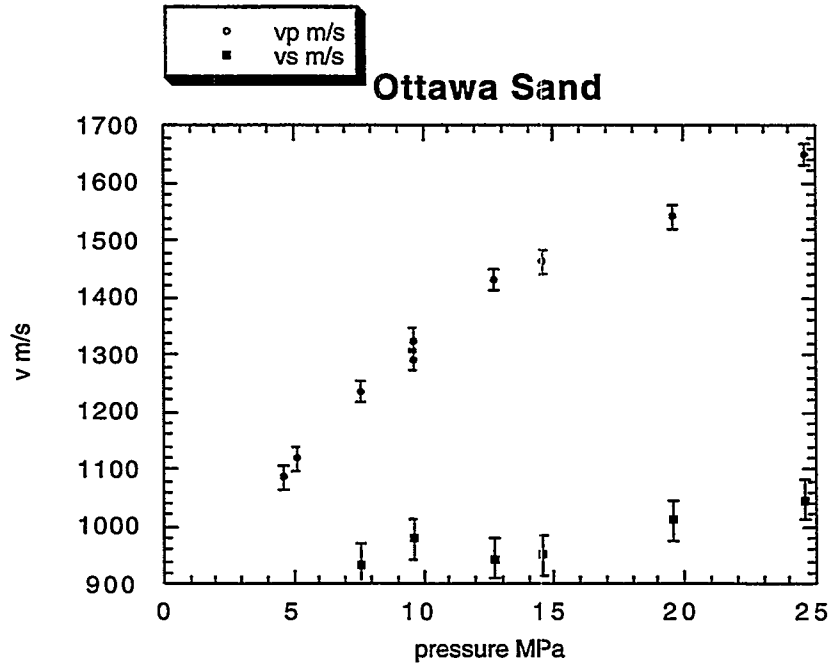

Figure 5: P - and S- wave velocities for Ottawa sand tested in the same apparatus. Data was only collected on the loading legs.

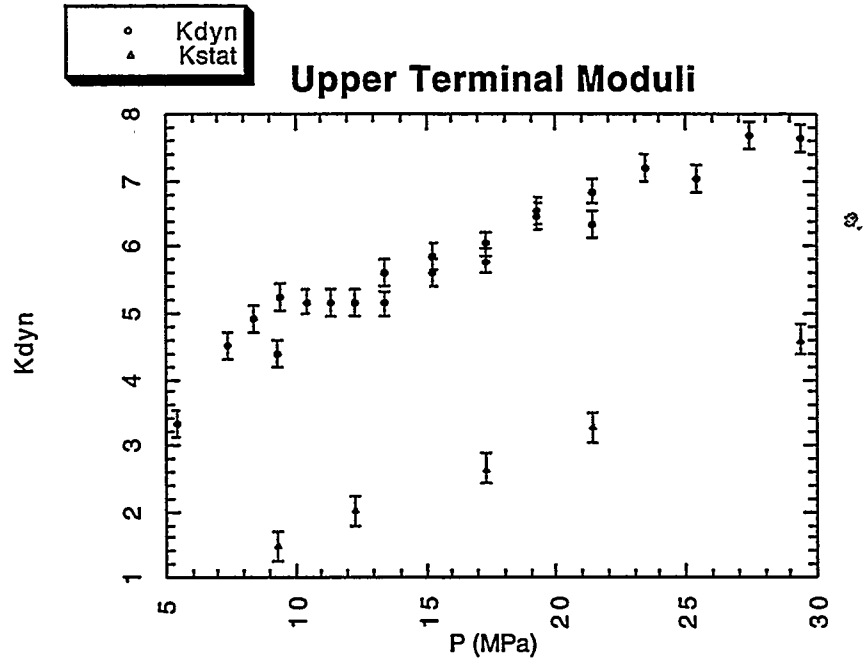

Figure 6: Bulk moduli of the turbidite sample. The static modulus (Kstat) shows the same increasing trend with pressure that the dynamic moduli (Kdyn) show, however it is significantly smaller than bulk modulus determined from wave propagation.

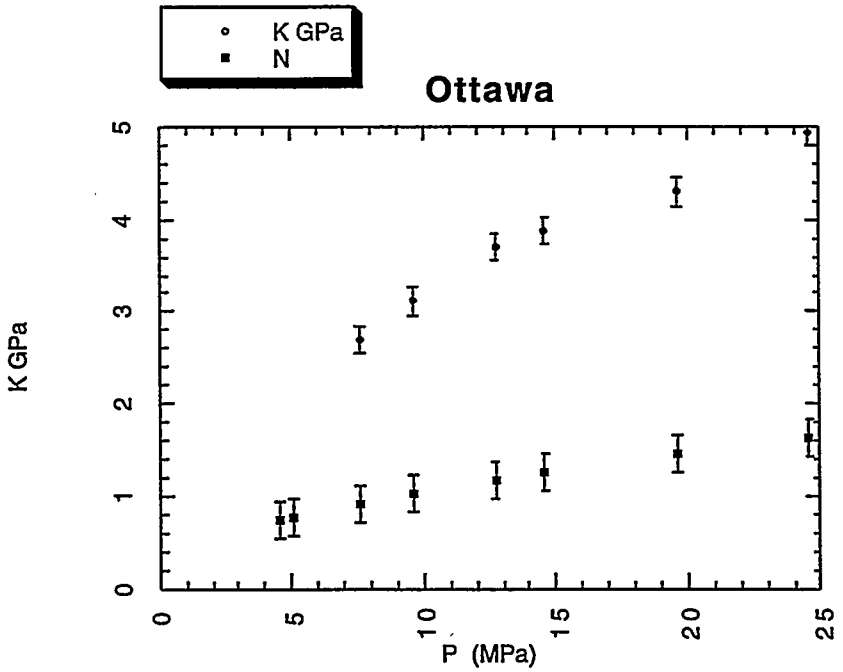

Figure 7: The Ottawa sand static moduli (Kstat) and dynamic moduli (Kdyn).

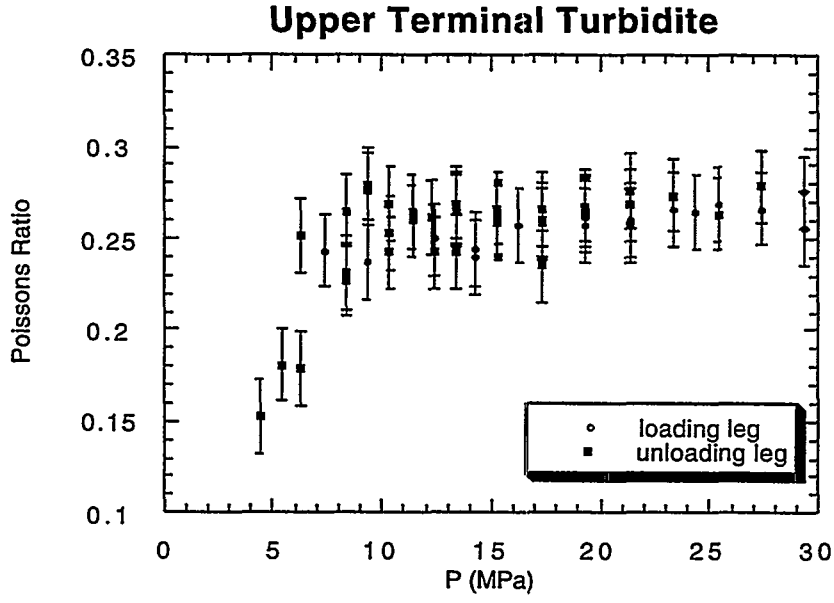

Figure 8: The Poisson's ratio of the turbidite. The measurement shows pressure sensitivity at low pressures.

DISCUSSION AND CONCLUSIONS

The Ottawa sand sample and the Upper Terminal zone turbidite have similar grain size and were treated similarly during sample preparation. However, one major difference is the presence in the turbidite of more than 10% by volume clay and as much as 20% by volume mica. To investigate this, we prepared two new samples of Ottawa sand, each with 15% by volume montmorillonite. The results of creep tests on these materials discussed in Chang et al. (Paper G7) demonstrate that the difference in behavior between the turbidite and clean Ottawa sand during testing can be explained by the presence of wetted clays and/or mica in the turbidite.

Differences between loading and unloading modulus of the turbidite are a consequence of irreversible compaction during loading, a behavior which can be appropriately modeled using elastoplasticity. However, differences between static unloading moduli and dynamic moduli of 300% persist. These can be explained by viscoelasticity associated with the clays and/or micas. As discussed in Paper G7, the static unloading and dynamic moduli were appropriate to describe the creep response of the turbidite. Using the viscosity required to fit the creep curve, the transition from low-frequency to high-frequency behavior occurs at a frequency which is several orders of magnitude less than seismic. Thus, it is appropriate to use the ultrasonic measurements of

dry modulus as inputs to Gassmann to predict the elastic properties of fluid-saturated sands in situ in the Wilmington field.

ACKNOWLEDGMENTS

Special thanks to Tidelands Oil and The Department of Energy who funded this research. Also, thanks to New England Research, who constructed the pressure vessel and acquisition/control system for the apparatus. And finally, thanks to Don Lowe of The Geology Department, Stanford University, for helping with the thin section analysis.

REFERENCES

Chang C., Moos D., Zoback M.D. "Mechanical Properties of unconsolidated materials", SRB 95 Annual Report, Vol. 58, Paper A5.

Bourbie, T., Coussy, O. and Zinser, B., 1987, "Acoustics of porous media", Gulf Publishing Company

Dominico, S. N.; "Elastic properties of unconsolidated porous sand reservoirs", 1977, Geophysics, Vol. 43, 7, p. 1339-1368.

Estes, C.A., Mavko, G., Yin, H., Cadoret, T.; "Measurements of velocity, porosity and permeability on unconsolidated granular materials", 1994, SRB Annual Report, Paper G1.

Han, D. H., personal communication, 1995.

Karig, D.E.; "Reconsolidation tests and sonic velocity measurements of clay-rich sediments from the Nankai Trough," Proceedings of the Ocean Drilling Program, Scientific Results, Vol. 131.

Mavko, G., and A. Nur, "Wave attenuation in partially saturated rocks", Geophysics, 44, 161-178, 1979

Murphy, W. F., III, Winkler, K.W.; "Acoustic relaxation in sedimentary rocks; dependence on grain contacts and fluid saturation." March 1986. (GEOPHYSICS ; Vol. 51, No. 3, p. 757-766)

Tutuncu A.N.; Podio A.L.; Sharma M.M; "Nonlinear Viscoelastic Behavior of Sedimentary Rocks: I. Effect of Frequency", submitted to Geophysics, February 1995

Winkler, K.W.; "Frequency dependent ultrasonic properties of rocks", GEOPHYSICS; VOL. 88, NO. B11, p. 9493-9499, 1983.

PAPER H6

HYDROCARBON SATURATION DETERMINATION FROM SONIC LOG DATA

Daniel Moos
Stanford Rock and Borehole Geophysics Project
Andrew Hooks
Magnetic Pulse, Inc.
Scott Walker
Tidelands Oil Production Company

ABSTRACT

Theoretical relationships, confirmed by laboratory and field data, suggest that hydrocarbon-bearing rocks in situ can be differentiated from rocks containing brines using sonic velocity measurements. A project to test this technique has been undertaken in the Wilmington Field, California, with co-funding from the Department of Energy (DOE cooperative agreement no. DE-FC22-95BC14934).

Results from M-499 (selectively completed in the Upper Terminal Zone) and 167-W (a Lower Terminal Zone injector) demonstrate that the theoretically predicted effects can be observed. Zones with producible oil can be differentiated from those which are watered out using acoustic logs recorded through casing.

THE WILMINGTON FIELD

The Wilmington field is located within a NW-SE trending faulted anticline beneath and immediately offshore of Long Beach, CA (Figure 1). The first successful well was drilled in 1936. As of 1967, more than 1.2 bbls of oil and 840 Tcf gas had been produced, and it was believed that more than 1.8 bbls of oil still remained. Initial production was enhanced by a waterflood started in the 1950's primarily to mitigate surface subsidence which had reached more than 29 feet in the center of the bowl directly overlying the region of greatest production. Injection wells are located at the margins of the field, and production continues from the center.

Production at Wilmington is from a thick sequence of clastic slope sediments (unconsolidated, low maturity, turbiditic arenites and clean arenites with porosities exceeding 25% and permeabilities of 100's of millidarcys, interlayered with sandy clays (wackes) containing 50%

or more detrital smectite). The producing horizons lie between depths of 2350 and about 6000 feet. The hydrocarbons produced at Wilmington range from API gravity 12 (Tar zone) to API gravity 18-19 (Ranger and Upper Terminal Zones) to API gravity 27 (Lower Terminal). API gravities as high as 30 are produced from deeper sections of the field (the Union Pacific, Ford, and 238 zones).

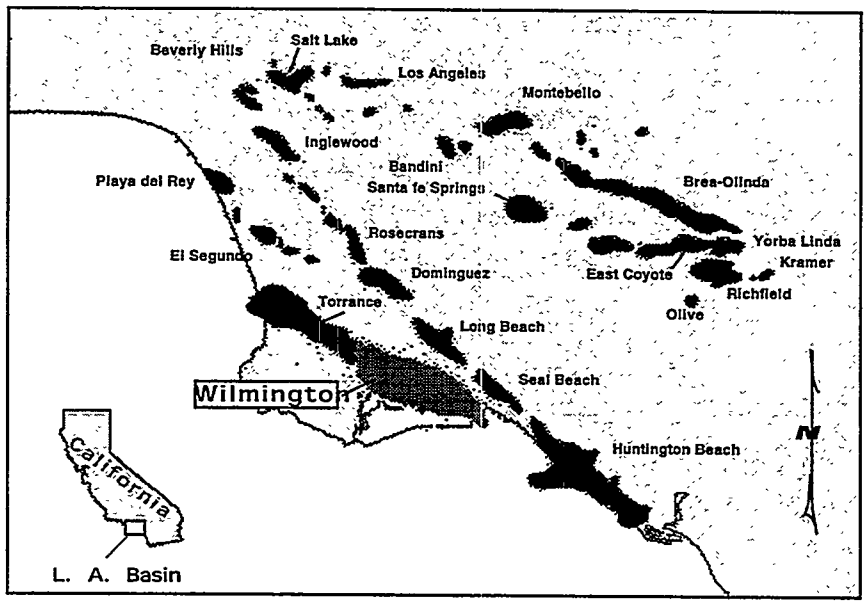

Figure 1: Location map, showing the Wilmington Field and other oil fields within the Los Angeles Basin (after Mayuga, (Mayuga, 1968)).

THEORETICAL BASIS OF THE SONIC DETECTION TECHNIQUE

Generally, when a rock is loaded under an increment of compression, such as from a passing seismic wave, an increment of pore pressure change is induced, which resists the compression and therefore stiffens the rock. The low-frequency Gassmann (1951) - Biot (1956) theory predicts the resulting increase in effective bulk modulus of the saturated rock. Gassmann predicted no change for the isotropic shear modulus with saturation. The Gassmann-Biot relation is valid only at sufficiently low frequencies such that the induced pore pressure is equilibrated throughout the pore space (i.e., that there is sufficient time for the pore fluid to flow and eliminate wave-induced pore pressure gradients). Laboratory measurements are under way to investigate whether this will be important at logging frequencies (Chang et al., this volume).

The ability to detect hydrocarbons using elastic waves depends both on the amount by which hydrocarbon properties differ from those of brines and the degree to which those properties control the velocities of the saturated rock. Several factors influence the properties of fluids at reservoir conditions. In general, density, bulk modulus and viscosity all decrease with increasing

API number (decreasing density) and temperature and increase slightly with increasing pressure. Gas in solution has a large effect, even in comparison to that of temperature, in reducing density and bulk modulus. Based on equations presented in Batzle and Wang (1992), live oils at reservoir conditions have significantly lower bulk moduli and densities than those of brine. And, the relatively low frame modulus (high pore compliance) of Wilmington reservoir rocks suggests that they will be quite sensitive to the properties of fluid saturants (see Fig. 3, Moos et al., this volume).

PREVIOUS RESULTS

Previously, theoretical models using values of fluid and formation properties typical of the Miocene-age turbidites within the target interval confirmed that it should be possible to differentiate between hydrocarbon and non-hydrocarbon bearing sands in this field using compressional and shear wave sonic velocity logs (Moos, 1995). And, results in a newly drilled well demonstrated that it was possible to record shear and compressional wave velocities through casing. Shear velocities recorded through casing in the frequency band between 0.8 and 2.4 kHz were virtually identical to the open-hole values. However, in the frequency band between 4 and 8 kHz, compressional velocities calculated using cased hole data were slightly less than those calculated using open-hole data, and open-hole velocities computed using data filtered to isolate energy propagating at 2.5 to 3.5 kHz were slightly greater than those calculated using the open-hole data at higher frequency (Moos, et al., 1995). Porosity estimated using an empirical relationship between shear velocity and porosity was similar to that determined from a density-neutron crossplot. Estimates of saturation were qualitatively similar to conventional (Archie's Law) values. The well was completed by selectively perforating zones with high Archie's Law predicted oil saturations, and outperformed adjacent wells completed using slotted liners and/or gravel packings.

To date six wells have been logged through casing, using several versions of the MPI XACT sonic logging tool. Two of these were also logged using the Schlumberger DSI tool. In M-499 and two of the newly logged wells, Schlumberger USI logs were run to investigate casing bond. A standard bond log was also run in M-499. The oldest wells were drilled in the 1940's. Deviations ranged from less than 2° to more than 40°. Casing diameters were between 6" and 8".

Table I: Summary of hole characteristics.

Hole	Depth*	Deviation	Year Drilled	Well Type
M-499	2.8-3.7	43°	1993	Prospect

167-W†	2.5-4.5	30°	1983	Injector
FY-67	1.6-3.7	17°	1948	Injector
Y-63	1.6-3.2	17°	1948	Prospect
X-32	3.0-5.6	-	1946	Prospect
J-15	1.2-2.9	vertical	1942	Prospect

*kft

†Steel casing extended to 4080 ft, below which fiberglass liner was installed and perforated to allow injection into selected zones.

Although compressional velocities have been determined in all but one case, shear-wave velocities have been obtained in only two of the six wells. In determining whether these logs actually measure the shear wave, independent recordings of arrivals on opposite sides of the tool are essential. Based on the results to date, the two most important determinants of success are the age of the well and the difference between shear-wave and tube-wave velocities. Neither standard cement bond logs nor bond estimates derived using acoustic reflections from casing could be used to unambiguously predict whether shear-wave logs could be obtained. Nor did the angle of deviation, as M-499, for which excellent data were obtained, was deviated 43°, and J-15, for which no shear-wave velocities could be determined, was vertical.

DATA

Data are now available from two wells to test whether producible hydrocarbons can be detected acoustically in the Wilmington Field. The first well, M-499, was drilled and selectively completed in the Upper Terminal Zone over the depth interval 3120 to 3540 feet (log depths are not corrected to true vertical depth). Excellent cased-hole compressional and shear velocities were obtained in this well (Moos, et al., 1995, Moos, 1995). The second well, 167-W, was drilled in 1984 and cased to 4080 feet. A fiberglass liner was placed below that depth and selectively perforated to allow injection into permable sands of the Lower Terminal Zone over the depth interval 4200 to 4680 feet.

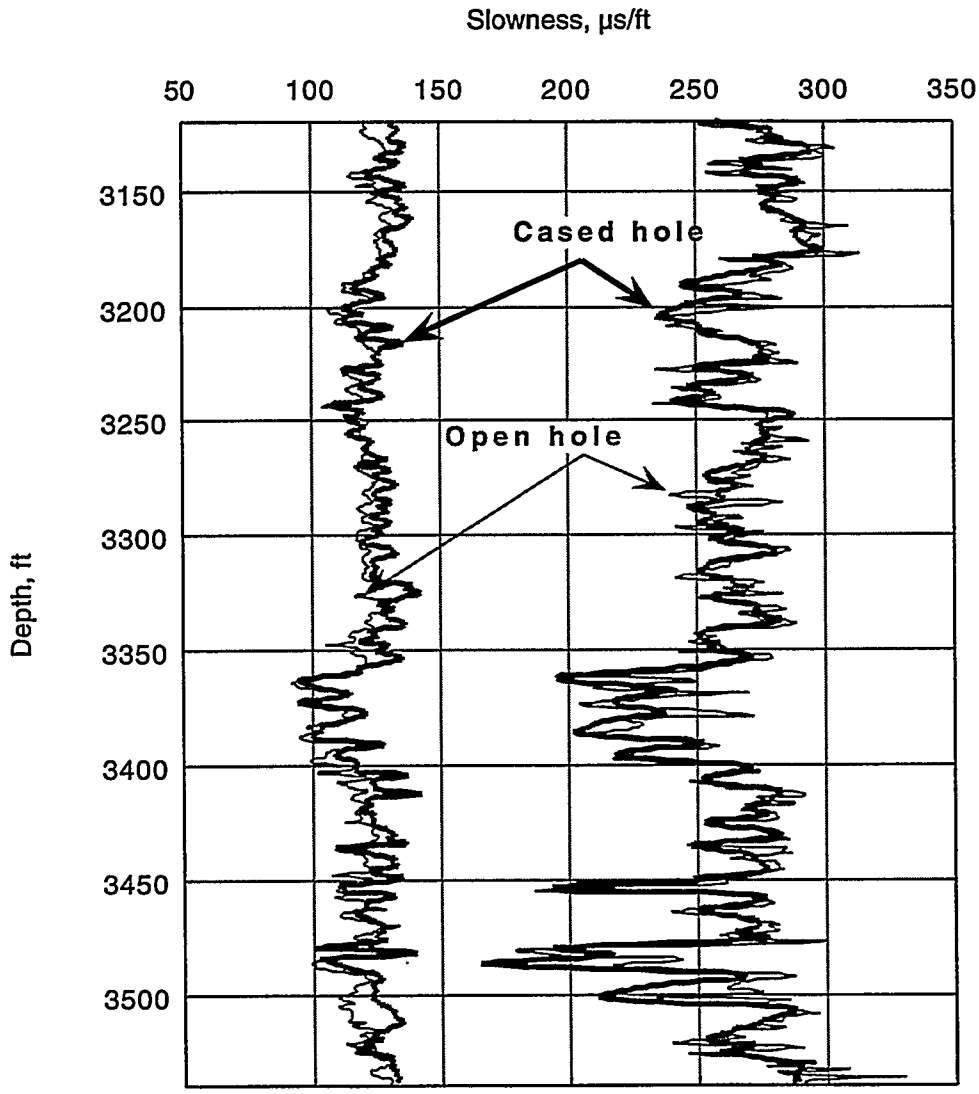

Figure 2. Cased-hole (heavy black lines) and open-hole (thinner gray lines) P- and S- wave slownesses calculated from monopole and dipole waveforms recorded in the Upper Terminal of M-499. Although dt_S is similar, dt_P measured in the open hole is slightly lower than that determined from the cased hole data.

Figure 2 shows P- and S- wave slownesses for the Upper Terminal Zone of M-499. Both cased- and open- hole slownesses are shown. As was discussed previously, dt_S is similar,

whereas dt_P is generally lower in the open-hole than in the cased-hole. The analysis presented in the remainder of this paper uses the cased-hole results.

Monopole and dipole sonic data were recorded in 167-W using both the MPI XACT tool and the Schlumberger DSI tool. Initial results using both tools allowed determination of the P-wave slowness throughout the well, and of the shear-wave slowness in the section of fiberglass liner below 4080 feet. Results in the cased hole were ambiguous.

A second log of the hole was run with the XACT tool, configured to allow independent surface recording of arrivals from opposite sides of the tool. In theory, this should allow unambiguous identification of the type of arrival, as monopole energy should arrive in phase on opposite sides of the tool, and dipole energy should arrive out of phase. Standard tools using crystals as receivers take advantage of this effect, by summing or differencing signals from opposite sides of the hole before transmitting data to the surface. This has the advantage of increasing signal-to-noise, thereby maximizing dynamic range, at the expense of uncertainty in the identity of a "mixed" mode which is not completely eliminated by the downhole mathematics (either because of receiver missmatch, tool eccentering or other effects).

Analysis of the data recorded using separate crystals allowed determination of the intervals over which the tube wave interfered with the dipole mode. The tube wave overlapped the dipole mode in frequency. Above about 2900 feet, the dipole mode propagated more slowly than the tube wave. Below about 3300 feet, the dipole mode propagated more quickly than the tube wave. In the intervening interval, the dipole and tube wave arrivals overlapped in both frequency and time. Filtering to isolate the dipole mode, and travel-time analysis restricted only to the time interval within which tube wave interference was minimal, allowed determination of dipole mode slowness over much of the well.

Figure 3 compares delta-t values determined from monopole and dipole logs in the interval 4000 to 4600 feet in 167-W. Also shown is a gamma log, which reveals waterflooded intervals adjacent to perforated sections of the fiberglass liner due to their elevated gamma readings. The correlation between the two compressional logs is excellent, and even the shear-wave logs are similar. This includes the interval behind steel casing above 4080 feet. The thicker lines show the results from analysis of the data recorded independently on opposite sides of the tool; it shows a somewhat better correlation between dt_P and dt_S and will be used in the remainder of the paper to determine saturation.

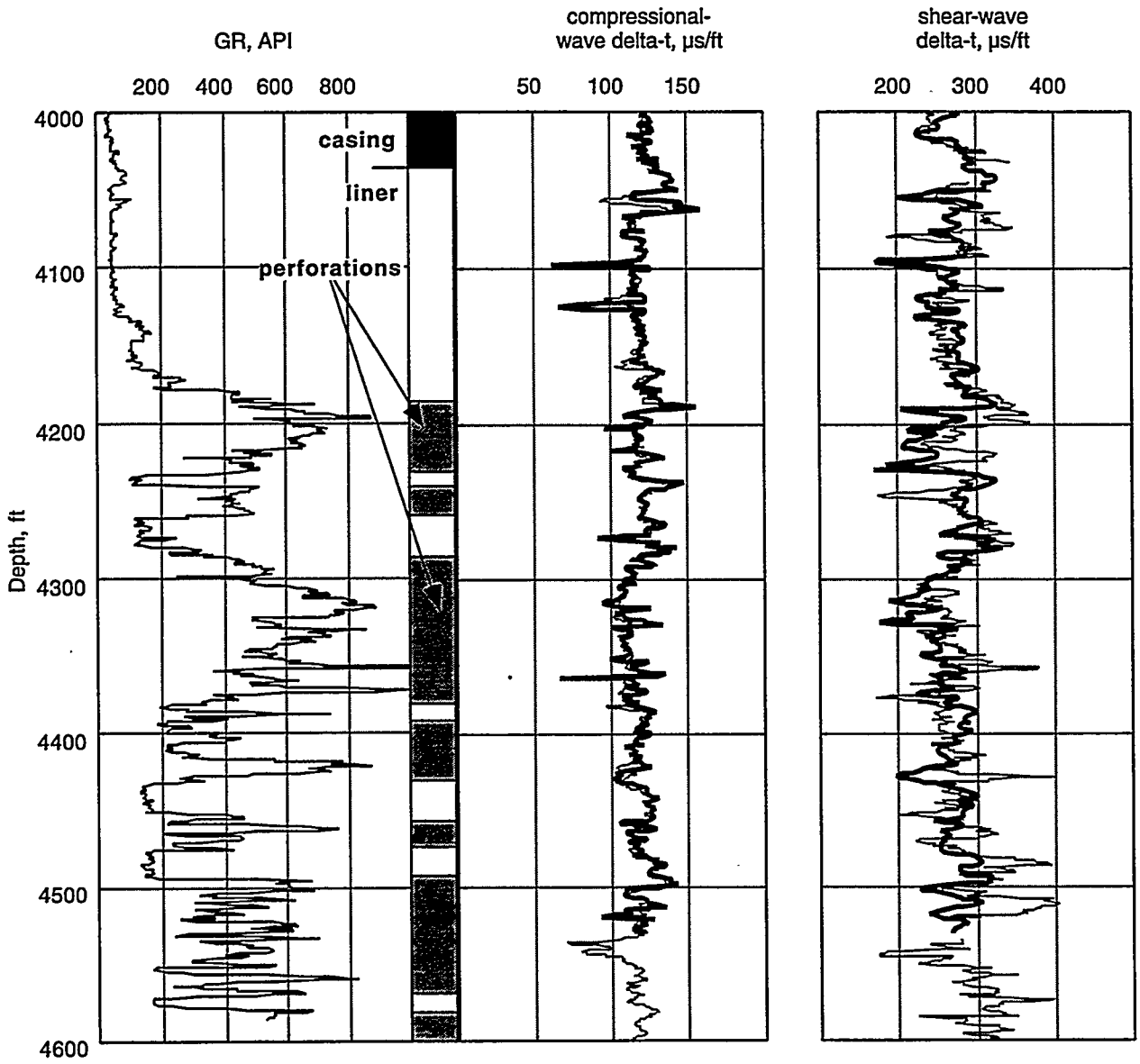

Figure 3. Compressional and shear-wave delta-t calculated from monopole and dipole waveforms recorded in the lowermost section of 167-W for two different logging sondes. Also shown is gamma (GR) and the locations of perforated intervals in this injection well. High gamma assocaited with perforated intervals indicates zones into which water has been injected.

SATURATION ESTIMATION IN WATER-FLOODED VS. PRODUCTIVE ZONES

Injection has been ongoing into the lowermost section of 167-W for more than 10 years. Thus it is reasonable to assume that all of the mobile oil has been flushed from the near-wellbore region. Since elevated gamma is found adjacent only to perforated zones, it is reasonable to assume that the injection process is associated with the high gamma readings. Thus a discriminator based on the gamma-ray log can be used to select only the sonic data recorded within the flushed zones.

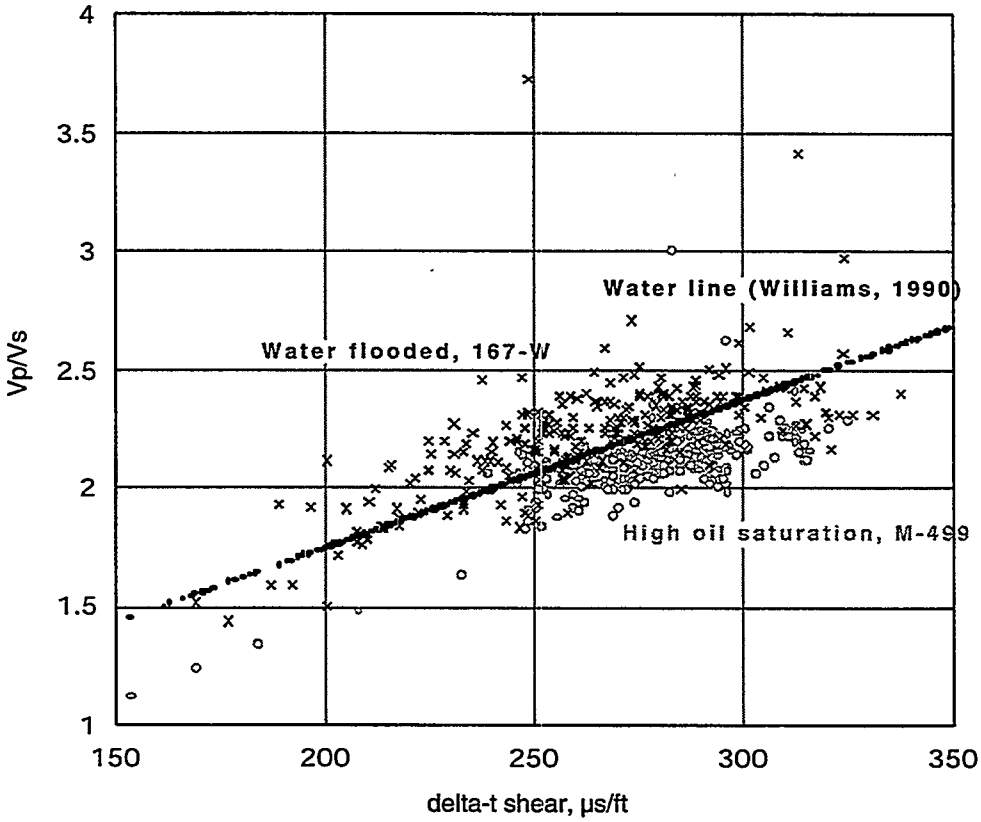

Figure 4. ALHI plot (Vp/Vs vs. dtS) of data from intervals with high oil saturation in M-499 (circles) and intervals with high water saturation in 167-W (crosses). Also shown is the empirical water line of Williams (1990), which is predicted to separate the two sets of data.

By comparing these data to sonic data recorded in zones within M-499 with high oil saturations detected using electrical methods, we can determine whether producible hydrocarbons could be detected using only the sonic data.

Figure 4 shows V_p/V_s plotted against dt_S (an ALHI plot) for data from water-flushed sands and wackes in 167-W (crosses) and high oil saturation zones within M-499 (open circles). Also shown is Williams' (1990) ALHI water line determined empirically, which should separate the two data sets. With only a few exceptions, all of the points from within high oil-saturated intervals of M-499 plot below the ALHI line, and all of the data from water-saturated intervals of 167-W plot above the line. This is particularly impressive when one considers that the oil saturation in M-499 is everywhere less than 0.5.

This initial result is quite promising. However, earlier work revealed that the sonic technique tended to yield "false positives" - i.e. it predicted that zones would be productive which were determined based on other data (but interestingly, not by actual testing!) not to be. And, it was not clear whether the effects could be predicted theoretically or from laboratory measurements, thereby putting the technique on a sound physical footing and allowing application in regions for which it had not been calibrated. These issues are under investigation in the remaining year of the project.

CONCLUSIONS

Results to date indicate that it is possible to discriminate between potentially productive intervals and those which are watered out using measurements of comrpessional and shear wave velocities recorded through casing using sonic monopole and dipole tools. In this field, the ALHI water line of Williams (1990) neatly separates zones which are likely to be productive from those which are not. A number of issues still need to be worked out. Of these, the single greatest problem continues to be how to acquire the data necessary to carry out the analysis.

REFERENCES

Batzle, M., and Wang, Z., 1992, Seismic properties of pore fluids: Geophysics, **57**, 1396-1408.

Biot, M.A., 1956, Theory of elastic waves in a fluid-saturated porous solid, II. Higher frequency range: J. Acoust. Soc. Am., **28**, 179-191.

Gassmann, F., 1951, Uber die elastizität poroser medien: Vierteljahrsschr. Naturforsh. Ges. Zuerich, **96**, 1-23.

Mayuga, M.N., 1968, Geology and Development of California's Giant - The Wilmington Oil Field *in* AAPG 53rd Ann. Meeting, Oklahoma City, OK, p. 47.

Moos, D., 1995, Using multipole acoustic logs in cased holes to determine porosity and oil saturation in clastic reservoirs, Paper F4 *in* Nur, A., Zoback, M.D., and Mavko, G., eds., Proc. SRB Annual Meeting, June 1995, Stanford, CA.

Moos, D., Hara, S., Phillips, C., Hooks, A., and Tagbor, K., 1995, Field test of acoustic logs for measuring porosity and oil saturation in a mature waterflood in the Wilmington Field, CA, SPE 29655 *in* SPE Western Regional Meeting, March 1995, Bakersfield, CA.

Appendix #6

PAPER H7

IDENTIFYING PATCHY SATURATION FROM WELL LOGS

Jack Dvorkin, Amos Nur, James Packwood
Stanford Rock Physics Laboratory

Dan Moos
Stanford Borehole Geophysics Laboratory

ABSTRACT

We consider two saturation patterns in a partially saturated rock. The first is the homogeneous pattern where saturation is the same at any location in the rock. The second is the patchy pattern where a fully-saturated patch may be surrounded by a dry region. In both cases, the global saturation value in a large volume of the rock is the same. At the same global saturation, the effective acoustic properties of the rock vary depending on the saturation pattern. We provide a practical method for identifying the dominating saturation pattern from well logs. This method performs well in soft rocks whose acoustic properties are most sensitive to the way fluid is distributed in the pore space. Well logs from high-porosity soft sands indicate that patchy saturation patterns do exist.

INTRODUCTION AND PROBLEM FORMULATION

The heterogeneous geological nature of porous rocks and soils often results in the heterogeneity of fluid distribution on scales greater than pore or grain size. In a partially saturated rock two end members of pore fluid arrangement can be considered: (a) the fluid is evenly distributed within the pore space, i.e., fluid distribution is homogeneous; and (b) the fluid is arranged in fully saturated patches that are surrounded by dry or partially saturated regions, so that fluid distribution is patchy. These patches may include thousands of grains.

It is important to identify the type of pore fluid distribution because:

a. The nature of oil/gas distribution in a pay zone affects the estimates of reserves, relative permeability, and dry-frame elastic properties. The dry-frame elastic properties are

needed for the "fluid substitution" procedure where the velocities in a rock with a new, hypothetical, fluid are calculated from those measured in the rock with the known fluid.

b. The patchy arrangement of ground water is probably common in undersaturated aquifer zones. To determine the details of such patchy arrangements is important for ground water flow calculations and watertable monitoring.

c. Industrial groundwater contaminants in the shallow subsurface may occur in patches, or may be evenly dispersed in the pore space. Determining the arrangement type will help select the remediation technique.

The problem posed is to identify the saturation pattern from well logs. In order to solve this problem, we assume that at every depth point of interest the following are available: P-wave velocity (V_p), S-wave velocity (V_s), density (ρ), porosity (ϕ), and saturation (S). In addition, we have to know the bulk modulus of the solid phase of the rock (K_s), as well as the bulk moduli of the liquid and gas phases (K_l and K_g, respectively).

SATURATION PATTERN, VELOCITY AND POISSON'S RATIO

Homogeneous Saturation

Consider a rock at saturation S. If the saturation pattern is homogeneous, the volumetric fraction of liquid in every pore is S, and the rest of the volume in the pore is occupied by gas. The effective bulk modulus K_f of such a liquid-gas mixture can be found from

$$\frac{1}{K_f} = \frac{S}{K_l} + \frac{1-S}{K_g}. \qquad (1)$$

The effective bulk modulus of the partially saturated rock (K_{Sat}) is related to that of the dry frame (K_{Dry}) by Gassmann's (1951) equation:

$$\frac{K_{Sat}}{K_s - K_{Sat}} = \frac{K_{Dry}}{K_s - K_{Dry}} + \frac{K_f}{\phi(K_s - K_f)}. \qquad (2)$$

The shear modulus (G) of the saturated rock is the same as that of the dry frame. These moduli can be found from the measured velocities and density as

$$K_{Sat} = \rho(V_p^2 - \frac{4}{3}V_s^2), \quad G = \rho V_s^2. \tag{3}$$

Once K_{Sat} is known from well-log measurements, we can calculate the dry-frame bulk modulus from equation (2) as

$$K_{Dry} = K_s \frac{1-(1-\phi)K_{Sat}/K_s - \phi K_{Sat}/K_f}{1+\phi-\phi K_s/K_f - K_{Sat}/K_s}. \tag{4}$$

Then the dry-frame Poisson's ratio (ν_{Dry}) is

$$\nu_{Dry} = \frac{3K_{Dry} - 2G}{2(3K_{Dry} + G)}. \tag{5}$$

Patchy Saturation

If the saturation pattern is patchy, the bulk modulus of the fully-saturated patches (K_0) is that of the fully-saturated rock:

$$K_0 = K_s \frac{\phi K_{Dry} - (1+\phi)K_l K_{Dry}/K_s + K_l}{(1-\phi)K_l + \phi K_s - K_l K_{Dry}/K_s}. \tag{6}$$

The bulk modulus of the dry patches (K_1) is that of the gas-saturated rock

$$K_1 = K_s \frac{\phi K_{Dry} - (1+\phi)K_g K_{Dry}/K_s + K_g}{(1-\phi)K_g + \phi K_s - K_g K_{Dry}/K_s}. \tag{7}$$

The shear modulus is not affected by the pore fluid. Therefore, the effective shear modulus of the mixture of dry and fully-saturated patches is that of the dry frame. The effective bulk modulus in this (uniform shear modulus) case is independent of the shape of the patches and can be found from Hill's (1963) formula:

$$\frac{1}{K_{Sat} + \frac{4}{3}G} = \frac{S}{K_0 + \frac{4}{3}G} + \frac{1-S}{K_1 + \frac{4}{3}G}. \tag{8}$$

The inversion of equations (6), (7), and (8) for K_{Dry} gives:

$$K_{Dry} = (-B + \sqrt{B^2 - 4AC}) / 2A, \tag{9}$$

where

$$A = cq + M(bq + cf), B = pc + dq - M(aq - bp - df + ce), C = dp - M(ap + de);$$
$$a = S[(1-\phi)K_l + \phi K_s], b = SK_l / K_s, c = \phi K_s - (1+\phi)K_l - K_l g / K_s,$$
$$d = K_l K_s + (1-\phi)gK_l + \phi gK_s, e = (1-S)[(1-\phi)K_g + \phi K_s], f = (1-S)K_g / K_s,$$
$$p = K_g K_s + (1-\phi)gK_g + \phi gK_s, q = \phi K_s - (1+\phi)K_g - K_g g / K_s;$$
$$M = \rho V_p^2, g = 4\rho V_s^2 / 3.$$

Example

In Figure 1a we plot V_p in Ottawa sand versus S, depending on the saturation pattern. The bulk and shear moduli of the dry rock at the effective pressure of 10 MPa are 1.75 MPa and 1.72 MPa, respectively (Han, 1986). Porosity is 0.33. The bulk moduli of the solid phase, liquid and gas are 38 GPa, 2.55 GPa, and 0.018 GPa, respectively. They correspond to pure quartz (Carmichael, 1990), brine of salinity 30,000 ppm, and methane at the pore pressure of 10 MPa and temperature of 50°C (Batzle and Wang, 1992).

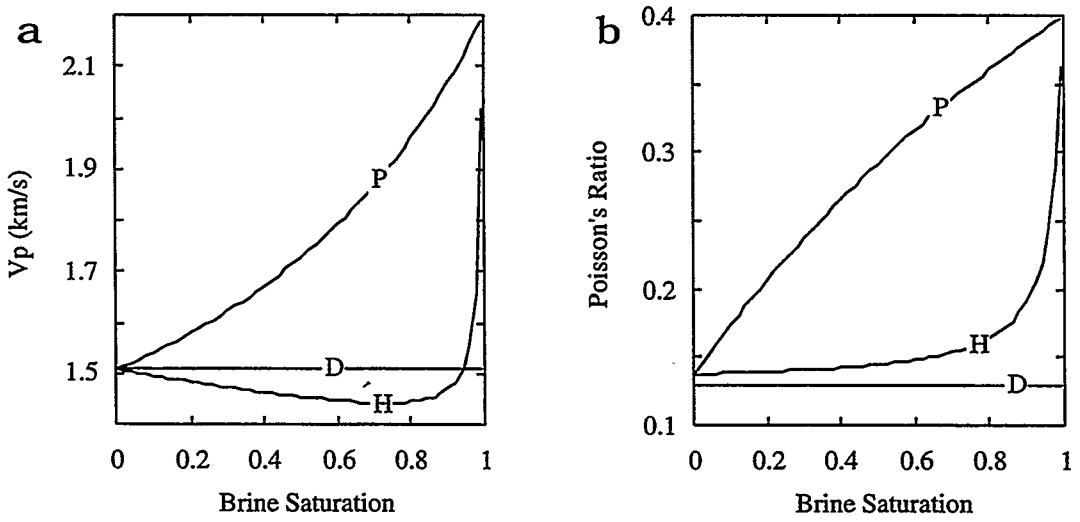

Figure 1: P-wave velocity (a) and Poisson's ratio (b) versus saturation in Ottawa sandstone. Letters on the curves mean: "H" -- homogeneous saturation, "P" -- patchy saturation, and "D" -- dry frame.

If saturation is homogeneous, the compressibility of the brine-gas mixture is very close to that of gas for almost all saturations. Only when water saturation approaches unity does

the compressibility of the mixture sharply decrease and approach that of brine. In this case, the bulk modulus of the rock is approximately constant for almost all saturations and sharply increases as the rock becomes fully saturated. At the same time, the density of the rock steadily increases with increasing saturation resulting in a slight V_p decrease with increasing saturation. Only at a very high saturation V_p approaches its value in the fully saturated rock. The situation is completely different if saturation is patchy. In this case V_p steadily increases with increasing saturation. This drastic difference in the acoustic response of a partially saturated rock emphasizes the importance of determining the saturation pattern in situ. Indeed, if acoustic well logs are interpreted to find the effective elastic properties of the dry rock, the results may be quite different depending on what saturation pattern prevails, and, accordingly, what inversion method is used. It is easy to imagine that the relative permeability of a rock may also strongly depend on the saturation pattern.

SATURATION PATTERNS FROM WELL LOGS

Method

In Figure 1b we plot the Poisson's ratio of Ottawa sand versus saturation. It is clear that this elastic constant is very sensitive to the saturation pattern. Therefore, Poisson's ratio may serve as an indicator of the saturation pattern. We propose the following saturation pattern identification scheme:

1. Find the dry-frame Poisson's ratio from equation (5) by using the inversion for patchy saturation as given by equation (9).
2. If this inversion gives unreasonable values for the Poisson's ratio, then the assumption that saturation is patchy is wrong, and, therefore, saturation is homogeneous.
3. Find the dry-frame Poisson's ratio from equation (5) by using the inversion for homogeneous saturation as given by equation (4).
4. If this inversion gives unreasonable values for the Poisson's ratio, then the assumption that saturation is homogeneous is wrong, and, therefore, saturation is patchy.

Synthetic Well Logs

We test this method on a synthetic well log. The log was created based on laboratory measurements of acoustic velocities and porosity in a suite of soft dry rocks from the Troll Field in the North Sea (Blangy, 1992). The effective pressure is 10 MPa. The liquid and

gas properties are the same as in the above example. We assumed saturation values and saturation patterns versus depth (Figure 2a) and calculated the "measured" V_p and V_s accordingly (Figure 2b).

We calculate the dry-rock Poisson's ratio using the assumption that saturation is patchy in the whole depth interval (Figure 3a). Obviously, the calculated Poisson's ratio values may be quite unrealistic at some depth intervals. In order to identify saturation patterns, we clip the calculated Poisson's ratio log leaving out unreasonable negative values (Figure 3b). What is left most likely corresponds to the patchy saturation pattern since the patchy inversion technique was used here. The rest of the depth interval corresponds to the homogeneous pattern. The intervals of different saturation patterns thus identified exactly correspond to those in the original log, except for one point at the depth of 1656.

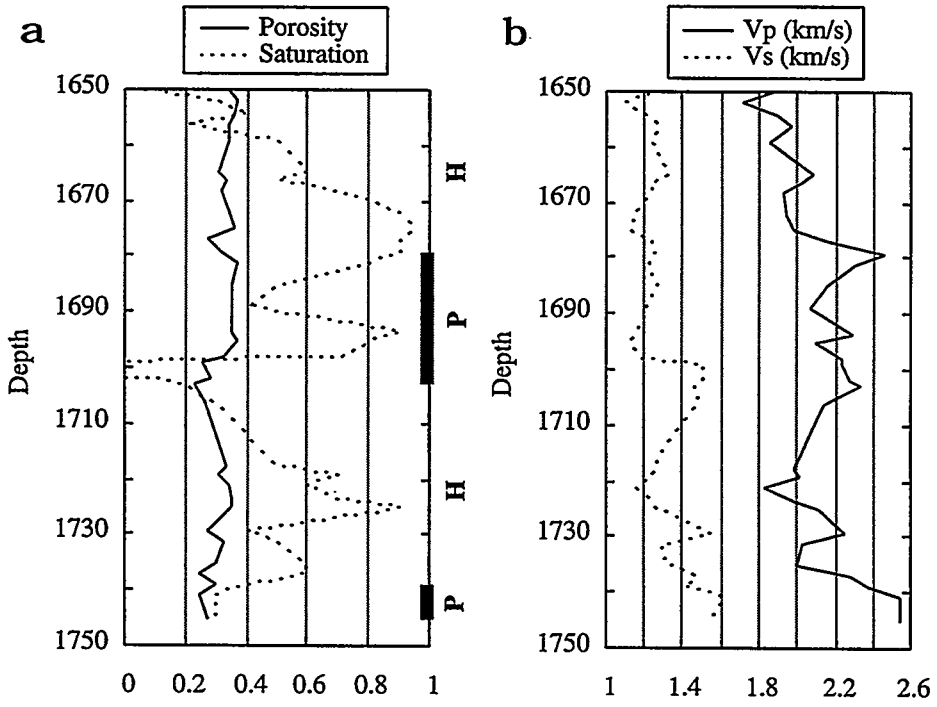

Figure 2: Synthetic well log. Depth given in fictitious units. a. Porosity and saturation versus depth. Bold vertical lines correspond to the depth intervals with patchy (**P**) saturation. The rest of the interval has homogeneous (**H**) saturation. b. Velocities calculated from dry-rock velocities and the assumed saturation values and patterns.

Figures 4a and 4b illustrate the importance of identifying the saturation pattern for determining dry-frame properties: unless the saturation pattern is known, the errors in calculating the dry-frame bulk modulus and P-wave velocity may be large. As a result, the fluid substitution procedure may give wrong estimates of seismic velocities and Poisson's

ratios in gas-saturated intervals. To obtain correct Poisson's ratio values is extremely important for AVO analyses.

The proposed method works well in soft formations because their elastic coefficients are extremely sensitive to the presence of low-compressibility pore fluid. This is not necessarily the case in a faster formation.

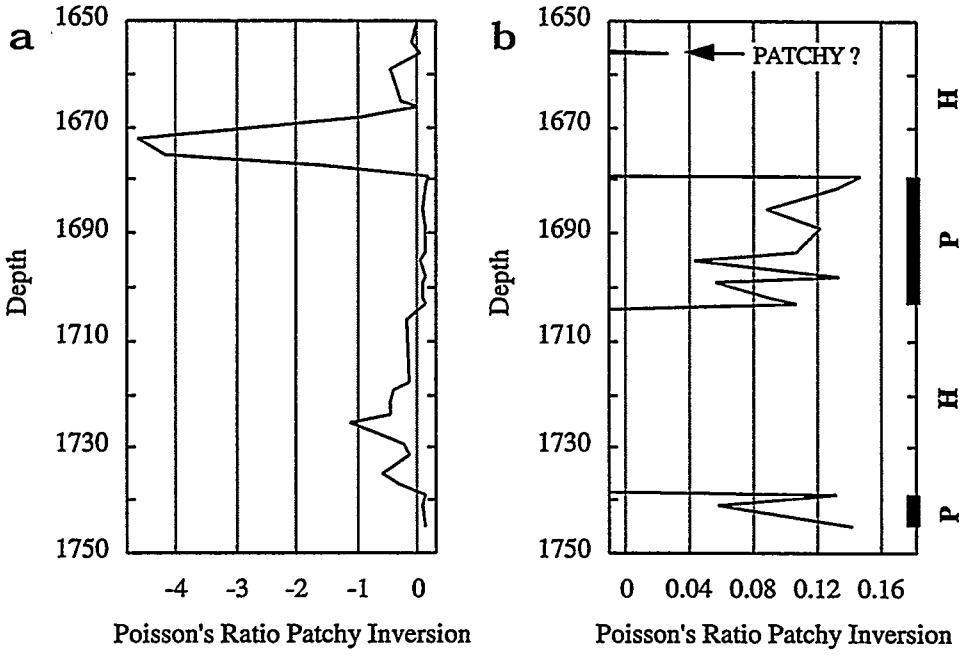

Figure 3: Synthetic well log: patchy inversion for the dry-frame Poisson's ratio. a. The whole range of the Poisson's ratio variation. b. Unreasonable Poisson's ratio values clipped. Bold vertical lines correspond to the depth intervals with patchy saturation. The rest of the interval has homogeneous saturation.

Consider, for example, high-porosity samples from the Oseberg Field in the North Sea (Strandenes, 1991). These granular rocks are quartz- and clay-cemented at their contacts, which results in high acoustic velocities. As in the previous example, we create a synthetic well log based on the laboratory measurement. Again, saturation values and saturation patterns vary with depth. Only at one point the wrong inversion of the dry-frame Poisson's ratio gives an unreasonably negative value (Figure 5a). Otherwise, it is impossible to determine the saturation pattern from the Poisson's ratio inversion. Still, the calculated dry-rock bulk modulus strongly depends on what saturation pattern is assumed during inversion (Figure 5b). However, the errors are not as large as in the soft-formation case.

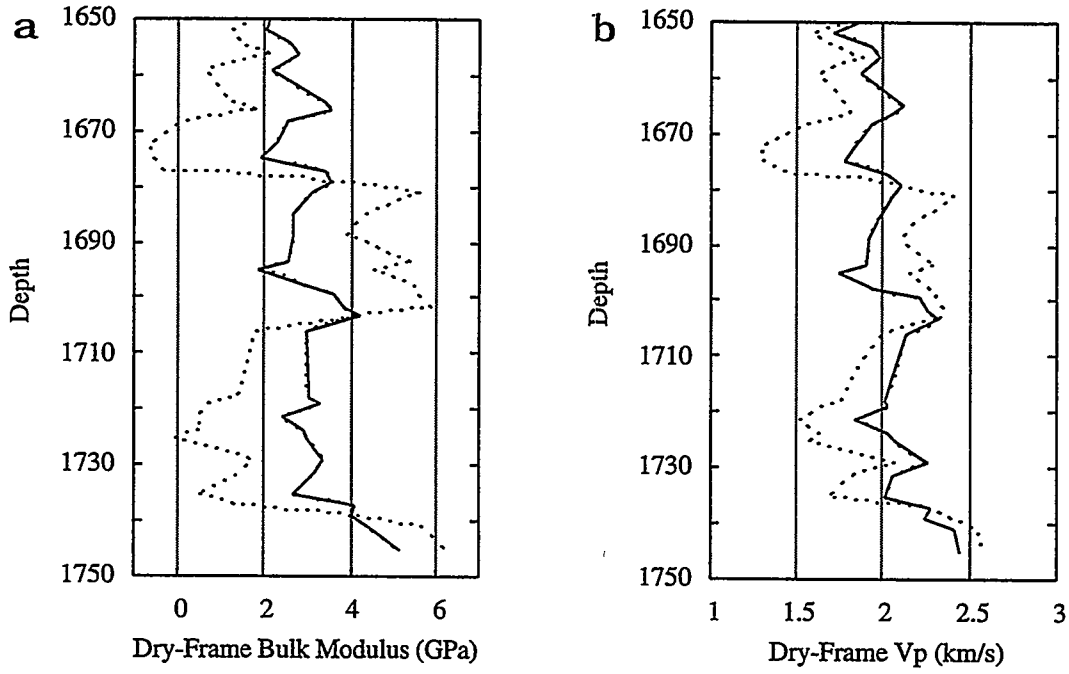

Figure 4: Synthetic well log. a. Determining dry-frame bulk modulus. b. Determining dry-frame velocity. Dotted lines -- wrong inversion, solid lines -- correct inversion.

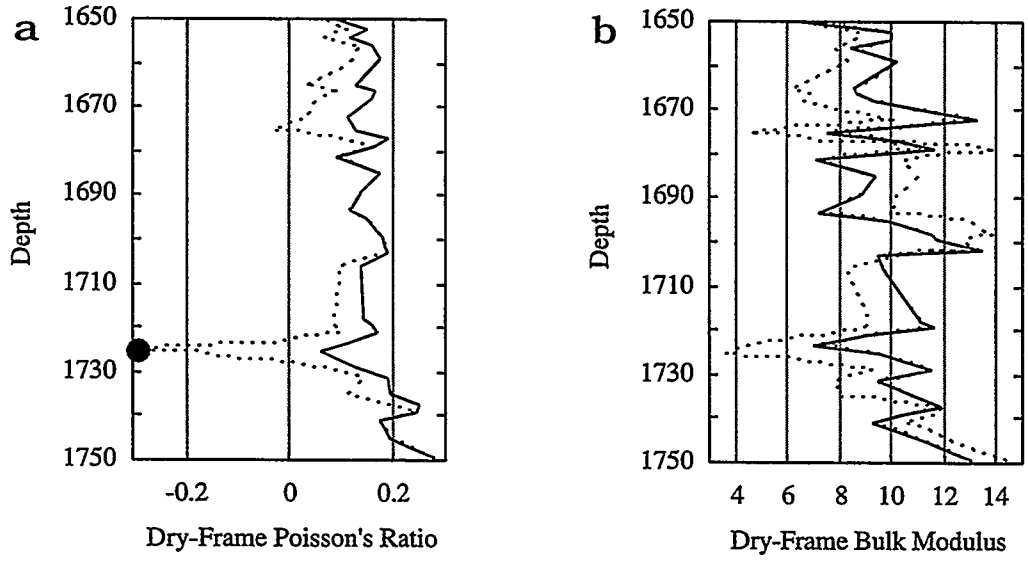

Figure 5: Synthetic well log for fast rocks. a. Dry-frame Poisson's ratio. One unreasonably negative value is shown as the filled symbol. b. Dry-rock bulk modulus. Dotted lines -- wrong inversion, solid lines -- correct inversion.

Real Well Log: Case Study

Two questions remain to be answered. The primary one is: does the patchy saturation pattern exist around real wells? The secondary one is: if it does exist, can it be identified from well logs?

To address these questions, we examine open-hole logs obtained in a well that penetrates unconsolidated gas sands (Figure 6). The frequency of both P- and S-wave sonic tools (Figure 6a) was low, which allowed for the investigation of the uninvaded zone. We select a relatively clean (Figure 6b) high-porosity (Figure 6d) interval with low brine saturation (Figure 6e). The calculated Poisson's ratio (Figure 6f) sometimes exceeds 0.3, which, in a partially-saturated rock, may indicate the patchy saturation pattern (see example in Figure 1b).

To calculate the dry-rock Poisson's ratio, we sequentially use the homogeneous-saturation and the patchy-saturation inversions. The brine and gas bulk moduli (2.88 GPa and 0.0365 GPa, respectively) were selected according to the salinity, and pressure and temperature conditions in the well. The results of the inversions are given in Figure 7a.

In this case it is much harder to separate the patchy-saturation zones from those with homogeneous saturation than in the synthetic log case (Figure 3). A possible indication of patchy saturation are anomalously high dry-rock Poisson's ratios obtained from the homogeneous inversion in the intervals marked with vertical bars in Figure 7a. Indeed, within these intervals, in sands with shale volume below 0.2 (Figure 7b), dry-rock Poisson's ratios exceed 0.2.

Spencer et al. (1994) report that many unconsolidated sands from the Gulf of Mexico have dry-rock Poisson's ratios near 0.18, while other Gulf Coast reservoirs have these values as low as 0.115. Only on several occasions (among a large number of rock samples) do the dry-rock Poisson's ratios exceed 0.2, with the maximum value 0.237. To facilitate this point, we plot dry-rock Poisson's ratios versus porosity (Figure 8) for a suite of unconsolidated North Sea sands (Blangy, 1992) at effective pressure values which bracket the in situ pressure in the well under investigation. Again, these values do not exceed 0.2.

The patchy inversion gives smaller Poisson's ratio values in the marked intervals (Figure 7a). Still, these values may exceed 0.2, but they appear to be more realistic that those given by the homogeneous inversion. We speculate that it is likely that in the patchy saturation domain the dry patches are not completely dry, and the saturated patches are not completely saturated. This is a reason for the absence of clear separation between the two patterns. Of course, our inversion technique can be easily changed to take this impurity

into account. But this will introduce additional non-measurable adjustment parameters which should be avoided in any practical application method.

The dry-rock bulk moduli curves calculated from the two inversion methods are given in Figure 7c. In the proposed patchy-saturation intervals, the difference between the two may reach 25%. Such a difference has to be taken into account, as it may definitely affect seismic reflection interpretation for direct hydrocarbon indication.

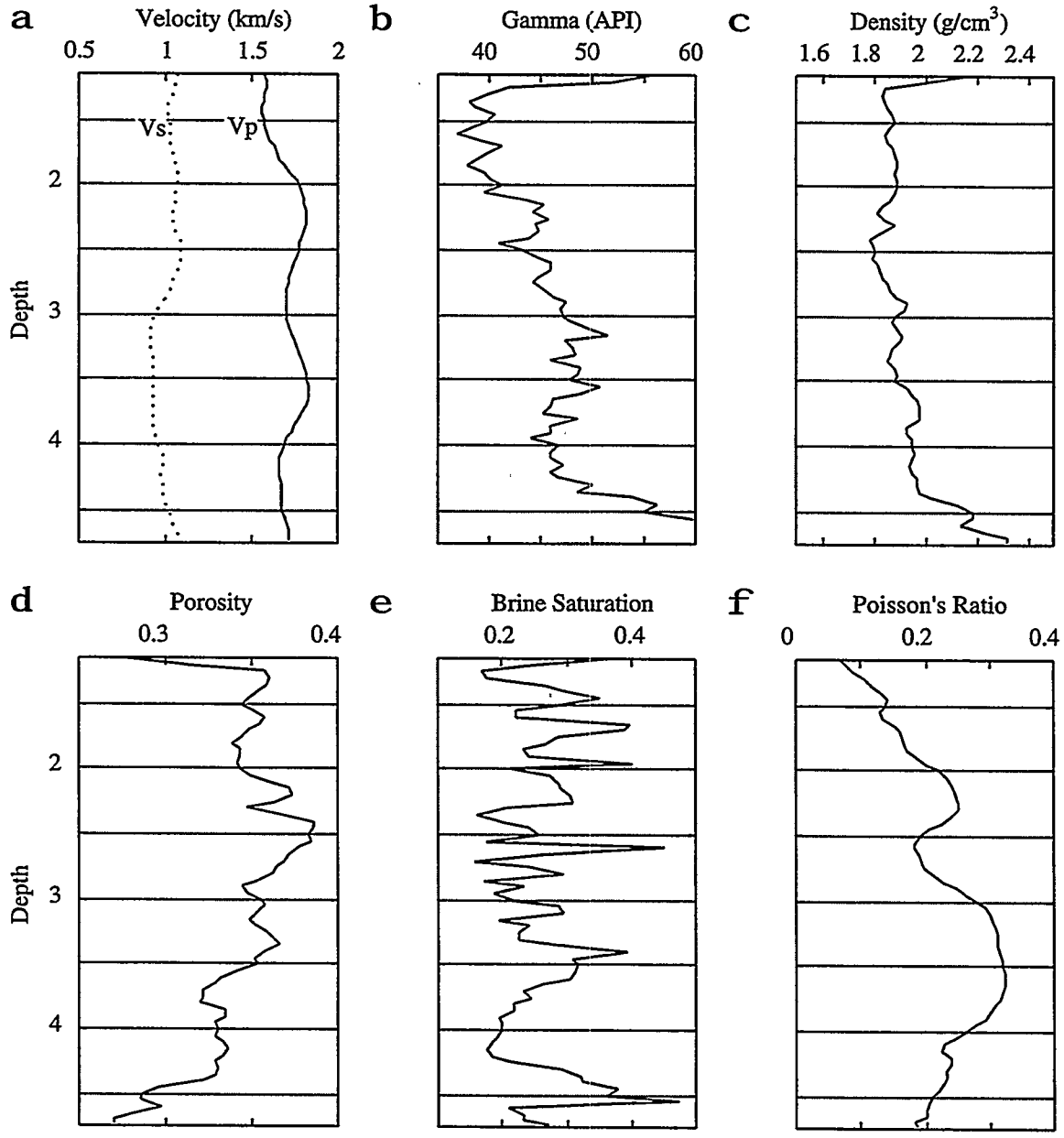

Figure 6: Open-hole logs. Depth is given in fictitious units. a. P- and S-wave velocity; b. gamma-ray log; c. density log; d. porosity (from neutron and density logs); e. saturation (from resistivity); and f. Poisson's ratio calculated from sonic logs.

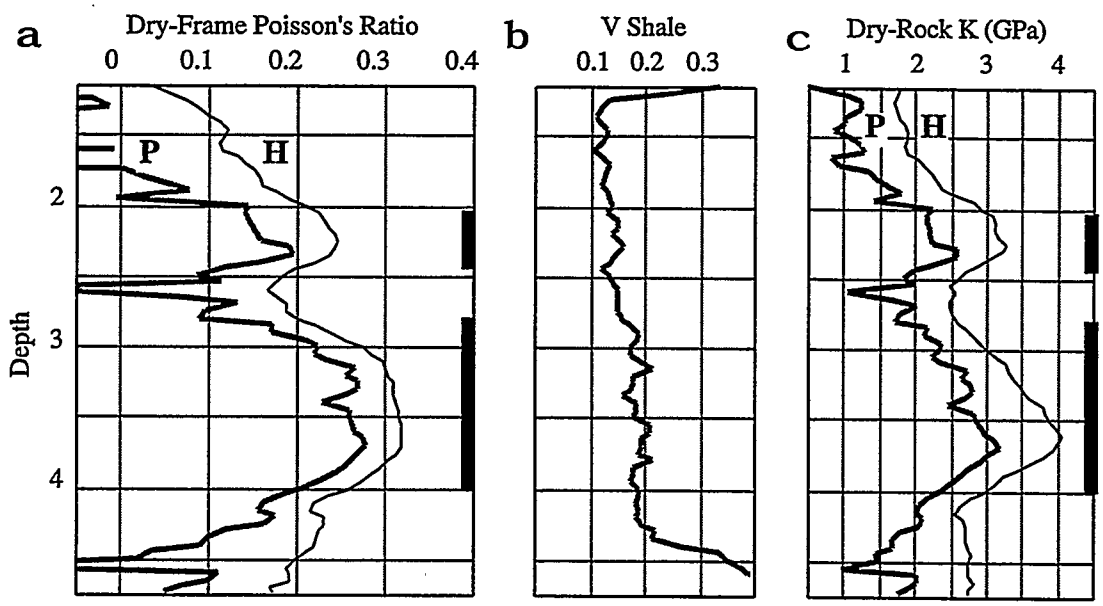

Figure 7: Inversion of the open-hole logs. Depth is given in fictitious units. Bold vertical lines mark depth intervals where patchy saturation is likely. The inversion curves are marked: **H** -- homogeneous saturation, **P** -- patchy saturation. a. Dry-rock Poisson's ratios; b. clay volume from gamma-ray log; and c. dry-rock bulk moduli.

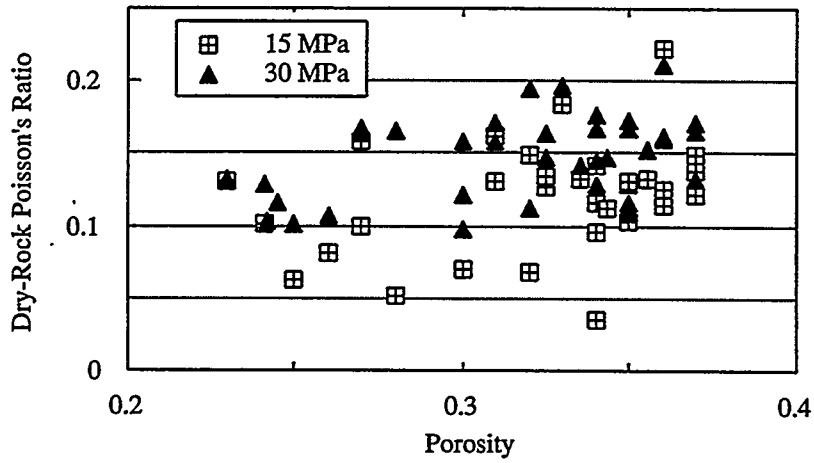

Figure 8: Dry-rock Poisson's ratios versus porosity in unconsolidated North Sea sands at the effective pressure of 15 MPa and 30 MPa (Blangy, 1992).

To summarize this case study we suggest that:

1. In unconsolidated partially-saturated sands two inversions -- the homogeneous saturation and the patchy saturation techniques -- should be applied to calculate the dry-rock elastic moduli from well logs.

2. If the homogeneous inversion gives dry-rock Poisson's ratios which exceed 0.2 - 0.25, and at the same time the patchy inversion gives lower and more reasonable values, the interval is likely to be patchy-saturated;
3. Then the dry-rock bulk moduli (for the fluid-substitution procedure) have to be calculated accordingly.

In any case, we recommend that both inversion techniques be used to bound the possible dry-rock Poisson ratio and bulk modulus values.

CONCLUSION

- At a fixed partial saturation, two saturation patterns may exist in rocks: the homogeneous one where saturation is the same at any location in the rock, and the patchy one where a fully-saturated patch may be surrounded by a dry region.
- It is important to identify the saturation pattern in order to correctly compute the dry-rock elastic moduli from well logs.
- A synthetic example and a case study show that the identification method where the dry-rock Poisson's ratio is computed sequentially based on the assumptions that the pattern is patchy, and that it is homogeneous, works in unconsolidated sands.
- We recommend that this method be routinely used to bound the dry-rock elastic moduli.

ACKNOWLEDGMENT

The idea of quantifying the patchy saturation pattern belongs to Gary Mavko. This work was supported by DOE (Office of Basic Energy Sciences) and by the Stanford Rock Physics and Borehole Geophysics Consortium.

Appendix #10

Increasing Waterflood Reserves in the Wilmington Field, CA: A Program Supported by the U.S. Department of Energy "Class III Oil Program: Near-Term Activities"

The DOE is co-funding a program to investigate new technologies to increase the waterflood reserves in the Wilmington Field, Long Beach, CA. These technologies include cased-hole acoustic logging to detect hydrocarbons, and improved completion techniques to selectively exploit sands with high residual hydrocarbon saturation.

The partners include the City of Long Beach, Tidelands Oil Production Company, Magnetic Pulse, Inc., and Stanford University.

Select the Appropriate Item for More Information:

- DOE CLASS PROGRAM HOME PAGE maintained by a DOE contractor.
- BPO FACT SHEET ON THIS CONTRACT (contract #DE-FC22-95BC14934) maintained by a DOE contractor.
- SPE PAPER: Acoustic Detection of Hydrocarbons in the Wilmington Field, CA.
- AGU ABSTRACT: Application of Laboratory and Theoretically Derived Rock Physics Relationships for Clastic Rocks to Log Data - Example from the Wilmington Field, CA
- Upcoming Papers, AAPG
- Upcoming Paper, ISRM
- GRL Paper (GRL v. 24 #3, pp.329-332):

  Application of theoretically derived rock physics relationships for clastic rocks to log data from the Wilmington Field, CA
- Acoustic Detection Works in Wilmington! Figure showing successful discrimination using acoustic data recorded through casing of watered out and oil bearing units.
- ROCK-LOG MODELS MATLab Application Screen.
- CONTACT ADDRESSES for more information.
- HOME PAGE FOR WILMINGTON STEAMFLOOD PROJECT maintained by Dr. Ershaghi of USC.

To learn more about research at Stanford related to this and other oilfield and geologic problems, select the Stress and Borehole Geophysics home page.

For reprints and other information on the ongoing project, contact
Dan Moos / moos@pangea.stanford.edu

Last modified March 23, 1997.

Appendix #11

Please find enclosed a preliminary version of the CD ROM that Tidelands has been working on as part of technology transfer for the DOE Projects.

Windows 95 is required for you to view the CD ROM. The CD ROM can be loaded as follows:

1. Access the CD ROM, tyically on D drive under the "My Computer" icon.
2. Load "QT32inst" from the CD ROM and follow the install instructions.
3. Load "Startpc" from the CD ROM. The program will load automatically and run through an introductory video. The video will end at the main interactive screen.

"TECH-TRANS-WARE"

OUTLINE OF

CD-ROM PRODUCTION

For: Tidelands Oil Production Company

By: DR. B. Ghaffary

Video And Animation Clips

- Nantional Oil Program ----(VAC.MOV)
- Southern California
- Long Beach
- Wilmington Field

Wilmington Field----------M000

- Background----------(A)
- Technology----------(B)
- DOE Projects----------(C)
- Operations----------(D)
- Environment----------(E)

- Tree -- Little man/Cross Reference---------- I000
- Help---------- H000

Background (A)----------A000

- (A1) History
- (A2) Reservoir Statistics---------(A002.TXT), (A002.PIC)
- (A3) Production Statistics---------(A003.TXT), (A003.PIC)
- (A4) Estimated Reserves---------(A004.TXT), (A004.PIC)

(A1) History

- (A11) Discovery----------(A011.TXT), 1x(movie A0119.MOV)

- (A12) Initial Development----(A012. TXT), 1x(movie A0129.MOV)
- (A13) Subsidence----------(A013.TXT), (A013.PIC), 1x(movie A013q.MOV)
- (A14) Steamflooding--------(A014.TXT), (A014.PIC),
  4x(movie A01479.MOV/A01478.MOV/A014912.MOV/A0149q.MOV)
- (A15) Waterflooding----------(A015.TXT)

Technology (B)----------B000

- (B1) Past Technology
- (B2) Current Technology
- (B3) Technology Innovations

(B1) Past Technology

- (B11) Reservoir
  Characterization----(B111.TXT), B111A.PIC), (B111B.PIC), (B111C.PIC)
  Management----------(B112.TXT)
- Operation
  (B121) Surface Facilities---------(B121.TXT),
  2x(movie B12198.MOV/B12199.MOV)
  (B122) Tertiary Recovery Projects-----(B122.TXT), (B122A.PIC), (B122B.PIC)

(B2) Current Technology

- (B21) Reservoir
  Characterization-------(B211.TXT), (B111C.PIC)
  Management---------(B212.TXT)
  Simulation----------(B213.TXT)
- (B22) Drilling----------(B022.TXT),
  3x(movie B022D1.MOV/B022915.MOV/B02252.MOV)
  (B22L) Extra video (large frame B022D2b.MOV)
- (B23) Operation----------(B023.TXT)
  (B231) Surface Facilities-------(B231.TXT), (B231A.PIC), (B231B.PIC),
  2x(movie B231.MOV/B231914.MOV)
  (B232) Injection/Production----------(B232.TXT), (B232A.PIC) (B232B.PIC),
  (A014.PIC), 1x(movie B232917.MOV)

(B3) Technology Innovations

- (B31) Reservoir Characterization/Management--------(B031.TXT), (B031.PIC),
  (B31L) Extra video (large frame B031SIM.MOV)
- (B32) Three-Dimensional Reservoir Simulation---------(B032.TXT)
- (B33) Drilling of Horizontal Wells----2x large frame (movie
  B033D34b.MOV/B033D5b.MOV)
  (B331) Well #1 (UP-955)--(B332A.TXT), (B332B.TXT), (B332A.PIC),
  (B332B.PIC), (B332C.PIC), (B332D.PIC)

(B332) Well #2 (2AT63)--(B333.TXT), (B333A.PIC), (B333B.PIC), (B333C.PIC), (B333D.PIC), (B333E.PIC)

- (B34) Hot Water Alternating Steam (WAS) Drive----------(B034.TXT)
- (B35) Underwater Steam Transmission Line--(B035.TXT), (B035.PIC), 3x(movie B035714.MOV/B035715.MOV/B0357BRI.MOV)
- (B36) Geochemistry of Rock/Fluid Interactions----------(B036.TXT)
- (B37) Through Casing Logging----------(B037.TXT)
- (B38) Advanced Well Recompletion Techniques
  (B381) Overbalanced Perforating Steam Injection Well Program (Well J-120)----------(B382A.TXT), (B382B.TXT), (B382C.TXT), (B382A.PIC), (B382B.PIC),(B382C.PIC), (B382D.PIC), (B382E.PIC)
  (B382) Overbalanced Perforating and Gravel Packed Inner Liner (Well A-173)--(B383.TXT), (B383A.PIC), (B383B.PIC), (B383C.PIC), (B383D.PIC)

Operations (D)----------D000

- (D1) City of Long Beach Department of Oil Properties
  - (D11) Background-------(D011.TXT), 1x(movie D001712.MOV)
  - (D12) Organization------(D012F.PIC)
- (D2) State of California State Lands Commission
  - (D21) Background---------(D021.TXT)
  - (D22) Organization--------(D022F.PIC)
- (D3) Tidelands Oil Production Company
  - (D31) History and Strategy----------(D031.TXT)
  - (D32) Present Operations----------(D032.TXT)
  - (D33) Organization----------(D033.TXT), (D033F.PIC)
  - (D34) Experience and Capabilities---------(D034.TXT)
- (D4) THUMS
  - (D41) Background----------(D041.TXT)
  - (D42) Present Operations--------(D042.TXT)
  - (D43) Organization----------(D043F.PIC)

Environment (E)----------E000

- (E1) The City of Long Beach----------(E001.TXT), (B111A.PIC)
- (E2) Surface Site Description----------(E002.TXT), (E002.PIC), 2x(movie E002739.MOV/ E002911.MOV)
- (E3) Environmental Concerns---------(E003.TXT), 1x(movie E003718.MOV)
- (E4) Environmental Precautions------(E004.TXT), 3x(movie E00474.MOV/E004916.MOV/E0049192.MOV)

U.S. Department of Energy Projects (C)----------C000

- (C1) National Oil Program and Class Projects

- (C2) Steamflood Project
- (C3) Waterflood Project
- (C4) Technology Transfer Documents

(C1) National Oil Program and Class Project

- (C11) National Oil Program-------(C011.TXT),
  (C011LV) Extra video (large frame C011b.MOV)
- Class Projects
  - (C1210) Summary----------(C012.TXT)
  - (C121) Class I Projects--------(C121.TXT)
  - (C122) Class II Projects--------(C122.TXT)
  - (C123) Class III Projects-------(C123.TXT)

(C2) City of Long Beach Class III Steamflood Project

- (C21) Abstract----------(C021.TXT)
- (C22) Highlights ----------(C022.TXT),
  2x(movie C022713.MOV/C0227u7.MOV)
- (C23) Team---------(C023.PIC)
  - (C231) U.S. Department of Energy
    - Background
    - Key Personnel
  - (C232) City of Long Beach
    - Background----------(C232A.TXT)
    - Key Personnel----------(C232B.TXT)
  - (C233) Tidelands Oil Production Company
    - Background----------(C233A.TXT),
      1x(movie C233413.MOV)
    - Key Personnel----------(C233B.TXT)
  - (C234) University of Southern California
    - Background----------(C234A.TXT),
      1x(movie C2347u7A.MOV)
    - Key Personnel----------(C234B.TXT)
  - (C235) David K. Davies and Associates
    - Background----------(C235A.TXT)
    - Key Personnel----------(C235B.TXT)

- (C24) Project Description and Results
  - (C2410) Project Summary----------(C2410.TXT)
  - (C241) Activity 1 Database
    - Summary----------(241T0.TXT)
    - Task 1 Production/Injection Completion Data--(C241T1.TXT)
    - Task 2 Well Logs and Core Data-(C241T2.TXT),
      (B111C.PIC),
      2x(movie C241T216.MOV/C241T24.MOV)
  - (C242) Activity 2 Advanced Reservoir Engineering
    - Summary----------(242T0.TXT)

Task 1 Basic Reservoir Engineering--------(C242T1y.TXT),
1x(movie C242T15.MOV)
Task 2 Characterization Data----------(C242T2y.TXT),
1x(movie C242T21.MOV)
Task 3 Deterministic 3-D Geologic Model---(C242T3y.TXT),
1x(movie C242T39.MOV)
Task 4 Stochastic 3-D Geologic Model-------(C242T4y.TXT),
2x(movie C242T42.MOV/C242T410.MOV)

(C243) Activity 3 Reservoir Simulation
Summary----------(243T0y.TXT)
Task 1 Deterministic 3-D Reservoir Model---(C243T1y.TXT),
1x(movie C243T1u3.MOV)
Task 2 Stochastic 3-D Reservoir Model--(C243T2y.TXT),
1x(movie C243T27d.MOV)

(C244) Activity 4 Reservoir Management
Summary----------(244T0.TXT)
Task 1 Horizontal Wells and Surface Facilities--
(C244T1A.TXT), (C244T1B.TXT), (C244T1C.TXT),
1x(movie C244T111.MOV)
Task 2 Horizontal Well Cyclic Steam Stimulation-.
(C244T2y.TXT),
1x(movie C244T210.MOV)
Task 3 Horizontal Well Steam Drive
(C244T3y.TXT),(C244T3.PIC),
1x(movieC244T313.MOV)
Task 4 Hot Water Alternating Steam Drive(C244T4.TXT),
(C244T4.PIC)
Task 5 Geochemistry of Rock/Fluid Interactions--
(C244T5y.TXT),
1x(movie C244T514.MOV)
Task 6 Steamdrive Mechanisms
Task 7 Reservoir Surveillance----------(C244T7y.TXT),
1x(movie C244T715.MOV)

(C245) Activity 5 Operational Management
Summary----------(245T0.TXT)
Task 1 Alkaline Water/Steam Injection
Completion(C245T1y.TXT),
1x(movie C245T119.MOV)
Task 2 Horizontal Well Completions-------(C245T2.PIC),
1x(movie C245T295.MOV)
Task 3 Profile Control in Horizontal Injectors-----
(C245T3y.TXT),
3x(movieC245T331.MOV/C245T397.MOV/C245T320.MOV
)
Task 4 Scale Control
Task 5 Determining Optimum Temperatures

(C246) Activity 6 Technology Transfer
Summary----------(246T0.TXT)
Documents

(C3) City of Long Beach Class III Waterflood Project----------F000

- (C31) Abstract----------(C031.TXT)
- (C32) Highlights---------(C032.TXT),
  2x(movie C022713.MOV/C0327u12.MOV)
- (C33) Team----------(C033.TXT), (C033.PIC)
  - (C331) U.S. Department of Energy
    - Background
    - Key Personal
  - (C332) City of Long Beach
    - Background----------(C232A.TXT)
    - Key Personal----------(C232B.TXT)
  - (C333) Tidelands Oil Production Company
    - Background----------(C233A.TXT)
    - Key Personal----------(C233B.TXT)
  - (C334) Stanford University
    - Background----------(C334A.TXT)
    - Key Personal----------(C334B.TXT)
  - (C335) Magnetic Pulse Inc.
    - Background----------(C335A.TXT)
    - Key Personal----------(C335B.TXT)
- (C34) Project Description and Results
  - (C3410) Project Summary----------(C3410.TXT)
  - (C341) Activity 1 Reservoir Characterization
    - Summary----------(341T0.TXT)
    - Task 1 Reservoir Extent and Structure
    - Task 2 Areas of High Oil Reserve Potential
    - Task 3 Geologic Reasons for High Oil Reserve Potential
    - Task 4 Rock-Log and Fluid-Log Models
  - (C342) Activity 2 Reservoir Engineering
    - Summary----------(342T0y.TXT)
    - Task 1 OOIP and Production / Injection Data
    - Task 2 Average Oil Saturations per Zone
    - Task 3 Material Balance
    - Task 4 Mapping of Production and Injection
    - Task 5 Recovery Factors
    - Task 6 Sands with High Remaining Oil Saturation
    - Task 7 OGCI Production Analyst Maps
  - (C343) Activity 3 Deterministic 3-D Geologic Model
    - Summary----------(343T0y.TXT)
    - Task 1 Deterministic 3-D Geologic Model-(C343T1.TXT)
    - Task 2 Cased Hole Pulsed Acoustic Logging-(C343T2.TXT),
      1x(movie C343T27u.MOV)
  - (C344) Activity 4 Cased Hole Logging
    - Summary----------(344T0y.TXT)
    - Task 1 Logging of 12 Wells
    - Task 2 Evaluation of Logs
  - (C345) Activity 5 Drilling and Recompletions
    - Summary----------(345T0.TXT)
    - Task 1 Overbalanced Perforating and Gravel Packed Inner Liner-(C345T1.TXT)

Task 2 Perforating and Gravel Packed Inner Liner
Task 3 Overbalanced Perforating Steam Injection--
(C345T3.TXT)
Task 4 Ultra-Short Radius Lateral Completion
Task 5 Short Radius Lateral Completion
(C346) Activity 6 Technology Transfer
Summary----------(346T0y.TXT)
Documents

(C4) Documents----------G000

- DOE reports
  Annual Reports
  Steamflood-------(C246T11.TXT)
  Waterflood---(C346T11A.TXT), (C346T11B.TXT), (C346T11C.TXT), (C346T11D.TXT)

  Quarterly Reports
  Steamflood----------(C246T12.TXT)
  Waterflood----------(C346T12.TXT)

- Publications
  Steamflood--
  Waterflood--

- Presentations
  Steamflood--
  Waterflood--

- Field Tours
  Steamflood--
  Waterflood--

THE END